UTS UNIVERSITY OF TECHNOLOGY SYDNEY

Design, Modelling and Experimental Evaluation of Energy Recovery Indirect Evaporative Cooling System

by Ahmed Y Taha Al-Zubaydi

Thesis submitted in fulfilment of the requirements for
the degree of

Doctor of Philosophy

under the supervision of Associate Professor Dr. Guang Hong
And Dr. Lee “Mickey” Clemon

University of Technology Sydney
Faculty of Engineering and Information Technology

December 2019

CERTIFICATE OF ORIGINAL AUTHORSHIP

I, Ahmed Y Taha Al-Zubaydi declare that this thesis is submitted in fulfilment of the requirements for the award of Doctor of philosophy, in the Mechanical engineering at the University of Technology Sydney. This thesis is wholly my own work unless otherwise reference or acknowledged. In addition, I certify that all information sources and literature used are indicated in the thesis. This document has not been submitted for qualifications at any other academic institution.

This research is supported by the Australian Government Research Training Program.

Signature: Production Note:
Signature removed prior to publication.

Date: 24.12.2019

Abstract

Design, Modelling and Experimental Evaluation of Energy Recovery Indirect Evaporative Cooling System

Heating, ventilating and air conditioning systems (HVAC) are essential for providing a comfortable and healthy indoor environment for human beings and required conditions for manufacturing and operations in industrial sectors. Maximizing energy efficiency and minimizing the environmental impact of HVAC systems has become more and more important to address the issues of sustainability and environmental protection. With the recent climate warming, the demand for air conditioning is expected to hit a new high. The dilemma of high demand while simultaneously reducing energy consumption requires a full-scale campaign to develop new technologies for HVAC systems.

Recovering wasted energy is one way to reduce the energy consumption in HVAC systems. In a modern building, the energy lost through ventilation can be more than 50% of the total thermal losses. In this study, two advanced technologies were investigated, the air-to-air heat recovery ventilation (HRV) and the indirect evaporative cooler (IEC). The energy wasted by the exhaust air was recovered by pre-cooling the supply air as the heat was transfer from the fresh air to the exhaust air in an HVAC system.

A test rig was designed, manufactured, modified and calibrated to meet the special aims of this research. It is a cost-effective and inventive test facility with the flexibility to be used for both dry (HRV) and wet (IEC) operation modes.

The experimental study of the HRV was conducted by testing two polymer heat exchangers with two different plate geometries, one with a flat plate and the other with a

dimpled surface plate. The key aims were to understand the effect of the surface geometry of the plates on the performance of the air-to-air heat exchanger. Regarding the performance of the HRV, the sensible efficiency of the heat exchanger with the dimpled surface was 50% to 60% higher than that of the heat exchanger with flat surface plate at lower air velocity and higher air initial temperatures. The highest COP of the heat exchanger with dimpled surface heat was 6.6; achieved under primary air operating temperature of 32.6 °C.

In the investigation of the IEC system, the main aim was to find the effect of water spray arrangement on the performance. Experiments were conducted with three water spray modes: (1) external spray, (2) internal spray and (3) mixed internal and external sprays. An ANSI/ASHRAE Standard 143-2015 evaluation indices with changing the primary air condition parameter (Primary air inlet temperature and velocity) were applied to evaluate the system performance with water spraying variation. The results show that the internal spraying mode performs better than the external spraying mode does in terms of the wet-bulb efficiency, cooling capacity and the COP of IEC. The mixed-mode improves the performance further but increases the water evaporation rate. The innovative internal spray system benefits the sensible heat transfer in the IEC system. The cooling load capacity increases by 12.5% with the internal spray mode and 25% with the mixed mode. The COP varies in a wide range under different water spraying modes and operating conditions with the highest of 19.12 achieved in the mixed-mode.

CFD modelling was also performed to further investigate the IEC system. An Eulerian-Lagrangian 3-D numerical model was developed which was capable of simulating a representative IEC system with realistic nozzles in the mixed-mode operation. A solid-cone spray representation in Eulerian-Lagrangian numerical models was applied in order to replicate real nozzles characteristics in the simulation. The model was verified by

experimental results. The verified model was employed to study the effects of primary air temperature, humidity ratio and velocity on the performance of the indirect evaporative heat exchanger (IEHX). Operating under variable inlet air temperature and humidity conditions, simulated results showed that the wet-bulb effectiveness for the mixed mode ranged from 68%% to 80% with a primary air supply temperature near dew-point temperature at primary air temperature lower than 28 °C and velocity less than 1.5 m/s.

Dedication

First to the memory of my father, Yassin Al-Zubaydi

To my mother Natheera Abdul-Baki, my wife Sarab Mansoor, my daughters Basma and Tanya and all my family

Acknowledgements

This work would not have been possible without the financial support of the Australian Government Research Training Program Scholarship and the help of the University of Technology Sydney – School of Mechanical and Mechatronic Engineering. I am especially indebted to my principal supervisor, Associate Professor Dr Guang Hong, for her continuous support. As my supervisor and mentor, she was the best example of how the researcher and academic should be. I appreciate all her contributions of time, ideas, and assistance to make my PhD experience productive and inspiring. The enthusiasm she has for her research was contagious and motivational for me during hard times in the PhD study.

In addition, I would like to thank my co-supervisors Mr John Dartnall and Dr Lee "Mickey" Clemon. John was the person who creates my deep engaging to the IEC technology, and he was the guide for long years extended to my master degree research time. Mickey is a positive addition to my study with his new experience, smart ideas and suggestions. A special thanks to Dr Terry Brown, Dr Benjamin Halkon and Dr Peter McLain, who have been supportive of my career goals and who worked actively to provide me with the protected academic time to pursue those goals. I am grateful to all of those with whom I have had the pleasure to work with during my time at the University of Technology Sydney. Each of my school members has provided me with extensive personal and professional experience. I would especially like to thank the UTS lab staff members Mr Carlo Giampietro and Mr Chris Chapman, who provided the help and technical backing just when I needed it. Furthermore, I have to thank Mr Ufuk Tiftik for his professional advice with CFD work.

To take the PhD ship to the shore, nobody has been more important to me in the accomplishment of this task than the members of my family have. I would like to thank my mother, whose love and guidance are with me in whatever I pursue. She is the ultimate idol. Most importantly, I am grateful to my loving and supportive wife, Sarab, and my wonderful daughters, Basma and Tanya, who provide unrelenting joyful and inspiration.

List of Publications

- Al-Zubaydi, A.Y.T., G. Hong, and W.J. Dartnall. 2016, CFD Modelling and Analysis of Different Designs Plate Heat Exchangers. In 10th Australasian Heat & Mass Transfer Conference. Brisbane, QLD.
- Al-Zubaydi, A.Y.T. and G. Hong, 2018.Experimental investigation of counter flow heat exchangers for energy recovery ventilation in cooling mode, International Journal of Refrigeration. 93: p. 132-143.
- Al-Zubaydi, A.Y.T. and G. Hong, 2019.Experimental study of a novel water-spraying configuration in indirect evaporative cooling, Applied Thermal Engineering. 151: p. 283-293.

Table of Contents

List of Figures

List of Tables

Abbreviation

3-D	Three Dimensional Geometry
AHRI	Air-Conditioning, Heating and Refrigeration Institute
AHU	Air-Handling Unit
ANSI	American National Standards Institute
ASHRAE	The American Society of Heating, Refrigerating and Air-Conditioning Engineers
BOM	Bureau of Metrology
CAD	Computer Aided Design
CFD	Computational Fluid Dynamic
CSIRO	Commonwealth Industrial and Scientific Research Organisation
DEC	Direct Evaporative Cooling
DIEC	Direct-Indirect Evaporative cooler
DNS	Direct Numerical Simulation
DOEE	Department of Environmental and Energy - Australia
DPM	Discrete Phase Modelling
HFC	hydrofluorocarbons
HMX	Heat and Mass Exchange
HRV	Heat Recovery Ventilation
HVAC	Heating, Ventilation and Air-Conditioning)

HX	Heat Exchanger
IEA	International Energy Agency
IEC	Indirect Evaporative Cooling
IEHX	Indirect Evaporative Heat Exchanger
LDPE	Low-Density Polyethylene
LMTD	Logarithmic mean temperature difference
M-Cycle	Maisotsenko Cycle
NGER	National Greenhouse and Energy Reporting
NTU	Number of Transfer Units method
PETG	Polyethylene Terephthalate Glycol
PHE	Plates Heat Exchanger
PVC	Polyvinyl Chloride
RANS	Reynolds-Averaged Navier-Stokes
R-IEC	Regenerative Indirect Evaporative Cooling
ε-NTU	Effectiveness-Number of Transfer Units

Nomenclature

A : Area, m^2

b : Gap between two plates, mm

c_{pa} : Specific heat of air, J/kg. °C

COP : Coefficient of performance

$eff._S$: Sensible efficiency, %

h : Enthalpy of air, J/kg

H : Height of Plate, mm

L : Length of Plate, mm

l_{fg} : Latent heat of vaporization of water, J/kg

$\dot{m}$: Mass flow rate, kg/s

N : Number of plates

p : Precision

P : Power, W

$\dot{Q}$: Heat Transfer Rate, W

RH : Relative Humidity, %

S_φ : The source term for the continuous phase

$S_{p\varphi}$: The additional source due to the interaction between air and water droplets

t : Temperature, °C

$u(x)$: The absolute uncertainty of directly measured variable, %

v : Air velocity, m/s

$\dot{V}$: Volumetric flow rate, m^3/s

V_w : Water evaporation rate, kg/hr

X : Total Width, mm

y : The indirectly measured variable

Z The differential pressure across the orifice plate, mmH_2O

Greek Letters

β : The sum of bias error

δ : The total uncertainty error, %

ε : Effectiveness

ϕ : Flow variable

Γ_φ : The diffusion coefficient

ρ : Air density, kg/m^3

t : Temperature depression, °C

ω : Relative humidity/moisture content of air, g/kg

Δx : The instrument accuracy

ΔP : Pressure variation, Pa

Δy : The absolute uncertainty, %

Δz : Plate thickness, mm

Subscripts

1 : Inlet

2 : Outlet

p : Primary air

s : Secondary air

DB : Dry-Bulb

WB : Wet-Bulb

Chapter 1

Introduction

1.1. Background

The increasing demand for power to supply modern-life activities has resulted in an uncontrollable greenhouse gas emission. The world is looking forward to effective, cheaper and environmentally clean power sources to prevent or at least slow down the catastrophic results of global warming. Most of the world's greenhouse gas emissions come from the burning of fossil fuels for energy (e.g. for electricity and transport). When oil, gas or coal burns, the carbon contained within it reacts with oxygen in the air to create carbon dioxide. Australia's produced 194.7 Mt CO_2^{-e} in 2016 for electricity generation (DOEE 2019), and the country steps up to reduce the greenhouse gas emissions to 5% below 2000 levels by 2020 and further to 26-28% below 2005 levels by 2030.

Global warming has led to a more extended period for cooling using air condition and consequently higher demand for electricity for HVAC (Heating, Ventilation and Air-Conditioning) systems (Burillo et al. 2019). The forecast shows that the temperature will rise in the coming decades (BOM 2019), resulting in a cooling load increase, which in turn will further contribute to global warming.

Traditional air conditioning systems that use direct expansion units and chillers are usually considered high-energy consumption systems. The HVAC systems electricity consumption represents up to 40% of Australian office buildings annual consumption (Lecamwasam, Wilson & Chokolich 2012). Furthermore, while the ventilation and

circulation fans consume part of the power, the majority of the energy is consumed in the chillers and cooling towers.

According to the International Energy Agency (IEA 2018), 1,600 million air conditioner systems are already operating in the world. The IEA predicted that by 2050, there would be 5.6 billion air conditioning units, leading to triple the electricity demand to operate these units. The impact of air conditioning on climate change is not limited to electricity consumption. Refrigerant gases, mostly hydrofluorocarbons (HFCs) can also be an issue for greenhouse gas effect if they released into the atmosphere at the end of their life span (NGER 2017).

The conventional air conditioning systems typically reach peak energy consumption during the hottest days in the year. The high power demand may exceed electricity transmission networks capacity, resulting in damage to the network and even disruptions in the power supply. Thus, it is commonly understood that reduced dependency on electricity for driving conventional air conditioning systems would lead to positive environmental outcomes. The recent improvement in "natural" ventilation systems has shown successful installations in some settings around the world (Gough et al. 2018). However, a substantial barrier to natural ventilation systems in Australia stems from the highly urbanised nature of the population. The fact that the vast majority of Australian buildings are located within large cities where ambient noise and smoke is commonly an issue (Chen et al. 2019). In the modern buildings, the ambient noise is reduced by "sealed building" design, with mechanical ventilation (Field 2015).

The building exhaust air is one of the energy-wasting forms in the traditional HVAC systems (Zeng, Liu & Shukla 2017). As shown in **Figure 1.1(a)**, a portion of the return air is mixed with the fresh air before treatment in the air conditioning system and supplied

to the zone. The other portion is sent to outside as exhaust air. The mixed air is contains some impurities and CO gas carried out from the conditioned zone. The exhaust air is a waste of energy. **Figure 1.1(b)** shows the installation of heat recovery ventilation [HRV] system to recover the energy from the return air to pre-cool the fresh air. The heat/mass recovery ventilation is an effective method to regain energy and provide better indoor air quality with 100% fresh supplied air. The indirect evaporative cooler as the heat recovery ventilation system enhances the heat recovery process in cooling mode.

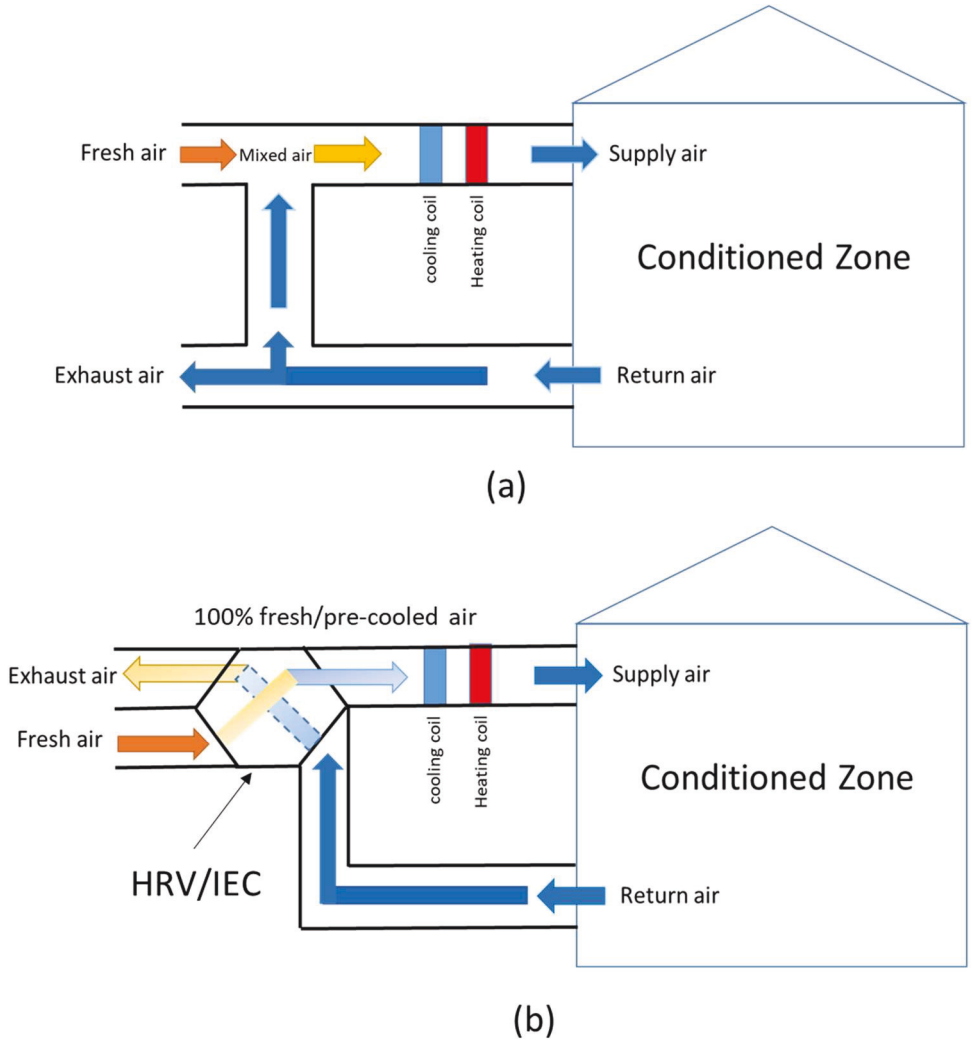

Figure 1.1. Schematic diagram of HVAC system: (a) Without heat recovery and (b) with HRV/IEC unit

The indirect evaporative cooling heat recovery system will enable the reduction of the power consumption by providing an extended compressor "sleeping" times and in consequence, a cut in the greenhouse gases emission. The device can also be applied as a high efficient/low consumption standalone air cooling system suitable for small to medium-size buildings (Bravo & González 2013). Both applications will improve the year-round building energy performance through the reduction in the energy consumption of the mechanical HVAC systems and enhance the building air quality in terms of higher ventilation rates. A dehumidification process may require as the system capable of processing the air at lower operating temperatures. The dehumidification of the supplied fresh air to the building is necessary to remove the excessive moisture contents to acceptable levels.

1.2. Research Objectives:

The overall objective of the present study is to meet the research needs discussed earlier by developing and experimentally investigating new techniques for water spray in IEC systems including the variation of nozzle locations and increasing water distribution area. Experiments were conducted on an IEC with installed nozzles for spraying water in multiple directions (vertically, horizontally and diagonally) within the wet channel to increase the wettability of the plates. Experimental results were analysed to compare the IEC performance in three different water spray configurations: external, internal and all-nozzles hybrid mode.

The secondary aim of the study is to reduce the existing experimental research gap discussed in Chapter 2 with extend analyses of laminar quasi-counter-flow fixed-plate heat exchangers and to measure the effect of small scale wall dimples. In particular, a new plate surface geometry design consists of longitudinal low amplitude dimples with specified arrangements. In this study, the impact of the surface geometry on the heat

recovery ventilation (HRV) system overall performance was experimentally investigated. Two polymer plates with different surface geometries, flat and dimpled, were tested under various operational conditions to compare the thermal performance.

An IEC system was developed to study the effect of the proposed novel water distribution arrangement. The device can be integrated into building exhaust ventilation systems to recover the energy from the building exhaust air. It thereby provides a pre-cooled air supply that could be reduce the energy demand of conventional air conditioning systems for cooling.

The specific objectives of the research identified as following:

1. To design, build and commission a standardised low-cost and flexible test facility to provide the accurate measurements of the energetic performance for all heat recovery devices with quasi-counter flow heat exchangers including the HRV and IEC systems.
2. To conceptually design and build air-to-air plate heat exchanger prototypes considering the structure/geometry, the material selection, air and water flow arrangement, and nozzle locations.
3. To conduct an experimental study on both the HRV and IEC prototypes and analyse the effect of the plate face geometry and water spraying distribution.
4. To develop and validate a detailed 3-D CFD model for the analysis and optimisation of the IEC system performance.

1.3. Research Methodology

To achieve the study objectives, a detailed review and analysis of the existing literature in indirect evaporative cooling (IEC) was conducted. The discussion focuses specifically

on two significant research features: the water spraying in IEC and the HRV heat exchanger. The aim is to analyse the existing water spraying arrangements deployed in the IEC systems. Moreover, developing heat recovery ventilation techniques to pre-cooling the fresh air temperature and increase the efficiency of the HVAC system. The research methodology flow chart is shown in **Figure 1.2.**

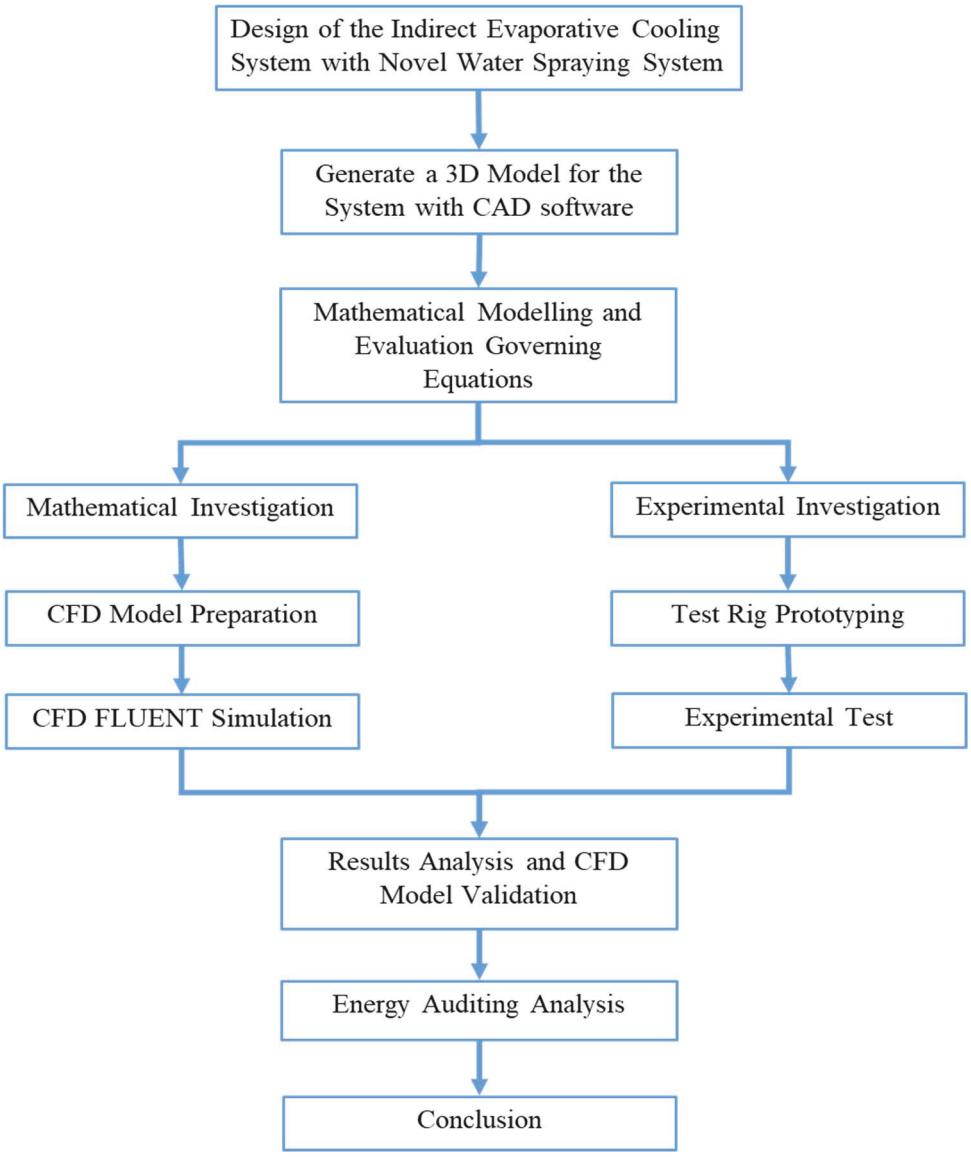

Figure 1.2. Methodology Flow Chart

A 3-D model will be used to prototype the test facilities and to perform the CFD (Computational Fluid Dynamic) simulation, analysis and optimisation. The CFD analysis created using the ANSYS FLEUNT package is capable of simulating the heat transfer,

airflow, water phase change process and pressure drop across the heat exchanger. A full set of data under a range of parameter variation can be collected via the CFD model.

The experimental test rig with designated heat exchanger will generate data under laboratory-controlled testing parameters. The generated experimental data are more realistic than the simulation data. The experimental data are used to validate the CFD model.

The CFD model and experimental work are applied in the system performance analysis and optimisation process.

1.4. Thesis Outlines

A summary of the thesis chapters is as follows:

Chapter 1: A brief introduction to the HVAC energy consumption and the increased demand, need for efficient air conditioning systems, significant energy recovery in buildings and its environmental impact are presented in Chapter 1. Chapter 1 also highlights the research concept of the proposed water distribution method for evaporative cooling, objectives and the methodology of the PhD research.

Chapter 2: To identify the gap in existing researches in the field of indirect evaporative cooling technology and specify the most accredited research methodology, a comprehensive literature review of existing researches in the field of indirect evaporative cooling technologies is presented in Chapter 2. This chapter presents the categorisation of different indirect evaporative cooling systems, in terms of working principles, heat exchanger geometry, airflow arrangement, construction material, water distribution system, performance, and the state of art of the commercially available systems.

The literature review identifies the technical problems, the advantages and limitations of the indirect evaporative cooling system. This chapter presents an analysis of numerical and experimental methods for evaluating the performance of indirect evaporative cooling and heat recovery technology.

In Chapter 3, a prototype of a multi-water spraying point's IEC cooling system was designed, fabricated and experimentally tested to validate the CFD model simulation. The details of material selection, heat exchanger and the test facility CAD models, prototype setup and data acquisition instruments are described in this chapter.

Chapters 4 and 5 include a detailed description of the experimental setup and the implementation of all examination methods. In addition, all test results are summarized and analysed. The results of the experiments and the effects of various testing parameters on the performance of the prototype were investigated in this chapter. The parameters include primary air dry-bulb and wet-bulb temperature, secondary air dry-bulb and wet-bulb temperature, the air channel velocity, feed water temperature and the spraying mode.

Chapter 6 reports the numerical method used in the present work for the evaluation of the experimental results. A devoted mathematical model of the indirect evaporative cooling system is presented based on assumptions and approximations. The mathematical model describes the governing equations of the heat and mass transfer and the effect of work parameters changing on the performance of the proposed hexagonal counter-flow heat exchanger. As part of this thesis methodology, Chapter 6 provides a CFD analysis of the novel indirect evaporative cooling system using the Computational Fluid Dynamic solver FLUENT integrated into the ANSYS commercial program package. Both the structure and the programming of the CFD analysis are explained. As an example, the meshes quality and grid verification, the turbulence model, the nozzle models and boundary conditions. The results of the CFD simulation are discussed and validated against the

experimental data collected. The CFD data and experimental data were employed to determine the accuracy of the CFD model.

To conclude this work, chapter 7 presents the conclusion of the most relevant results of the investigations carried out in the present work on the novel indirect evaporative cooling system in the form of a summary. The chapter concludes with an outlook on continuing research into the modelling of new indirect evaporative cooling systems with a focus on the water circulation methods.

Chapter 2

Literature Review

2.1. Introduction

To identify the gap in existing researches in the field of indirect evaporative cooling technology and specify the most accredited research methodology, a comprehensive literature review of existing researches in the field of indirect evaporative cooling technologies is presented in Chapter 2. This chapter presents the categorisation of different indirect evaporative cooling systems, in terms of working principles, heat exchanger geometry, airflow arrangement, construction material, water distribution system, performance, and the state of art of the commercially available systems.

The literature review identifies the technical problems, the advantages and limitations of the indirect evaporative cooling system. This chapter presents an analysis of numerical and experimental methods for evaluating the performance of indirect evaporative cooling and heat recovery technology.

2.2. Energy recovery ventilation

Air-to-air heat exchangers are classified into heat recovery ventilators (HRVs) and energy recovery ventilators (ERVs). HRVs are used for recovering the sensible heat only and ERVs for recovering both sensible heat and latent heat. The fixed-plate heat exchanger is one common unit used in HRVs and ERVs (O'Connor, Calautit & Hughes 2016). In HRVs, a non-porous material such as aluminium, steel or polymers are commonly used for the heat exchanger plates. Air-to-air heat exchangers have played an essential role in energy regeneration to reduce power consumption by using the energy wasted by the exhaust air in air conditioning systems. The fixed plate's heat exchangers can efficiently

replace the enthalpy wheel heat regeneration with shape flexibility and less operation cost (Chang et al. 2017).

The cross, concurrent and counter-current flows are the most common flow arrangements of ERV fixed plate heat exchangers. Among these three arrangements, the manufacturing process for the cross-flow heat exchanger is the least complicated, and the counter-flow heat exchanger has the best performance (Nasif et al. 2010). Munters presented the Thermo-Z® heat exchanger with a quasi-flow, which was a combination of cross and counter flows (Munters 2017). The quasi flow heat exchanger integrated the high performance of the counter flow arrangement and the ease of manufacturing property of the cross-flow heat exchanger. The shape modified later to a hexagonal shape with an apex angle at the entrance resulted in the reduction of air turbulence at the inlets and exits of the heat exchanger (Zhang 2010).

Manz and Huber (Manz & Huber 2000) reported experimental and simulation results of a combined duct/heat exchanger with comprising multiple parallel ducts for recovering the exhaust air energy. The heat exchanger unit they investigated was made of aluminium and used for air transport and heat recovery. Its recovery efficiency was up to 70%. Chen (Chen, Yang & Luo 2016a) performed experiments on heat recovery ventilation systems in four modes, including dry air-to-air, and using an aluminium fixed plate heat exchanger in a cross-flow arrangement. They investigated the effect of condensation in the heat exchanger channels with high relative humidity (RH) in the secondary air stream. Their results showed that due to the significant latent heat, the HRV system acted as an indirect evaporative cooling system. Fernandez-Seara (Fernández-Seara et al. 2011) tested a polymer plate heat exchanger with a counter-flow arrangement for heat recovery ventilation. They investigated the fresh air-preheating mode. Their results showed that

heat exchanger efficiency varied with the temperature, relative humidity and airflow rate of the fresh air.

The HRV systems can also be used in a hybrid mode with indirect evaporative cooling, direct evaporative cooling and heat pumps.

Different HRVs have been developed, such as the Smartbox© by Smart faćade (CEPEZED 2017). A hybrid heat recovery system was experimentally investigated by Fucci (Fucci et al. 2016). Their results showed a significant increase in the heat pump's COP when the heat pump was working in parallel with a counter-flow heat exchanger. They verified that applying the static heat recovery to preheat the fresh air reduced the power consumption of the heat pump.

The surface geometry of the heat exchanger plate can intensify the sensible efficiency in the heat exchanger plate, mainly due to the turbulence generated in airflows (Vera & Quintero 2015). Increasing the surface area and improving the air distribution over the plate area can be achieved by changing the plate surface geometry to increase the heat transfer rate and the system efficiency (Vera & Quintero 2015). However, strong turbulence may increase the pressure drop across the heat exchanger and reduce the overall system efficiency. Therefore, to optimize the performance of a heat exchanger, the pressure drop must be considered. Nevertheless, the dimple arrangements and dimple pitch had a positive influence on the heat transfer rate (Vorayos et al. 2016). The CFD results showed that the dimpled surface of the heat exchanger resulted in 20% higher sensible efficiency than the flat surface did (Al-Zubaydi, Hong & Dartnall 2016).

Reducing greenhouse gas emissions is a critical contemporary world issue. It may be the critical point in a decision analysing different HVAC systems, not only from the environmental point of view but from an economic viewpoint as well, especially after the

carbon tax charges in many countries, including Australia, have been applied. An extra cost is thus added to the operating costs of HVAC systems depending on their reliance on conventional energy. By increasing the air conditioning system efficiency, the HRV systems can save a significant amount of energy consumption required in building thermal comfort, and this energy-saving can be represented as a reduction in greenhouse gases emission (Mardiana-Idayu & Riffat 2012).

The extensive literature review shows that there is a substantial need for research on understanding the quasi-counter flow HRV system in cooling mode. In sum and experimental studies are required to investigate the influence of the plate surface geometry on the HRV heat exchanger performance. Part of this work experimentally tested the effect of the plate surface geometry on the parallel plates heat exchanger (PHE) performance. The results analysis was published in the International Journal of Refrigeration (Al-Zubaydi & Hong 2018) and further discussed in **Chapter 4**. An environmental study of the greenhouse gases reduction with the HRV system applications is an advanced scope in the HVAC studies.

2.3. Indirect evaporative cooler: Historical background

In 1935, Walter J. Ray (Ray 1935) described in his patent, a process with a capacity of cooling the air below the wet-bulb temperature of the incoming air to the installation without using mechanical refrigeration or external cooling means. The solution was achieved by the combination of an indirect evaporative cooler and an adiabatic cooler, what known later as the DIEC (Direct-Indirect Evaporative cooler), where the water of the adiabatic cooler is used to lower the air temperature entering the indirect evaporative cooler.

The Plate type indirect evaporative cooling as known today was first introduced by Watt early 1950s (Watt 2012). Watt described the first models of basic plate-type indirect evaporative cooling units built and tested in 1952 and 1953 for the United States Navy air bases. The two plate-type heat exchangers presented were made of a cross-flow parallel heat exchanger with aluminium sheets of 1.22 m length by 0.3 m wide. One with a 9.5 mm gap between the plate and spacing while the other with a 6.5 mm gap. When the two coolers mounted vertically, the system was able to cool down the primary air to 69% of wet bulb effectiveness.

Since the mid-1960s, a group of a scientific researcher of the Commonwealth Industrial and Scientific Research Organisation (CSIRO) developed a distinct program aiming the developing of the plate type indirect evaporative technology. The Australian IEC's pioneers researchers added a lot to the technology (Watt 2012). For example, the researchers introduced the revolutionary use of plastic plate heat exchanger, the energy recovery ventilation IEC and the turbulence generators dimples to increase the system efficiency.

Due to heavyweight and high cost and corrosion ability of the aluminium sheets, Donald Pescod (Pescod 1968) suggested the use of plastic sheets plate heat exchanger for the IEC system. Among the cellulose acetate, polystyrene and rigid PVC, the PVC proved to be the best in application mainly due to the strength, durability and forming ability by with thermoforming process. The limitation of the plastic low thermal conductivity (0.19 W/m.K) was minimised by using thin plastic plates.

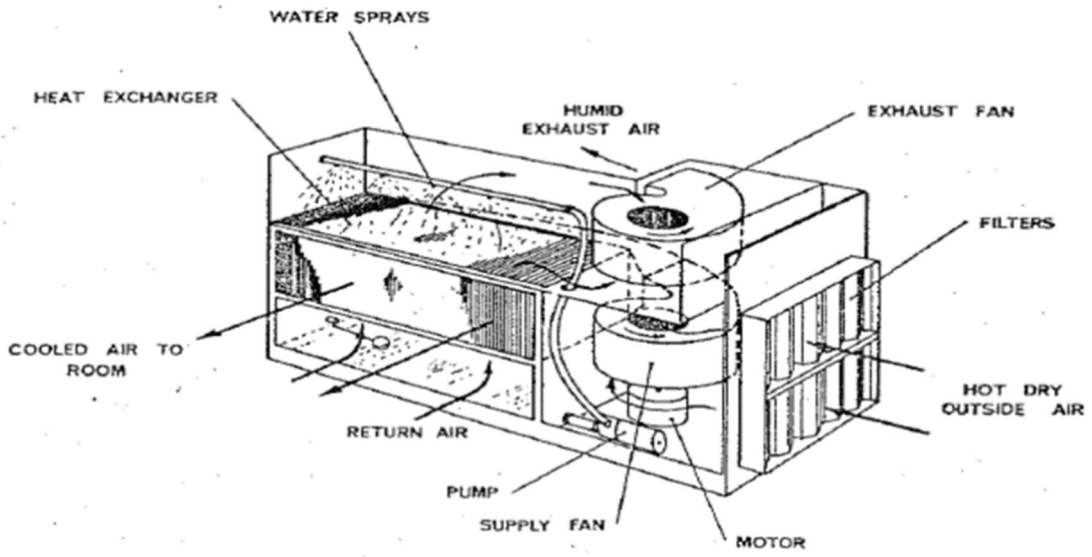

Figure 2.1. PHE cooling system by indirect evaporation (Pescod 1979)

In his later study, Pescod (Pescod 1979), promoted the first energy recovery IEC, applied the principle of using the zone exhaust air as secondary air in a wetted plastic heat exchanger. The same principles applied to an air conditioning unit built and commissioned in 1980 for Telecom building cooling (Pescod & Prudhoe 1980). The unit shown in **Figure 2.1** was commercially built in South Australia. Several hundreds of units installed in commercial offices, telephone exchanges and electricity substations. As shown in **Figure 2.1**, the unit is consists of a crossflow plastic heat exchanges with 2-4 mm plates' gap, twin centrifugal fans, water pump and low-pressure water sprayers. The medium size unit supply was in the range of 2-5 m^3/s and was able to achieve a full cooling load capacity of 3 kW.

In 1981, in what considered to be the first tracked academic IEC research, Svedeman (Svedeman 1981) master degree research discussed the simulation of an advanced indirect evaporative cooling system in conjunction with a vapour compression unit. The system consisted of an air-to-air heat exchanger, in which the secondary air (fresh air) it passes through the wet side before used for heat rejection from the condenser unit. While

the primary air (fresh air), is pre-cooled in the dry channels before bypass the cooling coil. The result shows an increase in the COP of the vapour compression system by 25%, while the cooling capacity increased by 43% compared to the standalone vapour compression system.

Similar to Svedeman system, the modified indirect evaporative cooling system presented by McNab (McNab 1990) which also known as Dual Indirect Cycle Energy Recovery (DICER), is a combined IEC and vapour compression system. The system represents an ideal solution to extend the performance of the indirect evaporative cooling despite the relative humidity of the intake of fresh air, which usually limits the system efficiency. At the same time, because the system combined with a vapour compression-cooling unit, it can reduce the energy consumption with its heat recovery. However, the system was introduced in 1990, but it was not analysed or experimentally tested since then.

Many of the known studies ignored the economic feasibility analysis of the IEC system, i.e. initial cost and payback period. Very few researchers presented the economic analysis, e.g. Hunn and Peterson (Hunn & Peterson 1996) presented the simulation results of the indirect evaporative cooling system used in commercial buildings in the typical weather of Texas. Acceptable figures of energy save and payback periods resulted for the different building type (Based on 1996 energy prices), with 0.3 years payback period and $ 3,300 annual energy saving for the cooling system used to air condition a restaurant in Huston, Texas while the results for other building types varied between promising and promisingly.

The electrical power consumption saving will result in a greenhouse gases emission reduction, which will define as the environmental impact. Robert Foster (Foster 1998), Bruno et al. (Bruno & Liu 2009) and Maheshwari et al. (Maheshwari, Al-Ragom & Suri 2001)generally described the advantages of the evaporative cooling systems different

arrangements energy saving and environmental impacts. Delfani et al. (Delfani et al. 2010) developed a statistical method to calculate the electricity-saving by using the IEC system as a precooling stage for the air supplied to an air handling unit.

There are different types of air-to-air heat exchangers used in the indirect evaporative cooling systems, including; Crossflow, parallel flow and regenerative M-type heat exchangers (**Figure 2.2**). In the cross-flow plate heat exchanger, the primary air flows in a direction perpendicular to the direction of the secondary air in the wet channels. Because of its simplicity, many works presented the modelling of the crossflow plate heat exchangers.

The parallel-flow heat exchangers as the name refer, the primary and secondary air streams flow in parallel levels, either in counter-flow direction or the same direction. The parallel-flow heat exchanger modelling was presented by Chengqin & Hongxing (Chengqin & Hongxing 2006). A comprehensive comparison between the cross-flow and parallel flow was presented by Zhan et al.(Zhan, Duan, et al. 2011).

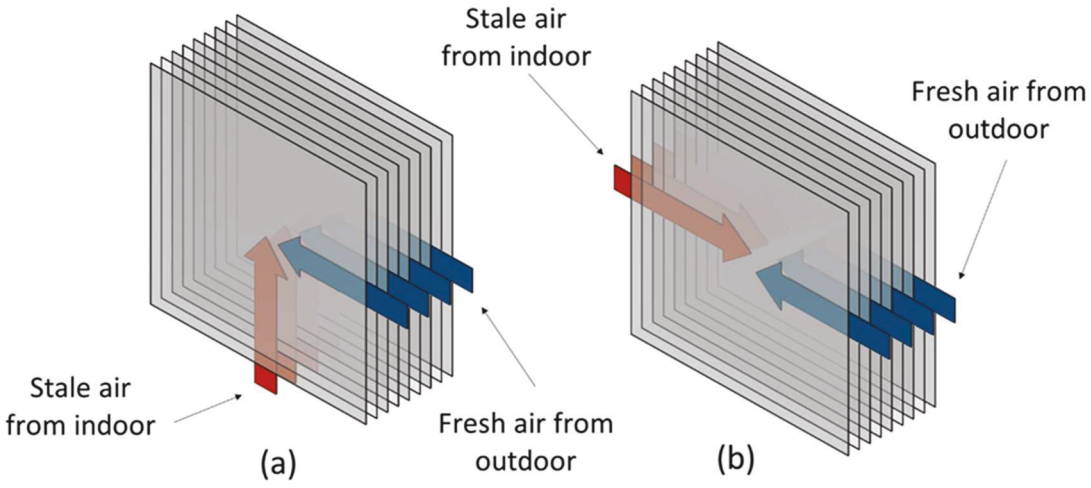

Figure 2.2. (a) Counter flow heat exchanger, (b) Cross flow heat exchanger

The third type is the regenerative heat exchanger type described earlier. In this type, there is only one inlet air stream, which passes all the way through the dry channel before the

split into two streams, one flow in a counter direction in the wet channels through small holes in the heat exchanger sheet, while the remaining air is supplied as the cooled air. This air cycle is also known as Maisotsenko heat exchanger, this cycle allows the fluid to be cooled below the wet bulb and within the dew point temperature. Moreover, no added moisture to the product air stream. The heat exchanger is patented in the United States (Gillan et al. 2010).

Coolerado® adopted the Maisotsenko cycle to develop a heat and mass exchange (HMX) technology and applied it to their products range of air conditioners, Coolerado M30, M50, C60 and H80. The cycle is modelled and simulated in work by Caliskan (Caliskan et al. 2011). A new modified regenerative heat exchanger models are analysed and presented by Lee et al. (Lee, Choi & Lee 2013; Lee & Lee 2013). Sergey Anisimov and Demis Pandelidis from Wroclaw University of Technology, Poland, enriched the M-Cycle researches with a series of publications between 2014-2019 (Anisimov & Pandelidis 2015; Anisimov, Pandelidis & Danielewicz 2015; Anisimov et al. 2014; Anisimov, Pandelidis & Maisotsenko 2016; Pandelidis & Anisimov 2016; Pandelidis et al. 2017). Their works provide data based on both experimental and numerical analysis that can be used as a solid base for M-Cycle researches.

2.4. Operating principles of the evaporative cooling systems

2.4.1. Direct evaporative cooling

In the direct evaporative cooling system, the system consists of a wet evaporative pad/membrane and water distribution arrangement. **Figure 2.3** illustrates the working diagram and thermal process of the direct evaporative cooling system representing on a psychometric chart.

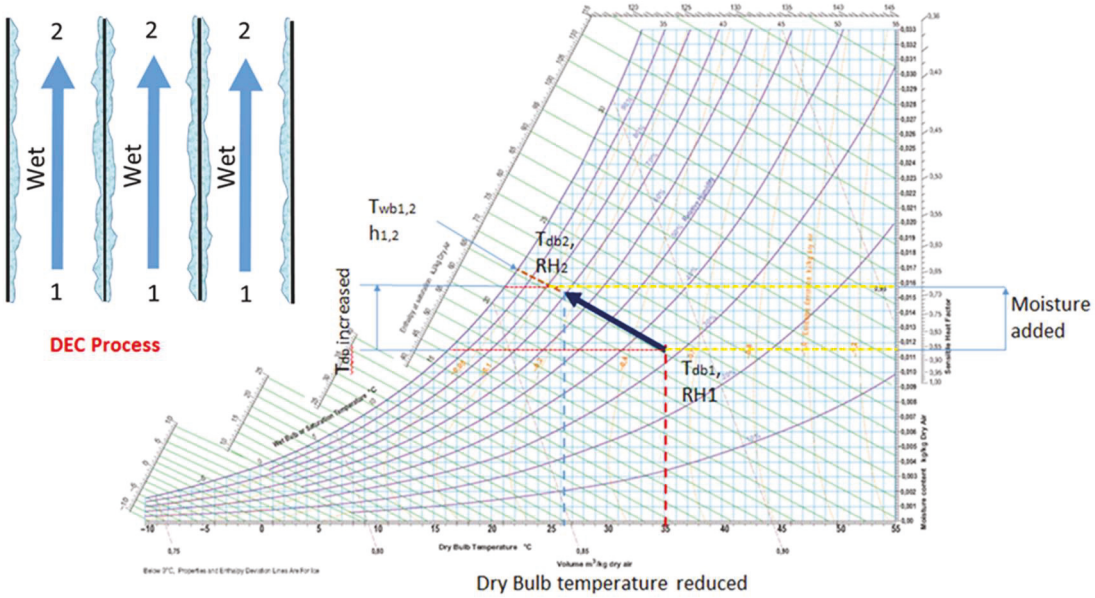

Figure 2.3. Working diagram and thermal process on the psychrometric chart of direct evaporative cooling

The water (at inlet air wet-bulb temperature) is sprayed on an evaporative pad. The evaporative membrane pad is thoroughly wet by water absorption. As the warm air passing through the evaporative pad channels, it has rejected the sensible heat to the cold water that absorbs it as latent heat. Consequently, water vapour is produced due to the increase in the latent heat and released adding moisture to the air stream and increasing its humidity. The water absorption of the sensible heat reduces the product air temperature, but adding the latent heat in the form of water vapour will result in almost no change in enthalpy value (ASHRAE 2012; Pandelidis 2016; Porumb et al. 2016).

At hot, humid inlet air the evaporation process could continue up to the saturation point, thus adding more moisture to the product air, results supersaturated supply air with high moisture contents and higher dew point temperature (High latent heat), and this is the main disadvantage of the direct evaporative cooling system.

As the working principle of the direct evaporative cooling system is the latent heat generated from evaporation of water to lower the temperature of the hot dry air, and

because the energy remains the same (adiabatic process) the moisture is added to the product air creating a cool, moist air, thus adding moisture to the conditioned space. Accordingly, the direct evaporative cooling system application is limited to hot arid weathers only, where both cooling and humidification are required (ASHRAE 2012; Pandelidis 2016).

2.4.2. Indirect evaporative cooling

The principles of the indirect evaporative cooling system sensible cooling overcome the moisture adding to the supply air. Thus, the system is more attractive and applicable rather than the direct evaporative systems in terms of comfort. Regardless of the type of heat exchanger (Counter-flow, Cross-flow and Generative) used in the indirect evaporative cooling system, the thermodynamics principle of heat transfer would remain the same as shown in **Figure 2.4**.

As shown in **Figure 2.4**, the heat exchanger is divided into a contiguous pair of parallel channels. A single pair consists of a dry channel (Air only) and a wet channel (air and water layer over the walls of the channel). As shown in Figure 2.3, the product air (also known and the primary air) is passing through the dry channels' over the heat exchanger plate surface from point 1, while the working air (also called the secondary air) is passing through the wet channels from point 3. As in the direct evaporative cooling system, the working air and the water temperatures difference would cause the water evaporation through conjunction heat transfer, releasing the latent water heat to the working air, thus the air temperature and water temperature drop. On the other side of the plate, the cold plate surface (cooled by conduction with water over wet channel wall) absorbs the heat from the product air (by convection) and producing a cold air without adding moisture.

The product air temperature will reach the initial wet-bulb temperature of the working air in the ideal process (Point 2). At the exit, the secondary working air temperature to be in one of the following cases:

1- Lower than its initial wet bulb temperature in case of no saturation (Point 4a), at a constant wet-bulb temperature as the initial value when the saturation level reached the outlet (Point 4b) or,

2- Higher than the initial wet bulb temperature if the saturation occurs before the outlet (Point c).

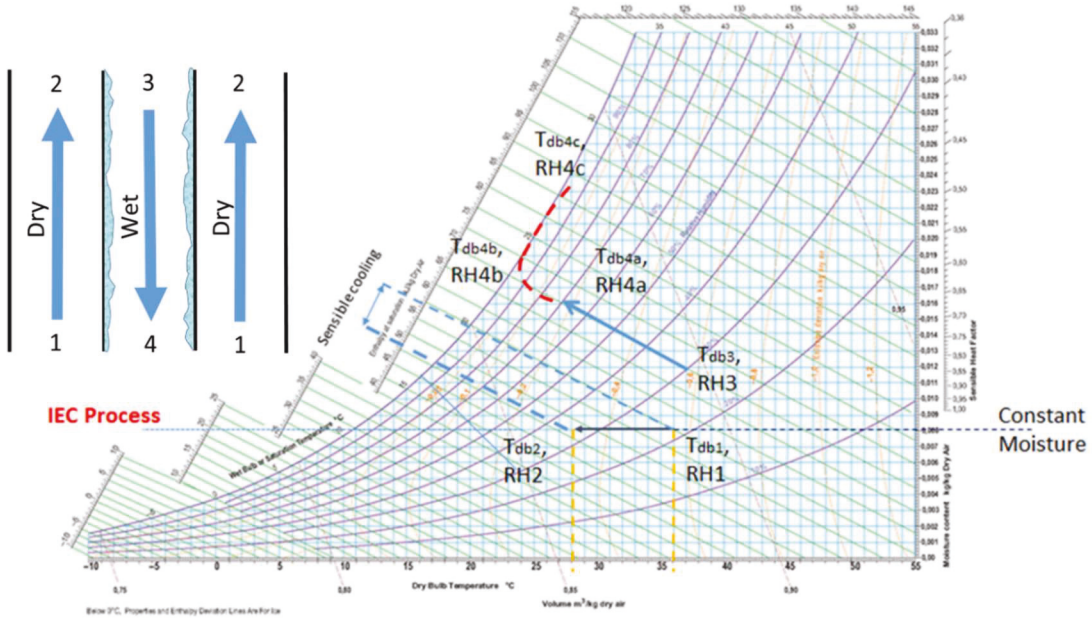

Figure 2.4. Working diagram and thermal process on the psychrometric chart of indirect evaporative cooling

However, as the other cooling process, the indirect evaporative cooling system process is not ideal. ASHRAE handbook (ASHRAE 2012) suggested that the wet-bulb effectiveness achieved for the typical indirect evaporative cooling system is in the range of 50 to 60%. That means that the supplied air temperature would be higher than the wet-bulb temperature of the inlet working air but lower than the dry-bulb temperature of the inlet product air, which is usually too high to cool the conditioned room space if the outside

air used in both two-stream (product and working air). To overcome this problem, the indirect evaporative cooling system is applied as an energy recovery system with indirect evaporative cooling, utilise the building return air as a working air (Al-Zubaydi & Hong 2019; Anisimov & Pandelidis 2015; Chen, Yang & Luo 2016a; Cianfrini et al. 2014; Costelloe & Finn 2003; Cui, Chua, Islam, et al. 2014; Dartnall 2015; Gómez, González & Martínez 2012).

However, the IEC (Indirect evaporative cooling systems) still experience similar restrictions of the direct evaporative cooling system. Thus, a lower wet bulb temperature is required for comfort air conditioning, and that is usually available in a dry climate (Al-Zubaydi & Hong 2019; Bruno & Liu 2009).

2.4.3. The regenerative indirect evaporative cooling

In the indirect evaporative cooling system, the secondary (working) air inlet temperature is the key for higher system effectiveness, i.e. lower secondary air temperature results in a lower supplied air temperature. The regenerative indirect evaporative cooling system utilizes a fraction of the supplied product air as the secondary inlet air; thus, lower temperature air will be the working air as described in **Figure 2.5**. In this case the secondary air is precooled in the dry channel to a lower wet bulb temperature than that of the secondary air in case of the indirect evaporative cooling system (IEC); consequently, the supply product air will be cooled further low (Moshari & Heidarinejad 2015).

The R-IEC process cycle is described in **Figure 2.5**. The Primary air (usually an outside air) enters the dry channel at the specified temperature and moisture content, the heat is transferred to the wet channel through the plate surface along the flow path resulting lower air temperature at the channel exit (Point 2). At the dry channel outlet, the air is divided into two streams, the significant fraction (usually 2/3) as a supplied air, while the

other 1/3 is introduced into the wet channel as the secondary air. In the wet channel, the same process described in the case of the indirect evaporative cooling system undergoes but with colder secondary air (Duan et al. 2016; Hasan 2012; Kabeel & Abdelgaied 2016).

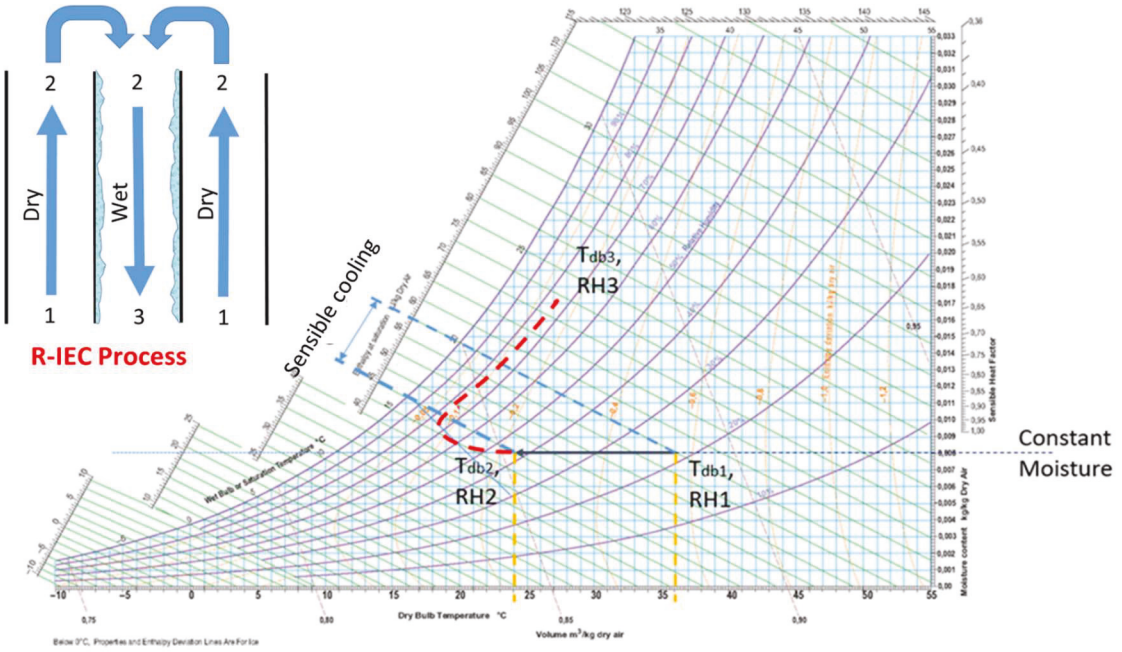

Figure 2.5. Working diagram and thermal process on the psychrometric chart of regenerative indirect evaporative cooling

As shown in the working process in **Figure 2.5**, the product air supply dry bulb temperature is below its value in the indirect evaporative cooling system. Further cooling takes the temperature of the primary air towards the wet-bulb temperature of the secondary air at inlet condition (Point 2). Accordingly, this type of indirect evaporative cooling system is called "**Sub wet-bulb IEC**" where dew-point effectiveness can reach up to 50% (Duan et al. 2016) .

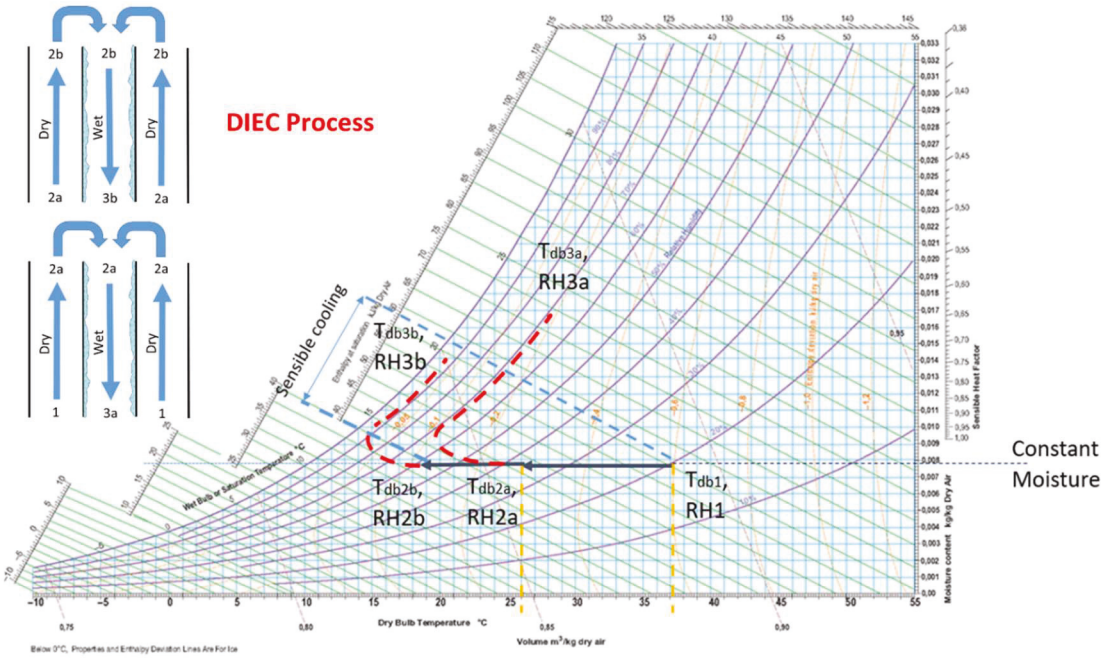

Figure 2.6. Working diagram and thermal process on the psychrometric chart of Double-Stage regenerative indirect evaporative cooling

The double stage regenerative indirect evaporative cooling arrangement is capable of reaching the dew point temperature of the primary air at the inlet condition. The double stage R-IEC cycle is described in **Figure 2.6**. As shown in **Figure 2.6**, the primary air exit from the first R-IEC from point 2a is fed to a second R-IEC system as primary inlet air. The second stage heat exchanger repeats the cooling process with cold air where its temperature is near the wet-bulb temperature of the original supplied air at point 1; thus the final product air at point 2b tends to be too close to or exactly at the dew point temperature of the original primary air supplied at point 1.

The main disadvantage of the R-IEC system is the low flow rate of both primary and secondary air when compared to IEC. This flow reduction increases as the number of stages increases. The second disadvantage is that the system cannot be applied as an energy recovery IEC, mainly because of the single inlet port design. However, the

advantage of cooling the air to near the wet-bulb temperature in the single-stage R-IEC and dew point temperature in the multi-stage arrangement is considerable.

2.4.4. Maisotsenko indirect evaporative cooling system

The Maisotsenko indirect evaporative cooling system is an advanced regenerative indirect evaporative cooling cycle with the capability to cool the product air to near the dew point temperature with a single-stage heat exchanger (Maisotsenko et al. 2004).

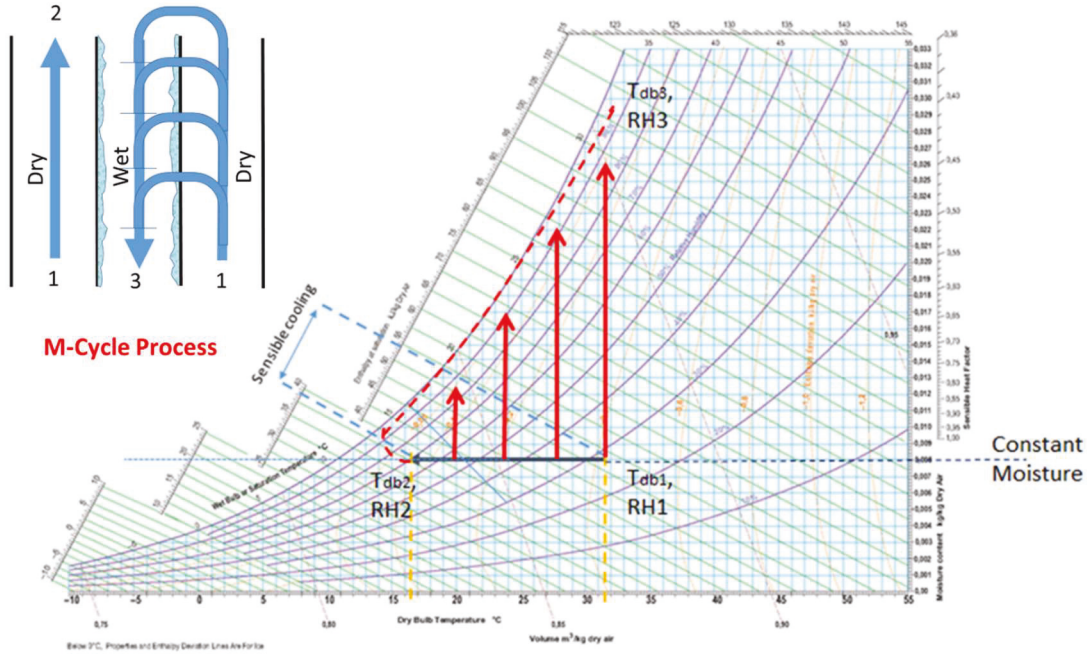

Figure 2.7. Working diagram and thermal process on the psychrometric chart of M-Cycle regenerative indirect evaporative cooling

The heat exchanger consists of two types of dry channels. The first type of dry channel is similar to the dry channel in a classic IEC system were 100% of the inlet primary air is supplied as a product primary air (No regeneration). The second type of dry channel has multiple air passages to the wet channel forming what can be described as an air bleeding system. The bled drawback air performing the regenerating process at multiple stages (levels) within the same heat exchanger plate where 100% of this air of fed to the second

dry channel is used in the wet channel (Anisimov et al. 2014; Anisimov, Pandelidis & Maisotsenko 2016).

As represented in **Figure 2.7**, the primary air enters the first type of dry channel at point 1, due to the sensible cooling through the plate with the air in the wet channel. The product air is exit at point 2 after cooled down to near the dew point temperature of the air enters at point 1 conditions (Maisotsenko et al. 2004, 2007; Pandelidis & Anisimov 2016; Zhan, Zhao, et al. 2011). The secondary air, in the wet channels, achieve a lower temperature (as low as the dew point temperature of the primary air). The higher performance is related to the multi-stage air bleeding arrangement that supply a pre-cooled air from the dry channel to the wet channel. The secondary air moisture contents increasing gradually at multiple levels until it is exit the heat exchanger at point 3.

The complex construction of the heat exchanger is the main disadvantage of M-Cycle IEC. However, the main advantage is the system capacity to cool the air to near dew point temperature with a single-stage regenerative cycle. Nevertheless, with the single inlet air stream, the system can not be used as an energy recovery system.

2.5. Indirect evaporative cooling for energy recovery – Literature Review

Evaporative cooling systems have been the subject of renewed interest in recent years. Direct evaporative cooling systems perform well in dry climates but are not suitable in areas with high humidity. Indirect evaporative cooling (IEC) systems have attracted more attention as they add no moisture to the product air and are suitable in both dry and humid environments (Chen, Yang & Luo 2016a). The potential for indirect evaporative cooling systems is vast – in addition to potential energy savings, IEC has less harmful effects on the environment than cooling systems with refrigerants only.

IEC can be applied as a standalone unit in moderate weather with low to medium humidity and hot arid weather, or as a pre-cooling system in conjunction with the conventional system, and as an energy recovery pre-cooling system recirculating the exhaust air. In all the above systems, the application of IEC as a pre-cooler may result in energy saving by up to 13% for building air conditioning (Jaber & Ezzat 2017).

The working principles of sensible indirect evaporative cooling described earlier are simple; with a set of parallel channels, pairs classified as wet and dry channels to form a heat exchanger. The latent heat released by evaporating water is transferred to the secondary air stream while the sensible heat is rejected from the primary airflow through the plate without adding moisture. However, the IEC performance is evaluated by the wet-bulb temperature efficiency (ANSI/ASHRAE 2015). Consequently, the system is limited to the wet-bulb temperature of the secondary air. Hence, when the humidity of the secondary air is high (high wet-bulb temperature), the IEC efficiency will be low, and the system may not be able to sufficiently cover the cooling load for buildings (Duan et al. 2017). The wet-bulb problem is moderate when the building exhaust air is recirculated in an IEC for energy recovery.

Since the early 1970s, many researchers focused on the analysis of IEC technology. The earlier studies were based on the experimental testing of full-scale operating IEC systems, i.e. Donald Pescod's works between 1968-1980 (Pescod 1968; Pescod 1979; Pescod & Prudhoe 1980). However, by the late 1970s and with the availability of computers for research work, many researchers adopted mathematical modelling as a tool to analyse the IEC system performance.

One of the earliest analytical work was presented by MacLaine-cross and Banks (Maclaine-cross & Banks 1981). MacLaine-cross and Banks presented a one-dimensional mathematical model to analyse the performance of a wet surface heat exchanger in an

IEC system. They use heat transfer and mass calculations for the entire area of the plate based on the average temperature and humidity ratio between the inlet and the outlet streams. The model assumed a unity Lewis number and 100% plate face wettability; as a result, the simulation results were around 20% higher than the experimental data reported by Pescod (Pescod 1979). To adjust the variation between the theoretical and experimental results, a model developed by Stoitchkov and Dimiltrov (Stoitchkov & Dimitrov 1998) introduced the effectiveness correction method determined according to the method presented by Maclaine-cross and Banks. They designed a new model where a layer of water flowing in vertical corresponds to the position of the heat exchanger. The method of Maclaine-cross and Banks was perfected by an approach for determining the average temperature of the water surface and the adaptation of a calculation equation of total heat compared to sensible heat in the light barometric pressure. The performances of the plates exchangers evaluated according to this calculation method agree with the solutions obtained by the finite difference method. The gap between the modelling results and the published experimental data is in the order of 2-4% (Stoitchkov & Dimitrov 1998).

Alonso et al. (Alonso et al. 1998) developed and simplified a heat transfer model for analysing the thermal performance of the cross-flow IEC including prediction of the energy consumption of the system, design system, configuration and optimization of the geometric dimensions of the system. This model has an equivalent water temperature that was used in the calculation of heat transfer between the primary and secondary air. In comparison between the experimental output and previous works, too small inconsistency in the primary air temperature was found (0.54 °C) (Erens & Dreyer 1993).

Chengqin & Hongxing (Chengqin & Hongxing 2006) developed an analytical model capable of simulating the improved heat transfer process and mass in the counter-flow

parallel IEC heat exchanger in various operating conditions. Unlike one-dimensional models mentioned above, this model has solved the coupled equations of heat transfer and mass taking into consideration of the variation of Lewis number, the wet surface condition, the effects of evaporation and flow, the temperature and the enthalpy of the water spray. In comparison to the one-dimensional model, the improved model results were slightly different in terms of the primary air temperature, the secondary air outlet temperature and absolute humidity.

Hettiarachchi et al. (Hettiarachchi, Golubovic & Worek 2007) have investigated the effect of longitudinal heat transfer by conduction in a compact plate heat exchanger with cross-flow using the Number of Transfer Units (NTU) method. Heat transfer by convection in the wet and dry channels and mass transfer in the wet channels were examined employing a system of equations; they have been solved using a numerical method iteratively. Jardi and Riffat (Jradi & Riffat 2014) presented a detailed two-dimensional numerical model to analyse the performance of cross-flow heat exchanger. The IEHX (Indirect evaporative cooler heat exchanger) dry channel length set to 500 mm and 5 mm gap to achieve 112% wet-bulb effectiveness and 78% dew-point effectiveness. Based on the simulation results, as the supply to intake air ratio increases, the supply air temperature increases from 19.2 C to 24.8 C where the supply air relative humidity decreases from 77% to 54%.

2.6. Most notable recent research

As mentioned earlier, the interest in the IEC system is continuously increasing since the 2000s. The number of researches and publications jumped to several hundred since 2000 (from tens between 1970's-1999), shows that the technology is a promising solution for the increasing demand for air-cooling. This research question of this study was based on a comprehensive literature review of previous studies. The analysis of the literature to

find the research gap classified the references based on the IEC type, the heat exchanger arrangement, the water distribution system and the research methodology.

The IEC researches evolution was summarised in many previous works (Anisimov & Pandelidis 2015; Duan et al. 2012; Pandelidis, Anisimov & Worek 2015; Porumb et al. 2016; Sadighi Dizaji, Hu & Chen 2018). The most recent IEC researches, mainly since 2015, are presented in Error! Reference source not found..

The 1-Dimensional numerical model simulation of a counter flow IEHX was presented by Pendelidies, Anisimov and Worek (Pandelidis, Anisimov & Worek 2015). The performance of an IEC with horizontal parallel plates heat exchanger core was numerically compared in four different scenarios: IEC, ERV-IEC, RIEC and suggested IEC with Counter-flow exchanger operating on exhaust airflow (wet channels) and ambient air (dry channels). The results shows that the regenerative unit is able to achieve the lowest outlet temperatures between other arrangements; however, it is characterized with the lowest cooling capacity. The counter-flow unit was found to be able to achieve similar efficiency when it is operating as a heat recovery unit in supply-exhaust system with cooling coil. The evaporative cooling process runs with higher effectiveness due to the low temperature of the exhaust airflow.

A cross-flow IEHX performance was investigated by Kim, Jeong and Jeong (Kim, Jeong & Jeong 2015). In addition, the authors presented a mathematical analysis for an IEC unit performance. The suggested IEC unit was experimentally tested to validate the numerical model. The results shows that 75% cooling effectiveness and 59% heat reclaim effectiveness could be achieved under wet and dry operating conditions. The proposed model show a potential 26% annual operational energy saving when applied as a fresh air pre-cooling system in conjunction with a conventional VAV unit.

Kabeel and Abdelgaied (Kabeel & Abdelgaied 2016) modified Riangvilaikul and Kumar (Riangvilaikul & Kumar 2010) RIEC unit, suggesting the various arrangements for the internal baffles in the dry channel. A mathematical MATLAB code was presented to optimise the baffles arrangement. It was found that the increasing of the baffles number resulted in the RIEC performance improvements in terms on wet bulb efficiency and cooling capacity. However, the pressure drop data were not reported.

Chen, Yang and Luo (Chen, Yang & Luo 2016a) studied the effect of the primary air moisture content on the IEC unit performance, i.e. the effect of the possible condensation incidence in the dry channel. The experimental work investigated the cross-flow IEC unit performance under two modes: 1- Low humidity and 2- High humidity. The unit was subjected to a variable test parameters include the primary air temperature and velocity, secondary air temperature and velocity. The results shows the capacity of ERV/IEC system to dehumidify the high humidity primary air when operating at lower secondary air temperatures. The humidity ratio found to have a negative impact on the IEC unit. The effect of the primary air intake moisture content was confirmed by Lin et al. (Lin et al. 2017a). To investigate the effect of the supply air humidity effect on the IEC system performance, Lin et al. built a regenerative IEC (RIEC) prototype consisted of a cross-flow horizontal plate heat exchanger, fans and water supply system. The prototype subjected to experimental investigation and numerical simulation under variable operating conditions. The authors suggested that a pre-dehumidification is required to minimise the effect of the high humidity on that reduce the IEC efficiency.

Analytical and experimental research presented by (Zheng et al. 2019) to assess the performance of a cross-flow IEC with consideration of condensation in the dry channels. The 2-D model validated against the experimental work results. The results confirms the negative effect of the water vapour condensation on the IEC wet bulb effectiveness (30%

reduction); however, the condensation increased the overall heat transfer rate in the system (mainly due to the increase in the latent heat in the dry channels). The water consumption rate was increased under the condensation state because of the increase in the total heat transfer. The visualisation of the operating IEC heat exchanger reveals that the condensation mainly occurred in the cold ports, i.e. the entrance of the secondary air and the exit of the primary air.

The economic study by Duan et al. (Duan et al. 2017) investigated the potential energy saving of applying the RIEC as a cooling system in Chinese weather. The RIEC with counter-flow configuration has been experimentally tested under variable primary air conditions. The empirical outcomes and the relationship between the testing parameters have been used to calculate the IEC cooling loads and energy saving based on the hourly metrological data for a selected Chinese cities. The proposed model achieved 53-59% energy reduction saving in China north – western provinces with providing 93-100% of the total cooling load. The saving rates are lower in higher humid zones (Southeast and southwest regions) with 13-28% power consumption reduction and 53-72% cooling load coverage. However, the results shows that the IEC system is promising in terms of energy saving in addition to the capacity of supplying a 100% cooled fresh air when required.

In order to achieve an optimisation of the RIEC system benefits of energy saving and indoor air quality, Chen, Yan and Yang (Chen, Yan & Yang 2018) proposed and advanced H-L or High-Low control system for the IEC unit. In comparison analysis between the H-L control system in to the traditional On-Off control system, A 1-D mathematical model was built to simulate the annual performance of the RIEC unit operates using the two controlling schemes. The H-L controller shows a superior improvement in terms of thermal comfort, indoor air quality and energy saving, mainly in the transition season were the control is mostly required.

An experimental and numerical analysis with 1-D and 3-D models was presented by Pakari and Ghani (Pakari & Ghani 2019). The 1-D and 3-D models where developed and validated to simulate the performance of RIEC. Pakari and Ghani compared between the results obtained from the 1-D and 3-D models shows that the 3-D model can be more predictable to the experimental data; still, the 1-D model is more advantageous based on the computational time and the hardware requirements.

Numerical analysis with ε-NTU model was presented by (Pandelidis et al. 2019) to compare performance of the IEC unit in cross-flow and counter-flow IEHX arrangements with consideration of condensation in the dry channels. The study presented a comprehensive mathematical description of the IEC system thermal performance. In general, due to the higher effective mass and heat flux over the heat exchanger plates, the counter-flow IEC performance found to be better than that of the cross-flow IEC. However, the thermal and energy performance of both IEHX configurations shown to be considerably affect by the same rate in case of water vapour condensation in the dry channel.

Table 2.1. IEC references based on configuration, study method, airflow arrangement and water distribution

Reference	Methodology	Flow type	Water distribution	η_{wb} (%)
(Kim, Jeong & Jeong 2015)	Experimental/Numerical model simulation	Cross-flow	Vertical-downward Parallel flow to the secondary air	75%
(Anisimov, Pandelidis & Jedlikowski 2015)	Experimental/Simulation	Cross-flow	45° - Downward Parallel flow	89%
(Sohani, Sayyaadi & Hoseinpoori 2016)	Numerical model simulation	Cross-flow	Theoretical	-
(Kabeel & Abdelgaied 2016)	Experimental/ Numerical model simulation	Counter-flow, Quasi-flow	Vertical-downward in counter-flow with secondary air	70%
(Duan et al. 2016)	Experimental	Counter-flow	Vertical-downward Counter flow	55%-106%
(De Antonellis et al. 2016)	Experimental	Cross-flow	Vertical-downward in Parallel and counter- flow	80%
(Chen, Yang & Luo 2016a)	Experimental	Cross-flow	Vertical-downward Counter- flow	65%
(Chen, Yang & Luo 2016b)	Numerical model simulation	Counter-flow	Vertical-downward Counter- flow	62%
(Xu et al. 2017)	Experimental	Counter-flow	Vertical-downward counter- flow against secondary air	114%

Table 2.2. IEC references based on configuration, study method, airflow arrangement and water distribution – cont.

Reference	Methodology	Flow type	Water distribution	η_{wb} (%)
(Lin et al. 2017a)	Experimental/Numerical model simulation	Cross-flow	Horizontal mist – Parallel flow	130%
(Kim et al. 2017)	Experimental	Cross-flow	45° - Downward in Parallel flow and Vertical downward (Parallel / Counter- flow), Paper wicked wall	70%
(Chen, Yang & Luo 2017)	Numerical analysis	Counter-flow	Vertical downward (Counter- flow)	60%
(De Antonellis et al. 2017)	Numerical model simulation	Counter-flow	45° - Downward Parallel flow	64%
(Duan et al. 2017; Huang et al. 2017)	Experimental/ Numerical model simulation	Counter-flow	Vertical – Downward counter to the secondary air stream	82%
(Nie et al. 2018)	Experimental	Quasi-counter flow	Water vapour flash	71%
(Lin et al. 2018; Meng et al. 2018)	Experimental	Counter-flow	Vertical Downward in Cross-flow against secondary air & Horizontal in parallel-flow to the secondary air	144%
(Zheng et al. 2019)	Experimental/Numerical analysis with the 2-D model	Cross-flow	Vertical downward against the secondary airstream	83%
(Pakari & Ghani 2019)	Experimental/Numerical analysis with 1-D and 3-D models.	Counter-flow	Vertical in cross-flow against the secondary airstream	125%

2.7. Indirect evaporative cooling literature summary

Plate surface wettability is the fundamental factor affecting the IEC system performance (Chen, Yang & Luo 2016b). Achieving a fully wet surface is practically hard due to the water surface tension, resulting in a reduction in evaporation surface area (Chengqin & Hongxing 2006; Xu et al. 2016). Surface treatment, including applying a wick material layer over the plates, may increase the wet area and improve the system performance (Xu et al. 2016). However, their research shows that the wick material built up on the heat exchanger plate surface and turned into a growth field for harmful microorganisms such as Legionnaires disease.

Airflow arrangement, surface geometry and the plate material in a heat exchanger can play a dynamic role in the surface wettability and the water film uniformity. Cross-flow heat exchanger is the most common arrangement used in IEC (De Antonellis et al. 2016; Hasan 2012; Heidarinejad et al. 2009; Maclaine-cross & Banks 1981; Pescod 1979). In IEC with cross-flow heat exchangers, the water is vertically sprayed at the top of the heat exchanger. The sprayed water, in large droplet sizes, flows downward in counter or parallel to the airflow direction. With its simplified geometry, cross-flow heat exchangers in a vertical position usually have low wettability. Advanced IEC systems with regenerative cross-flow or counter-flow heat exchanger (e.g. M-cycle) optimised the performance to a sub-dewpoint temperature (Duan et al. 2017; Lin et al. 2016; Mahmood et al. 2016; Sohani, Sayyaadi & Hoseinpoori 2016). However, in the regenerative IEC with one inlet air stream sub-divided into primary and secondary air streams, accordingly, the choice is selecting either the fresh air or building return air as the working/supply air is the main limitation (Bolotin, Vager & Vasilijev 2015).

In IEC systems wetting the wet channel, walls had a substantial influence on cooling efficiency (Duan et al. 2012). Early studies pointed out the significance of the surface wettability on the IEC performance (Guo & Zhao 1998; Maclaine-cross & Banks 1981; Wang & Reid 1996). Water distribution methods investigated by Duan et al (Duan et al. 2012) presented the necessity to develop new methods in order to achieve higher efficiency by increasing the wettability of plate surfaces and achieving uniform water flow distribution in the wet channels.

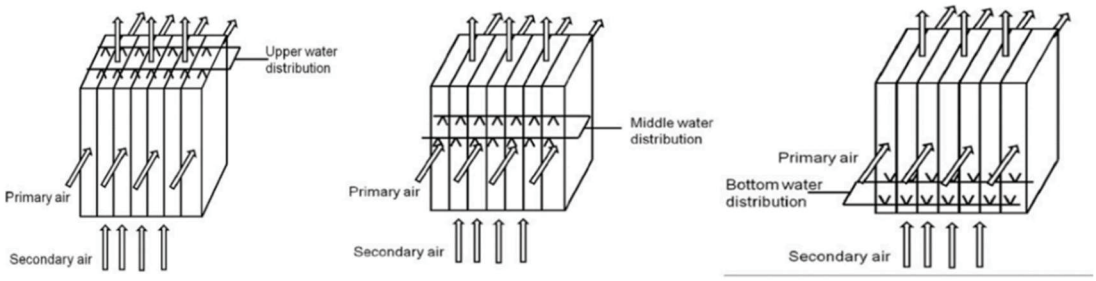

Figure 2.8. Three water distribution modes used in IEC by Zhou et al (Zhou, Huang & Di 2003)

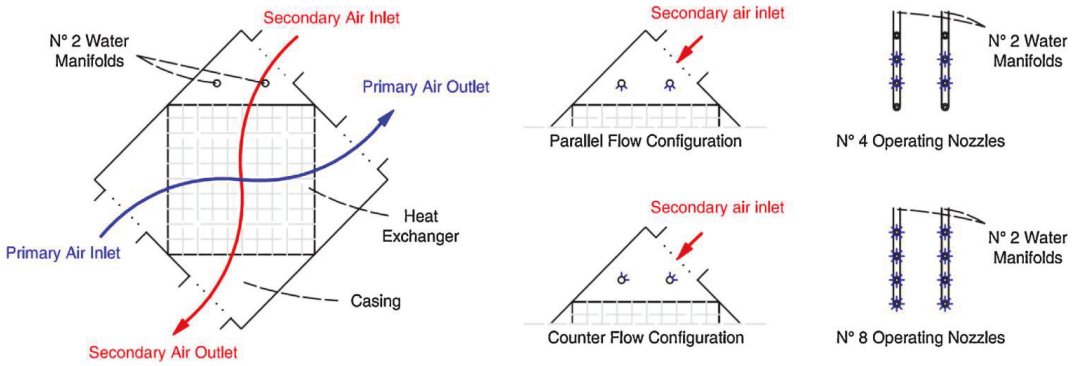

Figure 2.9. The different configurations of the investigated indirect evaporative cooling system by De Antonellis et al (De Antonellis et al. 2016)

The arrangement of water spray is the key in the IEC system. Zhou et al (Zhou, Huang & Di 2003) carried out an experimental study on the effect of the water spraying effect on the IEC heat and mass transfer. The three experimental water spraying arrangements tested by Zhou are shown in **Figure 2.8**. The results show that the middle and lower water

spraying arrangements resulted in an improvement in the IEC performance over the top water spraying mode. The middle spraying mode provided better water distribution with the possibility of increasing the channel gap and reduce the secondary air velocity. De Antonellis et. al. (De Antonellis et al. 2016) investigated the effect of water nozzle orientation at the heat exchanger entrance in two arrangements as shown in **Figure 2.9**: (a) parallel flow and (b) counter flow to the air stream direction, respectively. Their empirical results showed that the water mist spraying opposite the secondary airflow direction resulted in better system performance in terms of wet-bulb efficiency. It is common to spray the water vertically downward either in parallel with or opposite to the airflow, or in a fine water mist in the horizontal plates arrangement (Porumb et al. 2016).

Five different water nozzle – airflows configurations were experimentally tested by De Antonellis, Joppolo & Liberati (De Antonellis, Joppolo & Liberati 2019) to investigate the effect of spray position and airflows direction effect on the IEC system overall performance and to minimise the water consumption rate. The water spray configuration results are compatible with the author previous work (De Antonellis et al. 2016) where the water is to be spray at the top of the heat exchanger wet channels entrance against the secondary air airflow direction. This configuration increased the IEC wet bulb effectiveness in both vertical and horizontal heat exchanger orientation.

Water distribution system contributions to increase the IEC system efficiency could be achieved by designing an arrangement that can:

1- Provide equal water flow distribution for all wet channels.

2- Form a uniform water film over the plate surface.

3- Supply a constant water flow rate through the operation period.

4- Minimise maintenance required.

The broad literature review shows that there is a significant need for developing innovative water distribution systems. Extensive studies are required to investigate the influence of nozzle angles, sprayer mass flow rate, spray angles, and water temperature on the overall performance of IEC systems.

An experimental investigation can predict the accurate behaviour of the IEC performance under variable assessment parameters, i.e. the primary and secondary air temperatures, humidity, and velocity (Chen, Yang & Luo 2016a; De Antonellis et al. 2016; Duan et al. 2016; Gómez, González & Martínez 2012; Heidarinejad et al. 2009; Jradi & Riffat 2014; Lee & Lee 2013) . However, a mathematical model is essential to simulate the unit performance under a wide range of parameters variation; in addition, it is possible to vary the IEHX geometrical properties in order to optimise the IEC performance (Chang et al. 2017; Chen, Yang & Luo 2017; Delfani et al. 2010; Erens & Dreyer 1993; Kabeel & Abdelgaied 2016; Lin et al. 2017a).

Notwithstanding being a time consuming and required specialised computer hardware, 3-D modelling is more accurate and realistic than the 1-D and 2-D. The 3-D model can provide detailed information on the temperature, flow and moisture distribution in the IEHX considering the mass, energy, momentum and species transport conservation equations. In this work, a Computational Fluid Dynamics (CFD) simulation is used to simulate the 3-D model performance. The 3-D model originality in this work is to simulate a more realistic case with the assumption of the full wettability of the IEHX plate.

Chapter 3

Design and Construction of the Test Facility

3.1. Introduction

There was a necessity to design and fabricate a standardised innovate flexible test facility to achieve the specified research objectives sat for this study. The experimental IEC/ERV unit prototype was designed and constructed to accommodate the proposed internal spray system implanted heat exchanger. The main objective is the testing of heat recovery ventilation units utilise the building return air, the design principles of the experimental set-up were derived from two ASHRAE standards:

1- ANSI/AHRI Standard 1060- 2014 (AHRI 2014) for testing the performance,

2- Rating of Air-to-Air Exchangers for Energy Recovery Ventilation Equipment and ANSI/ASHRAE Standard 143-2015 (ANSI/ASHRAE 2015) for testing and rating the indirect evaporative coolers.

Both standards provide the guidelines to establish a reliable testing procedure to evaluate air-to-air heat and indirect evaporative cooling units serving as energy recovery systems.

The referenced ASHRAE standards also provide a comprehensive testing procedure and calculation method to evaluate the thermal performance of “Dry” and “Wet” energy and HRV systems with consideration of test facility air leakage, heat gain and losses through the casing, fans, pump and instrumentation power.

The heat exchanger with implanted sprayer tube was installed inside an experimental facility that designed operate as a typical air-handling unit with the ducts connected to form the selected open-loop concept adopted in this experiment. The experimental facility

size was designed to fit the available space in the lab. Instruments were selected to fulfil or exceed the test standard requirements.

The test facility subjected to an intensive experimental study to evaluate the performance of the IEC unit operates under different operating conditions to justify the research objectives 1, 2 and 3 of this study. This chapter presents the test facility and heat exchangers design, construction and commissioning. Afterwards, the experiments result of system performance and the effect of operation parameter effect on the cooling performance presented and discussed.

3.2. The Characteristics of the Experimental Facility

The test facility in ANSI/ASHRAE Standard 143-2015 (ANSI/ASHRAE 2015) with options for either open-loop or closed-loop operation is shown in Error! Reference source not found. schematic diagram. The size of the test facility must fit with the available lab space. As the study objective is to test the energy recovery units (HRV and IEC), the lab room temperature (22.5-24 °C) served as the assumed building exhausted air; thus, there was no need to make-up the secondary air conditions.

Based on the above considerations, the test facility was designed as:

1- An open-loop arrangement.

2- Heating, cooling and humidifying not required for the secondary air.

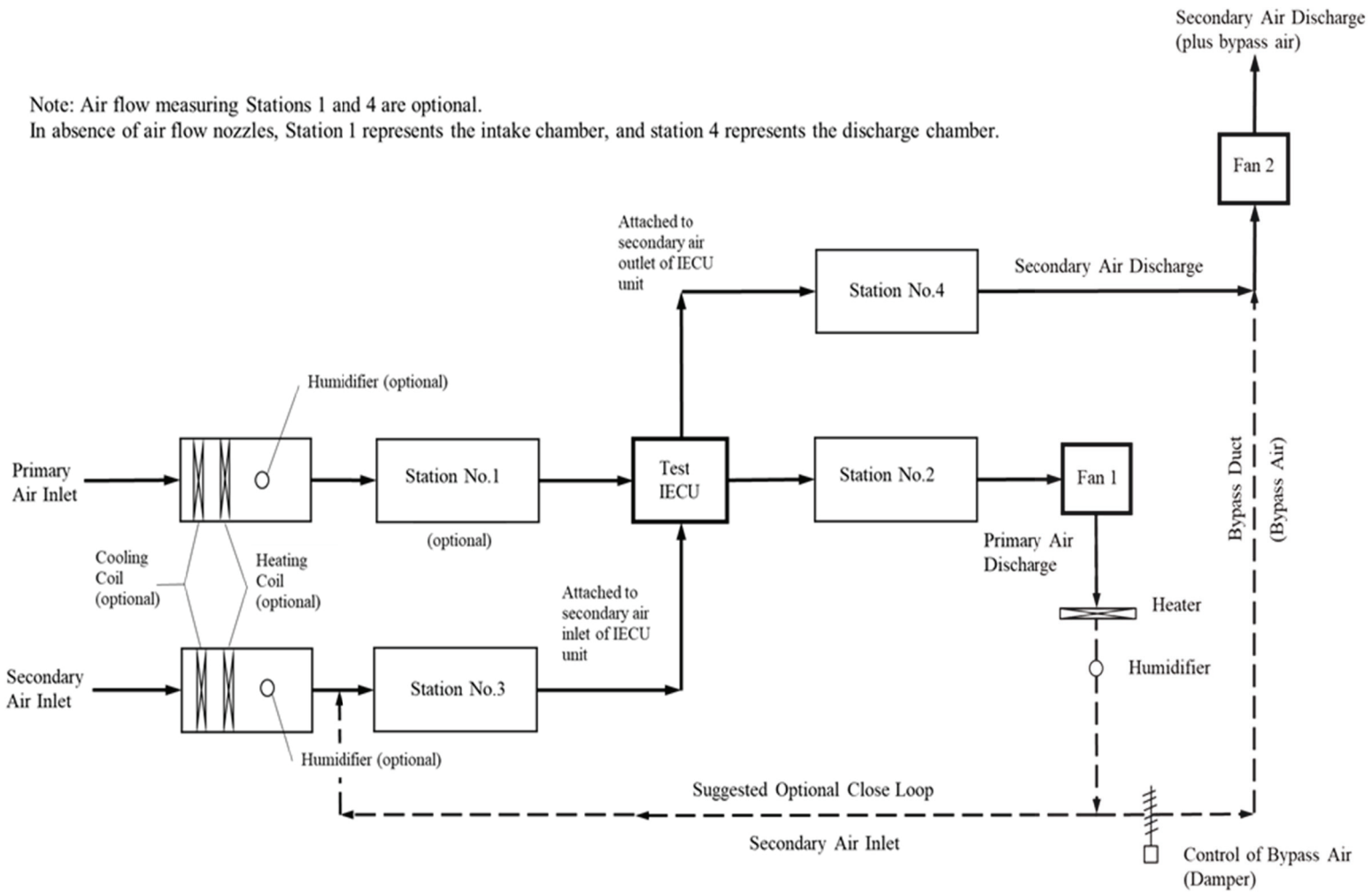

Figure 3.1. Schematic diagram of suggested open-loop-test equipment for indirect evaporative cooler (IEC) module (ANSI/ASHRAE 2015)

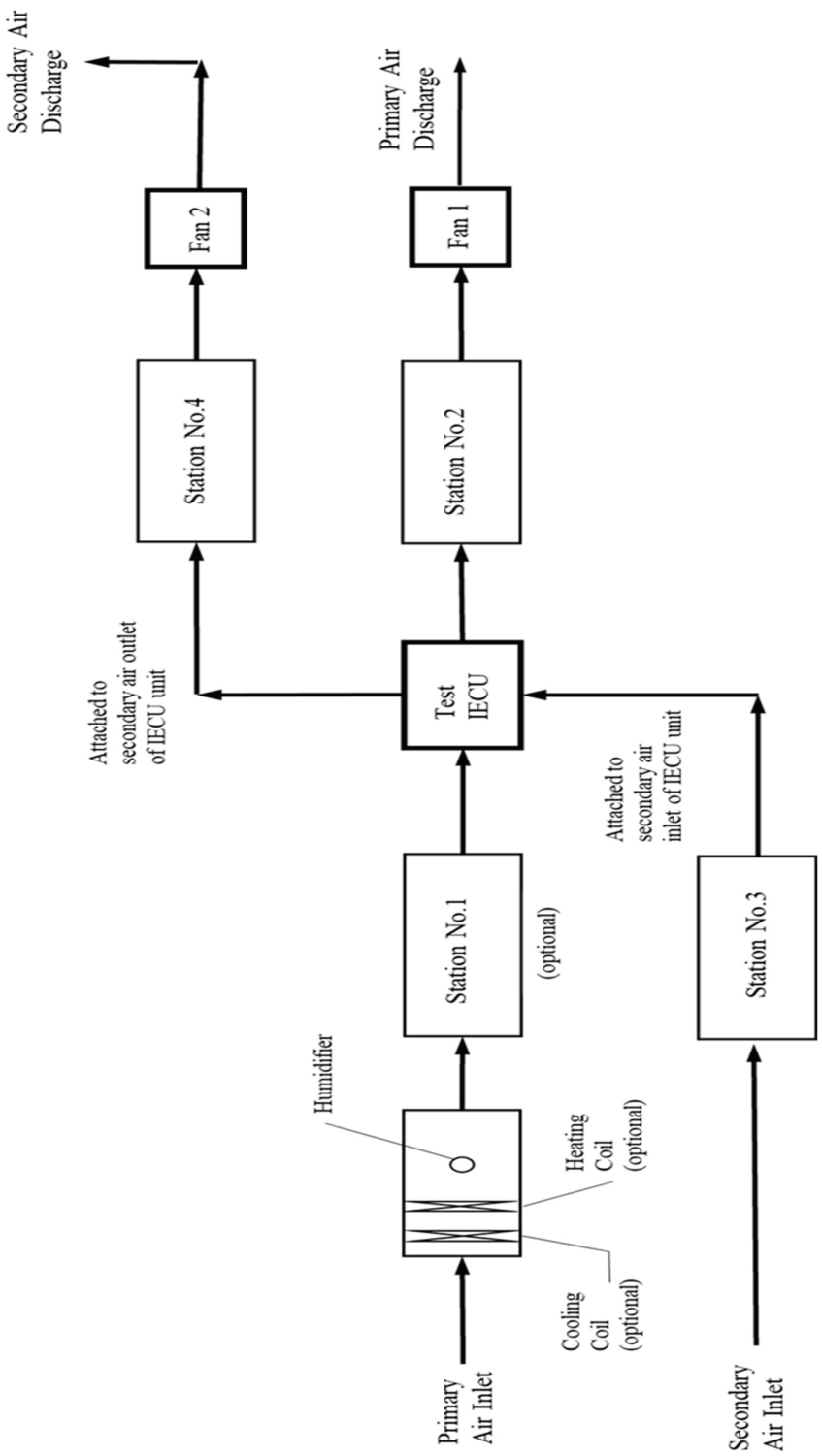

Figure 3.2. Schematic diagram of an open-loop-test facility for indirect evaporative cooler (IEC) module

Error! Reference source not found. shows the heat recovery test facility, which meets the ANSI/ASHRAE Standard 143-2015 and fulfils the present research requirements. The primary and secondary air was discharged to outside the building (or laboratory) to maintain the indoor zone conditions to be stable.

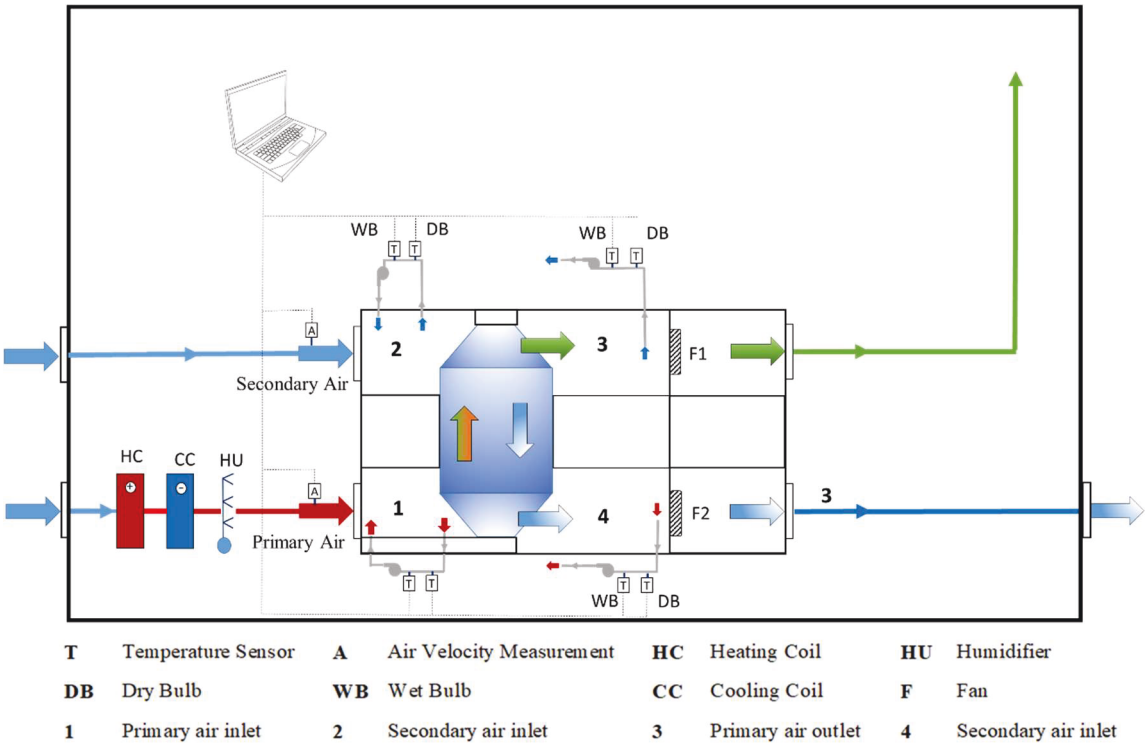

Figure 3.3. Scheme of the test rig for the HRV System

The schematics in **Figure 3.3** and **Figure 3.4** show that the heat exchanger was vertically positioned, mainly to let the water flows downward with gravity assist to cover the plate surface. The test rig is also able to accommodate different geometries of heat exchangers with simple modifications for future research. With the available space for a water sump, the experimental work on both dry HRV systems and IEC systems can be performed.

Measurement stations measure the air temperature, humidity and velocity. **Figure 3.3** and **Figure 3.4** show the locations of the measurement stations. The airflow velocities were measured using a pitot tubes manometers at the inlets ducts of the of air streams.

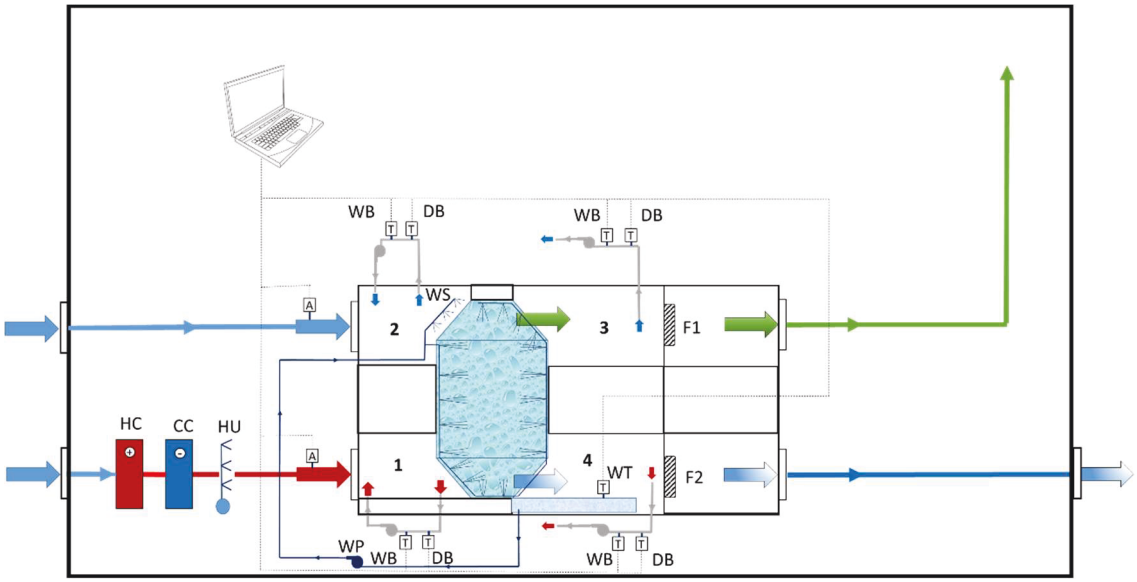

T	Temperature Sensor	**A**	Air Velocity Measurement	**WT**	Water Temperature	**HU**	Humidifier
DB	Dry Bulb	**WP**	Water Pump	**HC**	Heating Coil	**F**	Fan
WB	Wet Bulb	**WS**	Water Spray	**CC**	Cooling Coil		
1	Primary air inlet	**2**	Secondary air inlet	**3**	Primary air outlet	**4**	Secondary air inlet

Figure 3.4. Scheme of the test rig for the IEC unit

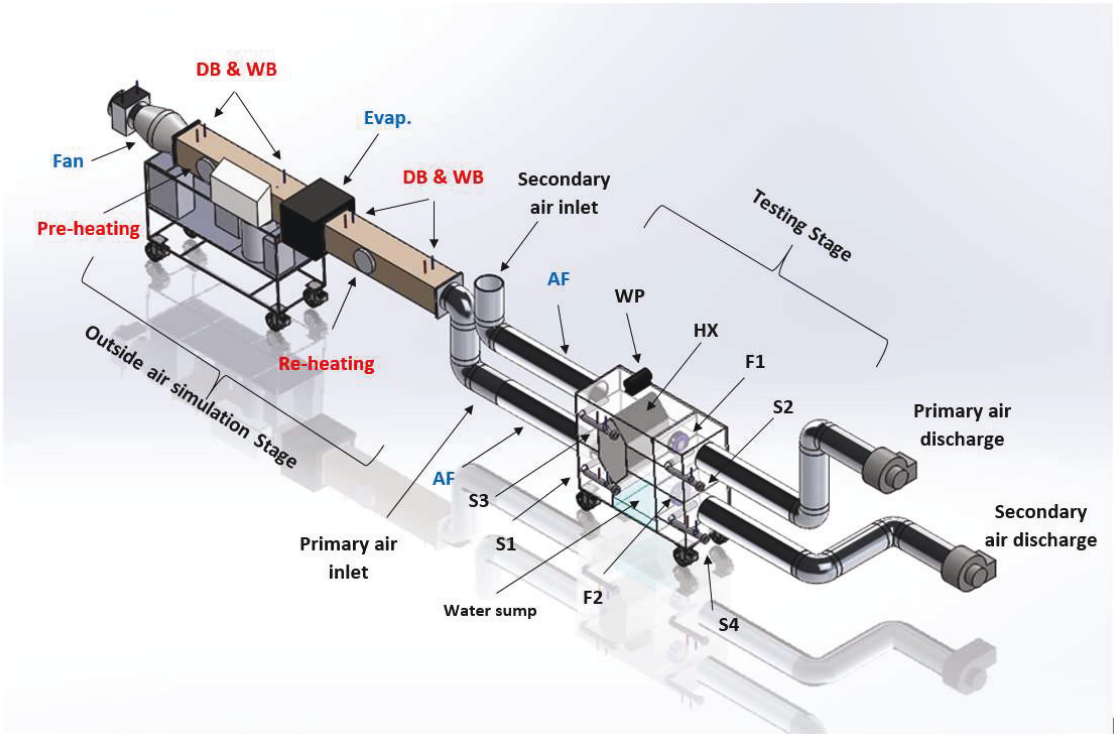

Figure 3.5. 3-D Layout of the Experimental facility

Figure 3.5 shows the 3-D view of the experimental facility. As shown in **Figure 3.5**, the open-loop test facility consists of two stages: the primary air-simulation stage and the IEC/ERV testing stage.

In the first stage, represented by the A660 laboratory HVAC test rig, the room temperature is conditioned to simulate outdoor air temperature and humidity ratio for average Sydney summers. The first stage outlet air is supplied to the second stage as the primary air inlet. On the other side, the air at room conditions is supplied as the secondary air of the IEC operation, to simulate the building exhaust air.

3.3. Experimental Facility Capacity

In addition to the mobility, the design criteria of the experimental facility considered the size the capacity of the primary air simulation unit (A660 Air Conditioning Laboratory Unit), the electrical power for fans and in-house manufacturing capacity.

The system was designed to cope with the range of the airflow. The maximum volumetric air flow rate was 445 m^3/hr based on maximum fan capacity. The average airflow required in the experiments is 316 m^3/hr. The minimum volumetric air flow rate was 140 m^3/hr. Experiments based on ANSI/AHRI Standard 1060 (AHRI 2014) require a minimum 12.0 °C temperature difference between the air streams across the heat exchangers plates. This requirement was met by using room air temperature at a constant 23 °C for the primary air inlet and hot air controlled to 35 °C entering the hot air loop side of the heat exchanger. The A660 air conditioning laboratory unit (P.A.Hilton 2018) was used to produce the primary air (Product air) at the inlet stage. The IEC/ERV system was subjected to summer conditions with test temperature ranged between 25 °C – 37 °C and relative humidity range of 35%-70%.

3.4. Construction of the Experimental Prototype

The IEC/ERV experimental facility was constructed in UTS laboratories. The construction of the facility components was based on the internal UTS manufacturing capacity. The fabrication procedure started after analysis of various design methodologies, including design for manufacturing (DFM), design for assembly (DFA) and design for environment (DFE). A detailed CAD model of each component was prepared with intensive analysis. Following the optimization and final decision making, component fabrication took place.

A- Casing

The air-handling unit (AHU) casing was made of a 10 mm clear Acrylic panels. The thickness provides good insulation to reduce the heat exchange with ambient air. All contact areas were sealed to prevent air leakage.

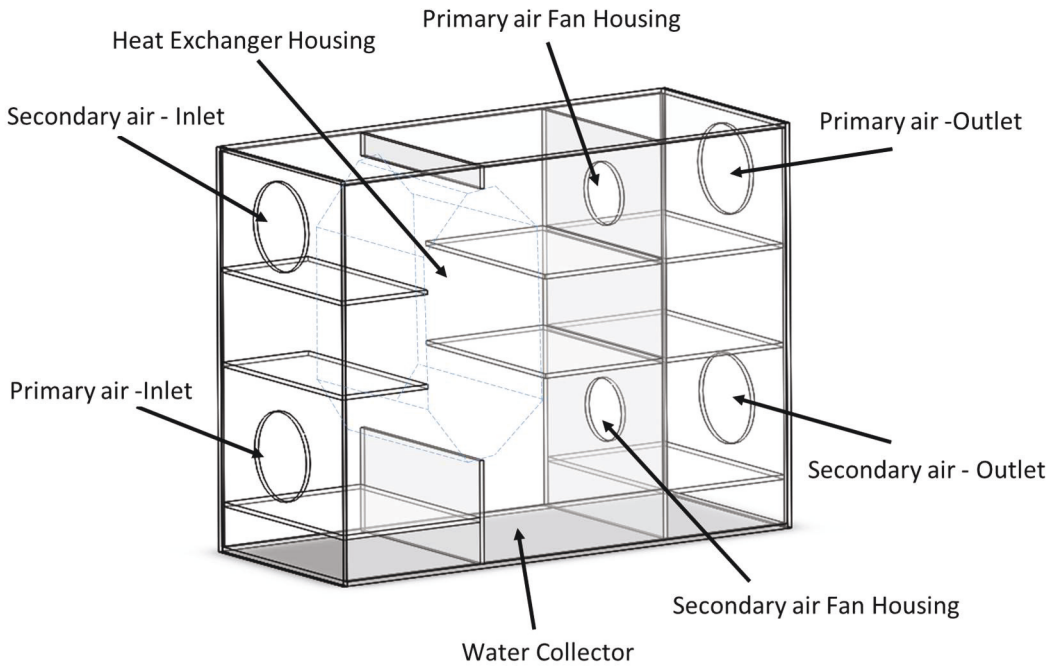

Figure 3.6. The CAD model of the AHU case

Figure 3.6 shows the schematic CAD model of the AHU. As shown in **Figure 3.6**, the unit was designed as a box with dimensions 900x500x1150mm for height, width and length, respectively. The interior consists of small rooms to provide a casing for the experimental heat exchanger, channels for the air streams, a water-collecting sump and measurements points. **Figure 3.6** also shows the locations for the air- inlets and air-outlets for primary and secondary air streams.

The Acrylic panels were cut by a specialist supplier based on the CAD drawing. The assembly process was completed at the university lab to reduce external labour costs. The assembled AHU is shown in **Figure 3.7**.

Figure 3.7. Completed Acrylic AHU Casing

B- Heat Exchanger Design and Fabrication

The main objective of this study was to design a heat exchanger as the core of an IEC/HRV system and to test the effect of water spraying outlets locations on the IEC

performance. An extended objective was the experimental evaluation of parallel-plate heat exchanger surface geometry on the performance of the HRV system in terms of pressure drop and thermal efficiency. Accordingly, two sensible polymers heat exchangers were designed, constructed and tested as described in (Al-Zubaydi & Hong 2018).

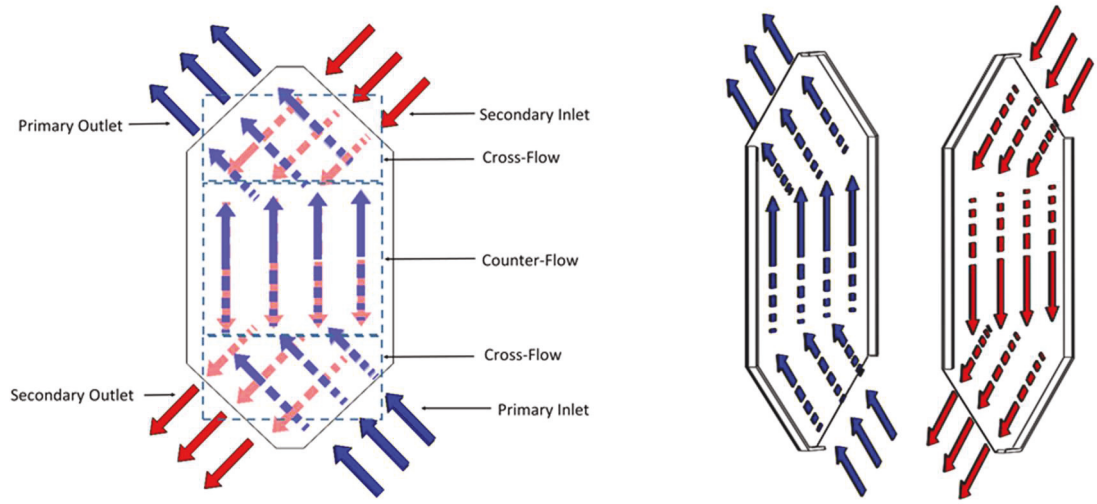

Figure 3.8. Heat exchanger flow pattern

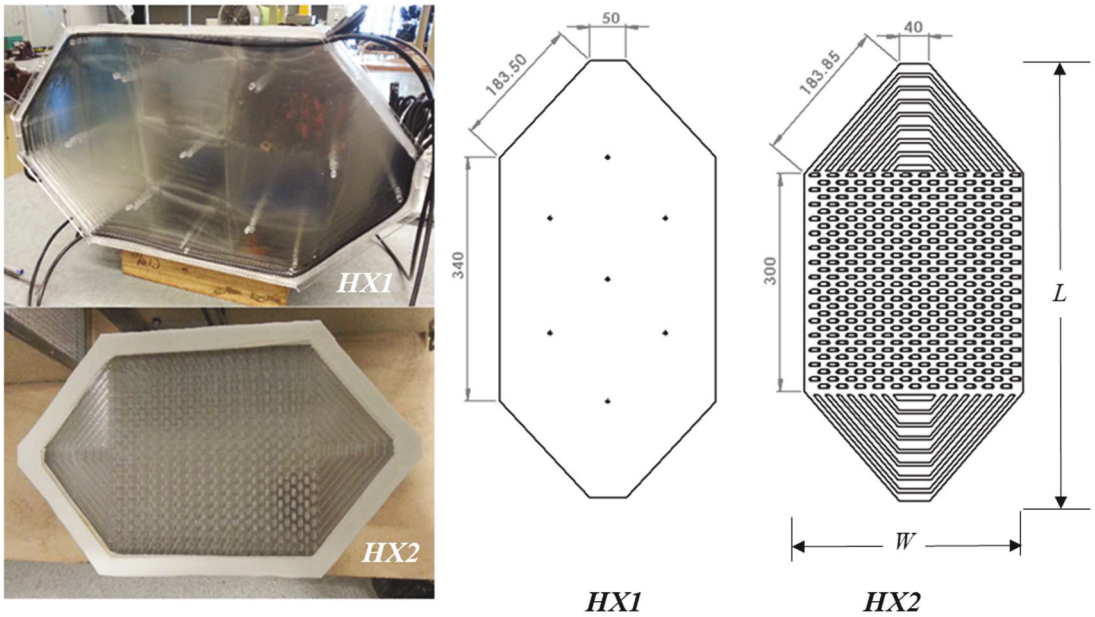

Figure 3.9. Surface Geometries and dimension of plates in two heat exchangers

The sensible quasi-counter-flow heat exchangers were made of PETG sheets in a hexagonal shape. **Figure 3.8** shows the airflow pattern in the heat exchanger. As shown in **Figure 3.8**, the quasi-counter-flow heat exchanger design was selected based on the properties of the airflow pattern to increase the counter-flow area and reduce turbulence.

The photographs and sketches of the plate heat exchangers are shown in **Figure 3.9**. The first heat exchanger (HX1) consists of parallel plates that have a flat surface and seven cylindrical spacers (4 mm diameter) in each channel to maintain the space between the plates with minimum air turbulence. The second heat exchanger (HX2) has a thermally formed PETG sheet in a hexagonal shape with a unique surface pattern proposed for this study, with the surface geometry comprised of multiple parallel rows of longitudinal dimples, upward and downward in sequence. The dimpled surface is aimed to generate high turbulence inside the channels to increase the surface area for heat exchange and hence increase the heat transfer rate, offset by the pressure drop increased by the complex geometry (Vorayos et al. 2016). The plate's surfaces were uncoated to minimize mould formation.

The dimensions of the HX1 plate was extended vertically by 40 mm in an attempt to compensate the area covered by the internal tube and make the total surface area equal to that in the HX2 plate surface with the dimples, as shown in **Figure 3.9**. In both heat exchangers, an acrylic frame of 5 mm height separated the plastic plates to form the channels. The channels were stacked to form the full heat exchanger, with 72 channels in total, equivalent to 460 mm depth. Following the criterion adopted by Kragh (Kragh et al. 2007), the design took into account the reduction of the pressure drop across the heat exchanger, minimizing the air leakage and mixing of both air streams, simplicity in the manufacturing process, maximizing the efficiency, and the robust design. The heat exchangers' geometrical specifications are listed in **Table 3.1**.

Table 3.1. Heat exchanger specifications and parameters

Parameter	HX 1	HX 2
Height of Plate H [mm]	600	580
Length of Plate L [mm]	300	300
Plate thickness Δz [mm]	0.5	0.5
The gap between the two plates b [mm]	5	5
Total Width X [mm]	460	460
Effective heat transfer area per plate [m^2]	0.19	0.192
The number to plates N	73	73
Number of hot air channels N_h	36	36
Number of cold air channels N_c	36	36

The novelty of this work is to introduce an internal water spraying arrangement in order to achieve the maximum water distribution over the plate, thus optimising the water film surface area in the IEC/ERV system. The proposed water spraying arrangement in this study consists of a flexible PVC tube with 4 mm internal diameter and multiple spraying holes. The tube inserted inside the wet channels, as shown in **Figure 3.10.** The design considered the pressure drop due to the tube length; accordingly, the tube inserted into two-thirds of the total number of the channels. The hole locations were selected to maximize and uniform the water distribution over the plate area, as shown in **Figure 3.10.b**. The tube was pre-tested under variable water flow rates and pressures.

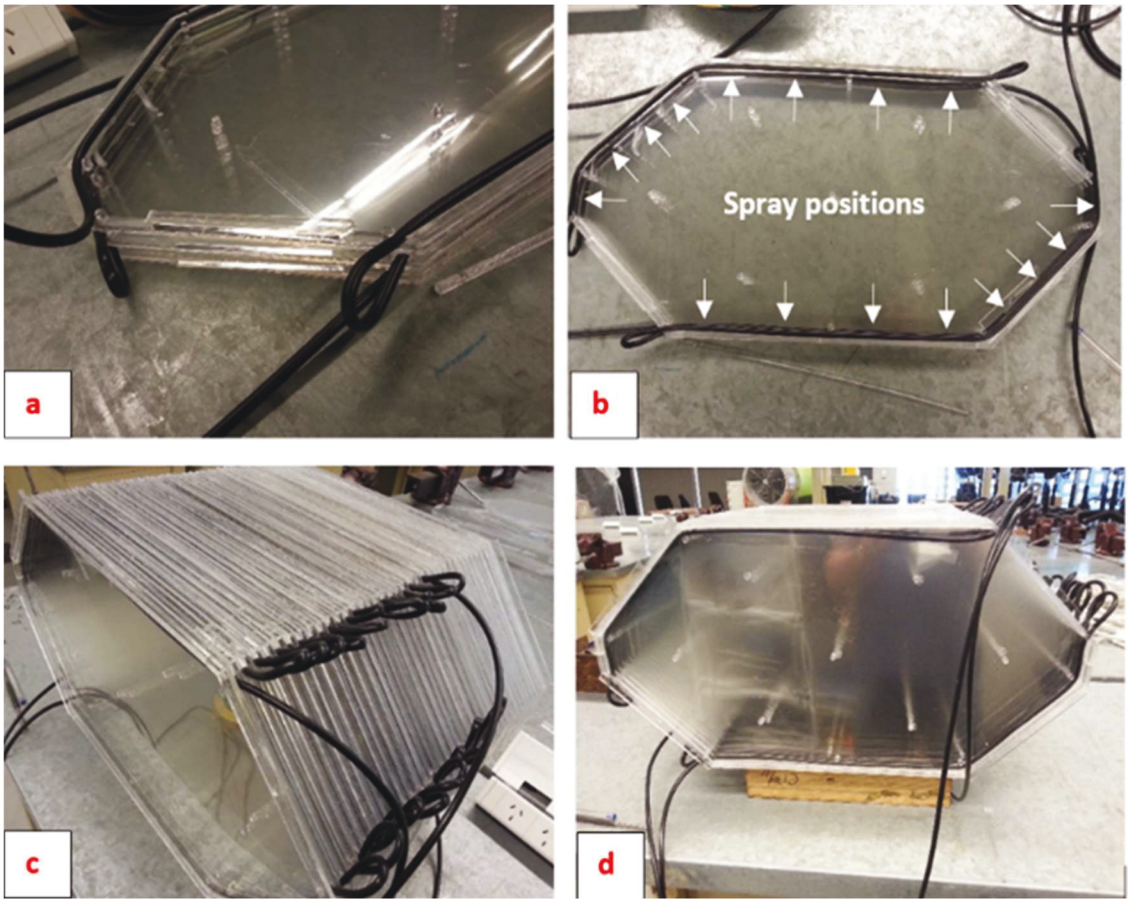

Figure 3.10. Water spray in the prototype heat exchanger (a) tubes. (b) Spray locations (c) side view of the tubes (d) front view of the tubes.

The assembly procedure of HX1 is shown in **Figure 3.11**. The polymer sheets and the channels frames were cut into shape and size with the laser-cutting machine. As shown in **Figure 3.11(a), t**he plates glued to the frames to assemble the 72 flow channels as individual pairs. The individual pairs were stacked on the top of each other to form a sub-assembly of 8 channels with the flexible low-density polyethylene (LDPE) tube in channels that were determined to be the wet channels (**Figure 3.11 (b), (c)** and **(d)**). The sub-assemblies are glued on top of each other to form the full heat exchanger, as shown in **Figure 3.11 (e)**. An extension duct was installed to the two inlets and the two outlets ports for accurate air data measurement, as shown in **Figure 3.11 (f)**. The heat exchanger

was tested for air leakage in a procedure adopted from (Liu et al. 2016). The possible leaking points and sides were cured and sealed with epoxy and duct tape.

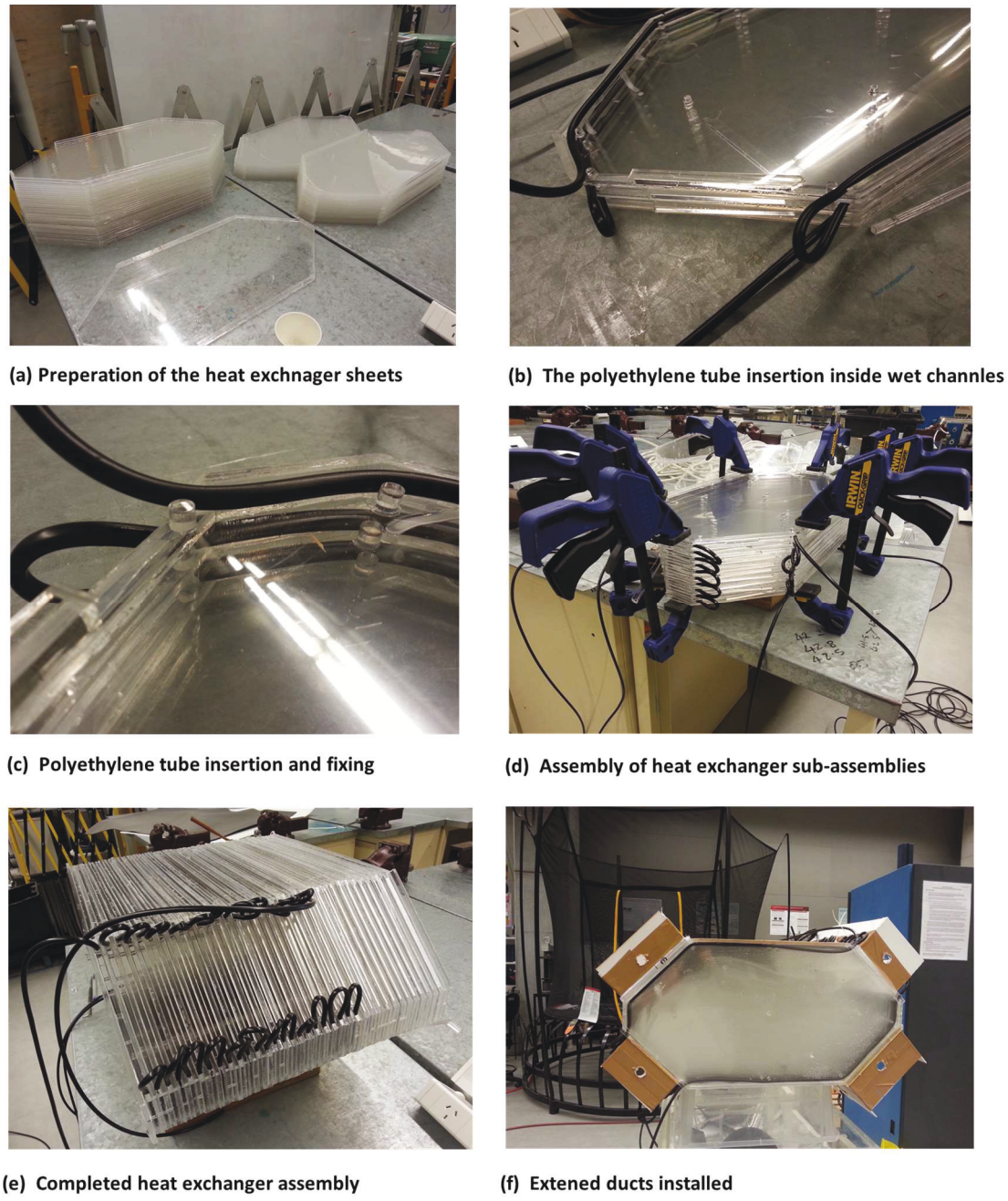

Figure 3.11. The construction process of experiment prototype heat exchanger

C- Air Supply System

During the experiments, the air was individually supplied to both mainstreams. Two ebm-papst fans model R2S175-AB56-01 backward curved centrifugal blowers fans were used

to circulate the air through the test facility. Each fan was coupled with a variable regulator that allows modifying the airflow rates to establish the primary and secondary air drive system. However, it is not possible to maintain exact values of the flow rate with the aid of the variable regulators, since the regulation units do not have definite positions, and since the flow rate provided for each position of the regulator will depend on the pressure drop of the particular fan that is connected to it.

D- Water pumps

In IEC mode, water is sprayed over the heat exchanger plates through the external nozzles and/or through the internal spraying arrangements using a circulating pump installed in the test facility. As circulating elements, small 12 V DC (30 Watt maximum power) with a maximum 4.0 lpm flowrate water pump was used. The DC motor capacity was varied with an adjustable DC power supply. The pump power supplied depends on the specific flow rate of the water system in each testing mode.

For circulating water, a 4 mm low-density polyethylene (LDPE) tube was used as a channelling medium in all configurations. Additional valves before the inlets of the tube branches were used to control and adjust the desired inlet flow rate of the water through the nozzles.

E- Air Temperature Control

In order to test different primary air temperatures, the IEC/HRV test facility has been combined with the A660 air conditioning laboratory unit described earlier. The A660 has two heating points, each with 2 x 1 kW heating elements. These heating elements were used to control the air temperature supplied to the test facility. For more incremental air temperature variation, a variable controller was applied to control the current supplied to the heating elements.

F- Humidity Control

In order to test different relative humidity levels, the A660 humidifying device was used. The humidifying device is an electrically heated boiler with 2.5 litres volume, working at atmospheric pressure and heated by 1 x 1.0 kW and 2 x 2.0kW heating elements. This system can produce steam at a rate of up to 10 kg / h, with the relative humidity range controlled from 20% to 100% by a controller that can work in different modes (proportional or modulating). The steam is injected after the reheating stage in the A660 unit with the help of a steam distributor device.

G- Air distribution systems

Figure 3.12. Image of flexible air ducts for the test facility

Flexible air ducts with a diameter of 250 mm have been used to connect the elements of in the test bench. A detail of these ducts is shown in **Figure 3.12**. The ducts will allow

the air transfer from the A660 climatic simulator to the IEC/HRV unit chambers, as well as from the unit to outside the lab.

3.5. Instrumentation

Experiments were conducted according to ASHRAE Standards. Four measuring stations as referenced in ASHRAE 84-2013 (ASHRAE 2013) are located at the heat exchanger entrances and exits to measure the dry bulb temperature, wet bulb temperature and air velocity.

A- Temperature and humidity measurement sensors:

1- TMC6-HD - HOBO

Temperature measurements were made using, TMC6-HD - HOBO temperature sensors in all locations. The dry bulb and wet bulb temperatures were measured at points 1-6 and sump water temperature, as shown in **Figure 3.3** and **Figure 3.4**. The TMC6-HD - HOBO is a 4-wire copper-coated sensor which can plug into the external input jacks of U12, UX120 HOBO loggers, directly. Although more costly than T and K-Type thermocouples, it is the most suitable material and has better characteristics due to its high degree of linearity and stability as well as high precision (0.15 ° C) when used with UX120 HOBO data logger. The working temperature range is -40 to + 100ºC in the air (www.Hobo.com).

2- RH-USB

For measurements averaging and data comparison, in accordance with ASHRAE test requirements, a parallel set of temperature and relative humidity measurements using RH-USB relative humidity/temperature sensors were used (**Figure 3.13**). The RH-USB sensor is using the capacitive effect to measure the air relative humidity. As the air moisture change, the electrical capacity of the metal oxide strip on the chip would change

based on the moisture collected on its surface. This electrical capacity variation is measured to calculate the air relative humidity. The RH-USB sensors from OMEGA® are pre-calibrated by the manufacturer with an accuracy of ±1ºC temperature measurement and ±3 % RH relative humidity precision measurement.

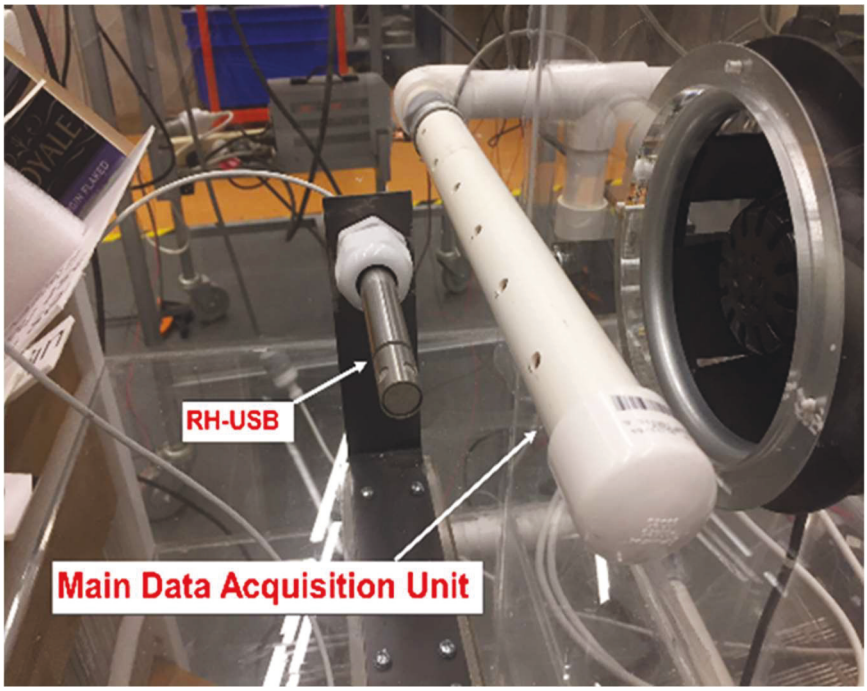

Figure 3.13. Primary and parallel measurement sets

The RH-USB sensor cannot be extended inside the channel. Consequently, the probes were fixed at the mid-position of the channel using L-shape stands, as shown in **Figure 3.13**. The diameter of the sensor probe head was 12mm. Four probes were used. The RH-USB probe was positioned at 150mm from each face of the heat exchanger.

3- Type K Thermocouple

The A660 unit is equipped with 'K' type thermocouples to measure the dry bulb and wet bulb temperature at multiple stages in the unit. The A660 type K Class 1 thermocouples were used to measure make-up air temperature supplied to the heat exchanger inlets and outlets for comparison. The 12 thermocouples in the A660 system were calibrated using

a hot water bath and a calibrated electronic platinum resistance thermometer from 19°C to 45°C. The thermocouple measured the air temperature in the hot water bath was accurately read using the calibrated platinum resistance thermometer and compared with the thermocouple readings.

B- Air Sampler

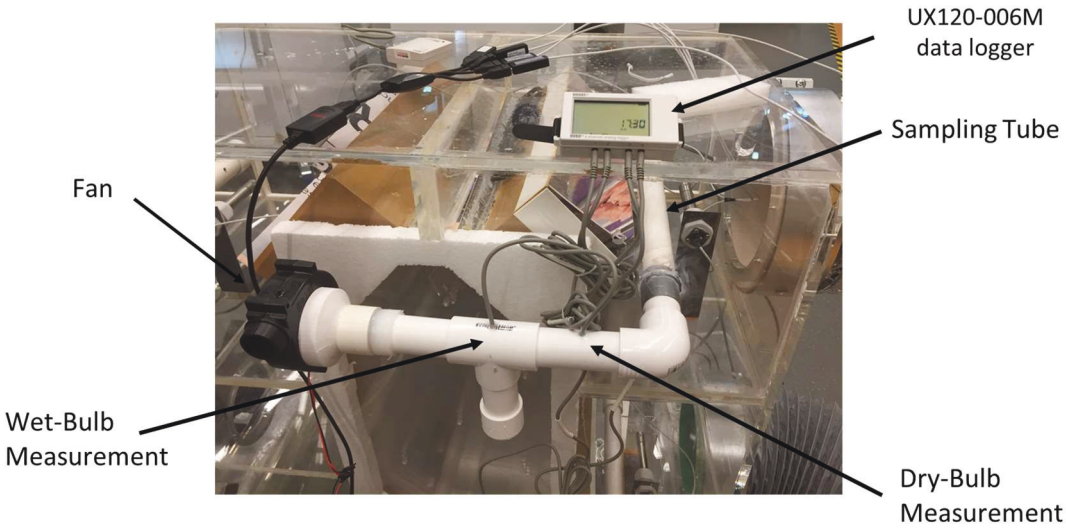

Figure 3.14. Airflow sampling system

Precise air temperature measurements at the heat exchanger inlet and outlet streams, a simple air sampling device was used to measure the temperature and moisture conditions. **Figure 3.14**shows the photograph of the sampling device. As shown in **Figure 3.14**, the sampling device consists of a 300 L x 25 D mm PVC sampling tube; the tube was positioned perpendicular to the air stream direction and provided eight sampling openings. The sampling tube is connected to the measurement tube. The sampling device contains two measurement points; the first is hosting a TMC6-HD temperature sensor for the dry-bulb temperature, followed by the second point with TMC6-HD temperature sensor enclosed with wick cloth that soaked partially in the water container was used to measure the wet-bulb temperature. Air sampler withdraws air from the main air stream

using a suction fan that connected to the end of the measurement tube. The air velocity of 6 m/s inside the sampling device is recommended to obtain the precise temperature measurement (Nasif 2008).

C- Water flowmeter

In order to measure the water flow rate in the water distribution system, 4-turbine flowmeters type USN-HS06PA-2 were used. The sensor has two 6mm hose barbs, with a measurement range between 0.2-2.5L/min and 1% error resolution.

D- **Measurement of differential pressure and air volume flowrate: Orifice plate**.

For the measurement of the air volume flow rate supplied to the heat exchanger inlets, the measurement equipment's from the A660 unit were utilised. The A660 unit inlet mixing duct and return duct are equipped with 150 mm diameter orifice and differential pressure sensors.

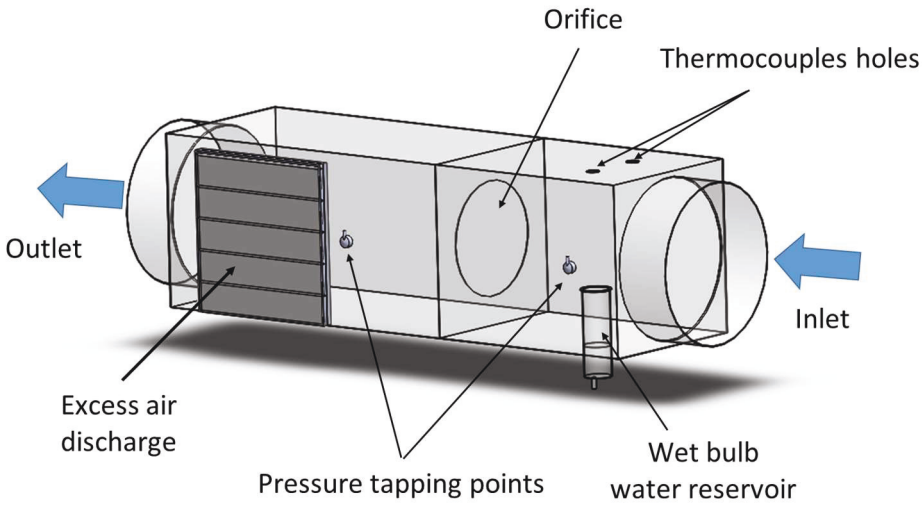

Figure 3.15. Sketch of the orifice plate used in the measurement of air volume flow rate

The structure of the return duct with an orifice is shown in **Figure 3.15**. The differential pressure measurements between the pressure tapping points on the sides of the orifice

plate were obtained. Electronic differential pressure transducers were used to collect the data for the range between 3-12.5 mmH_2O. An example of the calculation of the volume flow rate made by this procedure is presented in **Figure 3.16**.

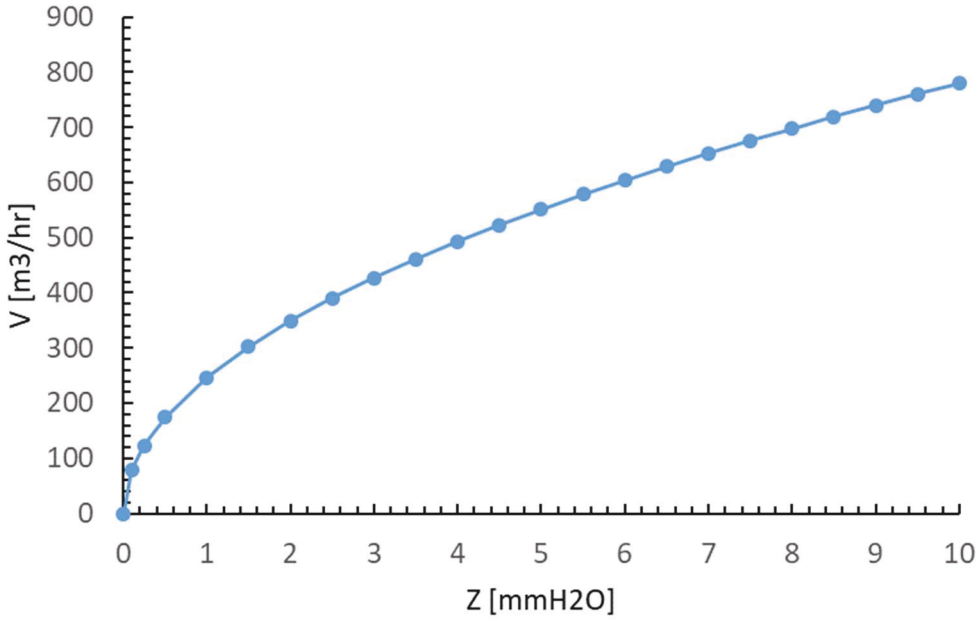

Figure 3.16. Volume flow rate curve measured with an orifice plate

Figure 3.17. Series 668 differential pressure transmitter

For the measurement of the pressure drop in the orifice plate, the differential pressure transducer is used, as shown in **Figure 3.17**, which provide a voltage output proportional to the applied pressure.

E- Measurement of Air Velocity

In addition to the air volume and mass flow rate measurement through orifice plate method, the velocity range of 1.0 m/s – 3.0 m/s to measure by a highly sensitive Testo-480 hot wire anemometer with a telescopic probe. The velocity measurements process based on Tchebycheff method procedure (ASHRAE 2008). Testo 480 Hotwire anemometer readings also applied for certainty temperature and relative humidity measurement.

F- Measurement of Power Consumption

The total power consumption in the test facility includes the two fans power consumption, in addition to the water pump consumption the wet mode test. Two power meters with data recorder model "Weidmuller Energy Meter 330" were used.

3.6. Acquisition system and data monitoring software

The system of instrumentation and data acquisition must enable the measurement of as many variables as possible with the appropriate precision. That requires the use of powerful and flexible instruments that acquire all the data and record it while making decisions and controlling the system. In particular, a HOBO UX120-006M analog data logger is used with all TMC6-HD sensors as the primary measurement system (Hobo Data Loggers).

A HOBO® data logger type UX12-006M and HOBO-Pro data analysis software was utilised for recording and analysing the data. A PC and TRHC_1.03.13.0919 Software as an alternative to the data logger to record the measured parameters by the parallel set of

temperature and relative humidity measurements (RH-USB relative humidity/temperature sensors).

The P.A. Hilton data logger recorded the A660 supply air streams conditions data including dry bulb, wet bulb and the differential pressure. The readings have been collected via data logging software in the span of 10 seconds. All the data were exported to an excel sheet for further calculations and analysis.

3.7. Experimental procedure

The test facility was used to investigate the performance of sensible energy recovery ventilation in both dry and wet operation. In order to ensure consistent test conditions, a pre-test of the test facility was completed. The pre-test comprises the smoke test for leak detection, the comparison of parallel measurement systems data, reliability of the calibrated sensors and the validation of the measurement locations.

The first step was to test the airflow rate in the primary and secondary channels. Both fans were switched ON to maximum speed. Two methods calculated the air mass flow rate: Using the differential pressure transducer reading (mmH_2O) and **Equation 3.1**:

$$\dot{m}_a = 0.0517\sqrt{\frac{Z}{v_a}} \quad \textbf{(3.1)}$$

Where $\dot{m}_a$ is the air mass flow rate in kg/s, Z is the differential pressure across the orifice plate in mmH_2O and v_{ia} is the specific volume of air at inlets (calculated) in m^3/kg. To validate the mass flow rate calculated with **Equation 3.1**, the air volume flow rate and the mass flow rate can be calculated by **Equation 3.2** and **Equation 3.3**, respectively:

$$\dot{V}_a = v.A_D \quad \textbf{(3.2)}$$

$$\dot{m}_a = \dot{V}.\rho \quad \textbf{(3.3)}$$

Where $\dot{V}_a$ is the air volume flow rate in m^3/s, v the air velocity in the duct (measured with the hot wire manometer) in m/s, A_D is the duct cross-sectional area in m^2 and ρ is the air density (calculated) in kg/m^3.

The fan speeds were adjusted to obtain multiple air velocities to investigate the effect of air velocity on the test unit's performance. The velocity range achieved with fan speed adjustment was from 2.0 m/s – 2.9 m/s. This velocity range falls in the velocity range specified by ASHRAE standards for air-to-air heat exchangers and indirect evaporative coolers (ANSI/ASHRAE 2015; ASHRAE 2013).

The next step was to validate the heat sensors. Equivalent air speeds were fixed for both streams. The temperature readings at a low primary air temperature were in the range of 15.4-16.2 °C. After this stage, the heat was added to the primary air stream by the heating elements. The variable controller controlled the current supplied to the heating elements as mentioned earlier; this enabled the tuning of the primary air temperature. The system required about 10 minutes to reach stability after heater supplied current tuning. The primary air temperature range was between 16 °C to 38.2 °C. To increase the air moisture content, the boiler was turned "ON". The boiler stability was reached after 15 minutes from heater activation. The steam injector was set to inject steam after the A660's evaporator unit, mainly to avoid the condensation. The heat additional heat from the hot steam was considered in the measurements. The system was able to vary the primary air moisture content from 9.1 g/kg to 18.24 g/kg.

Following the measurement system setup, the test facility was prepared for the experimental stage. The test procedure can be summarised as the following systematic procedure:

1) Switch ON the data loggers and computers. Inspect sensor connection and any possible reading error.
2) In the case of IEC testing, fill the water sump to the maximum capacity level.
3) Turn on the fans. Keep the system running for 10 minutes to reach the measurement system stability. Check the temperatures reading, the differential pressure transducer level and the corporation readings (air velocity, temperature and relative humidity with the hot wire monometer).
4) Turn on the vapour compression unit followed by the heating elements at maximum load and the steam boiler with 1 kW power. Re-check the measurement main and parallel system.
5) Keep the system operate for 60 minutes to ensure reaching the stability status for the system with the maximum primary air temperature and air velocities.
6) The test measurement started at the high primary air temperature and velocity. After each adjustment for temperature, humidity and velocity, the system was allowed to operate for 10-15 minutes before resuming the data collection.

The IEC unit performance rating under the three suggested modes implemented through empirical investigation. Each mode tested for 6-7 hours period for repeated tests with data recorded for minimum 10-minute time interval under steady-state conditions (variation in t_{p1} and t_{s1} is within 0.1 °C) before changing the inputs to collect the total 9000 different readings. In this experiment, the room exhaust air of 23 °C and RH 48-58% applied as the secondary air for the energy recovery IEC system. With the three water spray modes, the primary air inlet temperature [t_{p1}], the primary inlet air velocity [v_{p1}], the secondary air inlet velocity [v_{s1}] and spray water mass flow rate [$\dot{m}_w$] varied to create diversities in testing conditions. The primary air inlet temperature ranged between 24 °C to 37 °C, the

primary air and secondary air velocities ranged between 1.0 m/s to 3.0 m/s, while the mass flow rate of spray water varied between 20 g/sec to 50 g/sec using a DC pump controller. The pressure drop across the heat exchangers was measured by using total pressure differences between the inlets and the outlets.

The testing of different water distribution arrangements and varying the water mass flow rate are the main objective of this experiment. As mentioned above, a DC water pump with a variable controller was applied to control the water mass flow rate to suites the capacities of the nozzles of the specified arrangements. The water mass flow rate required in the external spraying modes was set to 23 g/s on average, while the internal spraying modes was around 25.0 g/s and the mixed-mode average mass flow rate of 50 g/s.

3.8. Pre-Test: Pressure drop across heat exchangers

As mentioned earlier, the test rig equipped with two fans to form the primary and secondary airflows. The two ebm-papst fans are backward blades centrifugal fans model R2S175-AB56-01 (ebm-papst 2016). The air velocity was varied by adjusting the fan speed via the analogue fan speed controllers. Increasing the air velocity may increase pressure losses. The static pressure measurement method was based on ANSI/ASHRAE Standard 84-2013 (ASHRAE 2013) “Method of Testing Air-to-Air Heat/Energy Exchangers”. **Figure 3.18** shows the variation of pressure loss ($\Delta P = P_{in} – P_{out}$) with the inlet velocity of the primary airflow. As shown in **Figure 3.18**, the pressure loss increases with the increase of the inlet velocity of the primary airflow. The effect of the air velocity on the pressure loss becomes much stronger at high velocity of the primary airflow. It is shown in **Figure 3.18** that the effect of the primary airflow velocity on the pressure loss is significantly stronger in HX2 than that in HX1. The higher pressure loss in HX2 is

mainly due to the turbulent flow generated by the more complicated surface geometry of the plates.

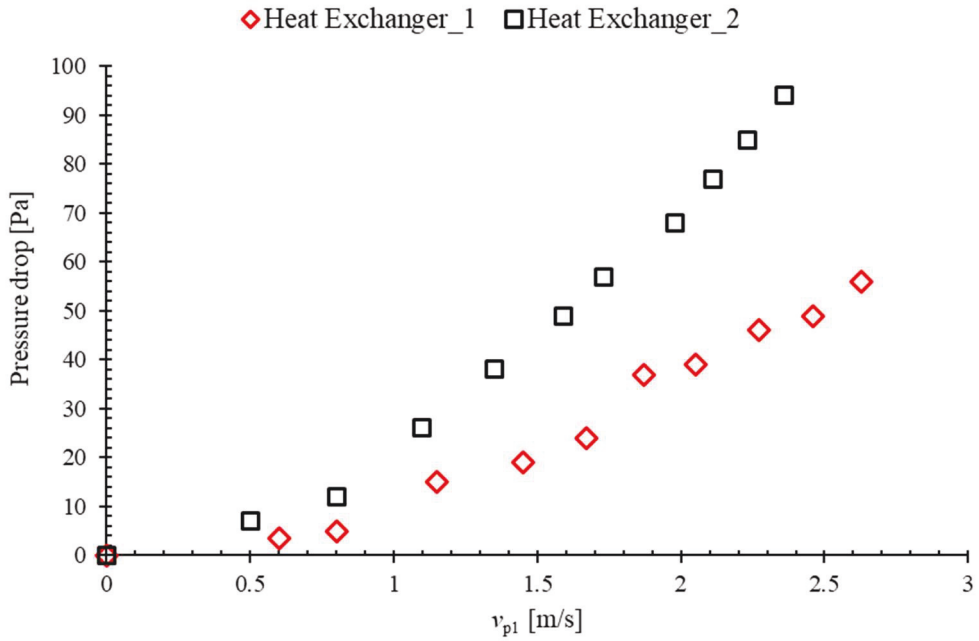

Figure 3.18. Variation of pressure loss with the inlet velocity of the primary airflow

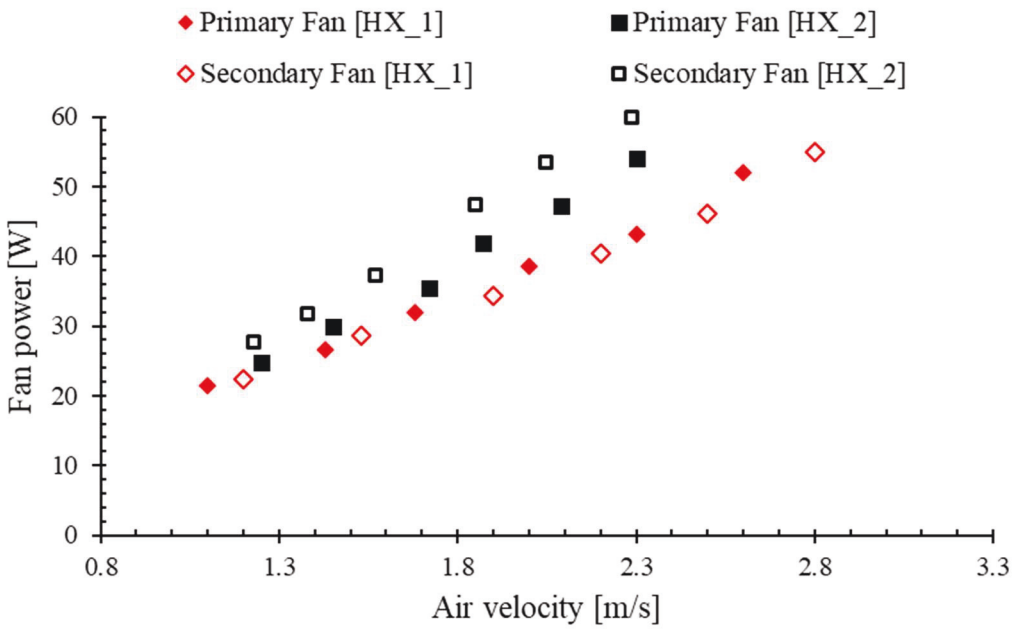

Figure 3.19. Fan power consumption measured under different air velocities

Figure 3.19 shows the fan power varied with the velocity of the primary and secondary airflows at six different velocities. As shown in **Figure 3.19**, the fan power consumption in HX2 is higher than that in HX1. This mainly due to flow resistance increased by the complicated surface geometry in HX2. The higher-pressure drop due to the internal turbulence generated in HX2 resulted in higher-pressure load on the fans, thus translated as higher power consumption. The measured fan power at full speed is 52 Watts and 55 Watts for the primary and secondary fan in HX1 and 54 Watts and 57 Watts for the primary and secondary fan in HX2, respectively.

3.9. Uncertainty Analysis

The confident level in the experimental measurements is based on both the accuracy of the measuring instruments and measurements precision. ASHRAE Guideline 2-2010: Engineering Analysis of Experimental data (ASHRAE 2014) suggested that all the experimental measurement should include the best value, uncertainty interval (+/-) and an associated probability with 95% confidence for sample number $N \geq 30$.

The total uncertainty error, δ, for one measurement can be calculated as the sum of bias error (The systematic error), β, and the precision (the random error), p.

$$\delta = \beta + p \tag{3.4}$$

Uncertainty analysis was conducted on the measured and calculated data to assess the effect of measurement errors and validate the results, based on the method presented by Coleman and Steele (Coleman & Steele 2009). The absolute uncertainty of directly measured variable depends on the instrument accuracy, Δx. The standard uncertainty for direct measurements can be calculated by **Equation 3.5**:

$$u(x) = \frac{\Delta x}{\sqrt{3}} \tag{3.5}$$

The standard uncertainty for the directly measured parameters is presented in **Table 3.2**.

Table 3.2. Standard uncertainties of the directly measured parameters

Measured parameters	Apparatus	Measurement range	Accuracy (Δx)	Standard uncertainty $(u(x))$
Air temperature (t_{DB}, t_{WB})	Temperature sensor Model: TMC6-HD HOBO	-40 to +100 °C	±0.15°C	±0.0866 °C
Relative Humidity and t_{DB} (averaging system)	RH and temperature sensor Model: RH-USB OMEGA	t_{DB}: -17°C to 49°C; RH: 2 to 98%;	Temperature: ±1°C; Relative Humidity: ±3%;	±0.523 °C ±0.017
Water temperature	Temperature sensor Model: TMC6-HD HOBO	-40° to 50°C	±0.15°C	±0.0866 °C
Water flow rate	Water flow sensor Model: USN-HS06PA-2	0.2-2.5 L/min	1%	±0.00577 L/min
Air velocity	Hotwire anemometer Model: Testo-425	0-20 m/s	±(0.03 m/s +5% of mv)	±0.01 Pa
Differential pressure	Dywer Series 668 DPT	0-20 mm H_2O	1%	0.0173 m/s
Power consumption	Power meter	0-2400 Watt	±2%	±0.0115 Watt

The indirectly measured variable, y, is a function of the independent direct measured parameters x_1, x_2,…x_n, and can be expressed as:

$$y = f(x_1, x_2, x_3, \ldots\ldots, x_n) \tag{3.6}$$

The absolute and relative uncertainties of depended and independent variables were calculated using the following equations:

$$\Delta y = \sqrt{\left(\frac{\partial f}{\partial x_1}\right)^2 (\Delta x_1)^2 + \left(\frac{\partial f}{\partial x_2}\right)^2 (\Delta x_2)^2 + \cdots . + \left(\frac{\partial f}{\partial x_n}\right)^2 (\Delta x_n)^2} \tag{3.7}$$

$$\frac{\Delta y}{y} = \sqrt{\left(\frac{\partial f}{\partial x_1}\right)^2 \left(\frac{\Delta x_1}{y}\right)^2 + \left(\frac{\partial f}{\partial x_2}\right)^2 \left(\frac{\Delta x_2}{y}\right)^2 + \cdots . + \left(\frac{\partial f}{\partial x_n}\right)^2 \left(\frac{\Delta x_n}{y}\right)^2} \tag{3.8}$$

Where: Δy is the absolute uncertainty and $\Delta y/y$ is the relative uncertainty of dependent variables. The relative uncertainty analysis for the calculated parameters: e.g. $\eta_{\cdot S}$, $\eta_{\cdot WB}$, $\dot{Q}_p$ and COP is listed in **Table 3.3**.

Table 3.3. Relative uncertainty analysis results for measured parameters

Indicator	Nominal value	Relative uncertainty
$\dot{V}_p$	0.126 m^3/s	4.98%
$\dot{V}_s$	0.123 m^3/s	5.1%
$\dot{m}_p$	0.1449 kg/s	5.0%
$\dot{m}_s$	0.147 kg/s	5.15%
$\eta_{\cdot S}$	60%	±1.87%
$\eta_{\cdot WB}$	73%	±1.52%
$Q_{sensible}$	946 W	±4.9%
COP	11.8	±5.0%

An energy balance between the primary and secondary air was conducted to verify the accuracy and consistency of the experiment. The energy balance is the comparison between the enthalpy changes in the primary air and secondary air obtained from **Equations 3.9** and **3.10** (Wang et al. 2017).

$$Q_p = \dot{m}_p(h_{p1} - h_{p2}) \tag{3.9}$$

$$Q_s = \dot{m}_s(h_{s2} - h_{s1}) \tag{3.10}$$

The energy balance variation found in the literature was around 5% (Duan et al. 2016). However, high values as 10-20% were used by Chen et al. (Chen, Yang & Luo 2016a).

Chapter 4

Counter Flow Heat Exchanger for Heat Recovery Ventilation in Cooling Mode

4.1. Introduction

In this chapter, Experiments were conducted to fulfil the aim of investigating the effect of surface geometry on the performance of the heat exchanger. The performances of two plate heat exchangers of different surface plate geometries were tested, i.e. Flat plate and dimpled face. The test evaluated the performance of each heat exchanger based on the evaluation parameters specified by ASHRAE (ASHRAE 2013) and similar work in the literature (Fernández-Seara et al. 2011; Nasif et al. 2010; Zhang 2010). Experiments were conducted on the quasi-counter-flow heat exchanger employed as an HRV (Heat recovery ventilation) system in both dry (sensible heat exchanger) or wet (Indirect evaporative cooling system) modes.

4.2. Experimental methods for meeting particular aims

As indicated in Chapter 3, the test facility was used to generate the inlet airflows required for experiments. The supplied primary air temperature decreases gradually from the maximum temperature of 37.4 °C to 24.5 °C over the 110-minute span. A similar variation was repeated for every test mode. The secondary air applied in this experiment was 23.0 °C, due to the absence of heat loads during the experimental work periods; the temperature was always within the range of 23 ± 0.5 °C.

Sample data of the test parameters were acquired in steady-state test conditions. The total time of all the tests is approximately 780 minutes. The average was taken in the range of

8-12 minutes, which was long enough to provide a sufficient sample size reliability, 100-120 samples were collected and analysed for every parameter. The data-sampling rate is set at one sample of the test parameters every 10 seconds (0.1 Hz).

4.3. Data analysis and criteria for assessing the performance

ASHRAE Standards procedures were adopted in the experiments, as done in similar experimental work (Fernández-Seara et al. 2011; Liu et al. 2016; M.F. & A. 2016). Each experiment lasted for 6 hours to collect sample data at a time interval of 8-minutes after changing the parameter on 10 seconds bases (3000 data per hour). In the first testing mode, both heat exchangers were operated at constant inlet air velocities of 2.6 m/s for the primary flow and 2.8 m/s for the secondary flow. The primary air inlet temperature as a testing parameter was varied in the range between 25 °C – 35 °C. The experimental data recorded range was between 27.6 °C to 32.7 °C to for HX1 and from 27.8 °C to 32.5 °C for HX2 over 120-minutes.

Table 4.1. Summary of the data ranges of various parameters

Parameter	**Symbol**	**Data Range**	**Unit**
Inlet primary air temperature	t_{p1}	25 – 35	°C
Inlet primary air humidity	w_p	11.23-13.45	g/kg
Inlet primary air velocity	v_p	1.1-2.6	m/s
Inlet secondary air temperature	t_{s1}	20.8-23.7	°C
Inlet secondary air humidity	w_s	11.05-12.87	g/kg
Inlet secondary air velocity	v_s	1.18-2.3	m/s

In the second mode, the air velocity for both streams was varied within a range of 1.1 m/s to 2.9 m/s at constant temperature and humidity to evaluate the effect on the heat exchanger evaluation indices. **Table 4.1** summarises the controllable experiment parameters.

4.4. Data analysis and Performance Indicator of HRV System

The sensible efficiency ($\eta_{.S}$) is used to evaluate the sensible heat transfer rate in the heat exchangers. According to AHRI standard 1060 (AHRI 2014), the sensible efficiency $\eta_{.S}$ is defined by **Equation(4.1**:

$$\eta_S = \frac{t_{p1} - t_{p2}}{t_{p1} - t_{s1}} \quad \textbf{(4.1)}$$

Where t_{p1} and t_{p2} are the dry bulb temperature of the primary air at the inlet and outlet, respectively. Where t_{s1} is the dry bulb temperature of the secondary airflow at the inlet of the heat exchanger.

In HRV systems, the fresh air is pre-cooled by the returning air. The cooling capacity of the heat recovery system is a major factor in system performance. The cooling capacity is the heat transferred from the primary air to the exhaust air, including sensible heat, $\dot{Q}_{sensible}$, and both the $\dot{Q}_{sensible}$ and the latent heat, $\dot{Q}_{latent}$, in the case with condensation. **Equation 4.2** defines the sensible heat rejected by the primary air, and **Equation 4.3** defines the latent heat:

$$\dot{Q}_{sensible} = \dot{m}_p . c_{pa} . (t_{p1} - t_{p2}) \quad \textbf{(4.2)}$$

$$\dot{Q}_{latent} = \dot{m}_p . h_{fg\_p} . (\omega_{p1} - \omega_{p2}) \quad \textbf{(4.3)}$$

Where $\dot{m}_p$ is the primary air mass flow rate [kg/s], c_{pa} is the specific heat of air [J/kg. °C], h_{fg_p} is the specific latent heat of vaporisation of water [J/kg], w_{p1} and w_{p2} are the absolute humidity of the primary air at the inlet and outlet, in the unit of kg water/kg dry air], respectively.

The total cooling capacity is the sum of the sensible heat and latent heat. The cooling capacity can also be calculated from the enthalpy change of the primary air, as shown in **Equation 4.4** (Chen, Yang & Luo 2016a):

$$\dot{Q}_p = \dot{m}_P.(h_{p1} - h_{p2}) \quad \textbf{(4.4)}$$

Where h_{p1} is the enthalpy of the primary air at the inlet of the heat exchanger and h_{p2} is the enthalpy of the primary air enthalpy at the outlet, in a unit of kJ/kg.

In an HVAC system, the performance is assessed by the coefficient of performance, COP, of the system. In a heat recovery heat exchanger, the power consumed by the system is the sum of electrical power to drive the fan and to operate the instruments and as defined by **Equation 4.5**:

$$P_{total} = P_{fan\_p} + P_{fan\_s} + P_{Instrument} \quad \textbf{(4.5)}$$

Where P_{fan_p} and P_{fan_s} are the power for driving the primary and secondary path fans, and $P_{Instrument}$ is the power consumed by the sensors and data acquisition system. The electrical power measurement is described in **Section 3.5.F**.

The COP of an air cooling system is defined as the ratio of the total cooling capacity to the total power consumption, expressed as (Chen, Yang & Luo 2016a):

$$COP = \frac{\dot{Q}_p}{P_{total}} \quad \textbf{(4.6)}$$

The system energy balance is required to validate the experimentally measured data. The energy transfer rates associated with the cooling capacity for the primary air and heat rejected to the secondary air were calculated based on experimental data. The enthalpies at inlet and outlet conditions were calculated using the standard equations for psychometric properties (Shallcross 2012). The rate of heat rejected by the primary flow is defined by **Equation 4.4** and transferred to the secondary flow by **Equation 4.7**:

$$\dot{Q}_s = \dot{m}_s(h_{s_2} - h_{s_1}) \quad \textbf{(4.7)}$$

And in the ideal operation case, the system balance is:

$$\dot{Q}_p = \dot{Q}_s \quad \textbf{(4.8)}$$

Where $\dot{Q}_p$ is the cooling capacity based on primary airflow and $\dot{Q}_s$ the secondary airflow.

The cooling capacity and the sensible efficiency for evaluating the performance of the heat exchangers were calculated with equations (4.1) - (4.6), based on the measured temperature, humidity and velocity of the primary and secondary airflows. The performance of the two heat exchangers with different plate surface geometries are compared to examine the effect of primary inlet temperature, the velocity of the primary and secondary inlet air flows on the evaluation indices: 1- Sensible efficiency, 2- Cooling capacity, 3- The coefficient of performance.

Theoretically, the heat rejected by primary air is equal to the heat gained by the secondary air. In practice, the difference in the heat transfer between these two flows may vary by up to 20% (Chen, Yang & Luo 2016a) due to causes such as the air by-pass. There is no main reason for the energy change difference as the error is related to many accumulated factors including: heat loss to surroundings, the heat stored within the heat exchanger plates and the measurement accuracies.

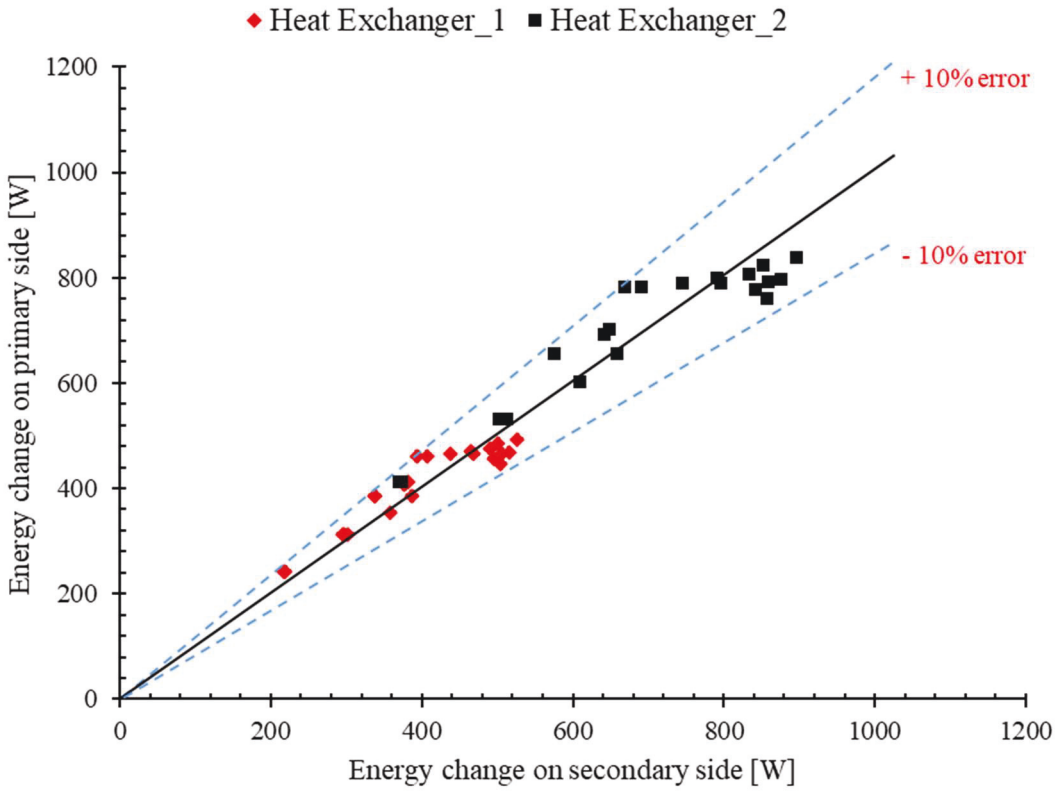

Figure 4.1. Energy balance of two air streams

The principles of energy balance in heat exchangers described in section 4 were applied to calculate the heat rejected by the primary stream, $\dot{Q}_p$, and the heat rejected by the secondary air stream, $\dot{Q}_s$. As mentioned above, the ideal heat exchanger to verify **Equation 4.8** ($\dot{Q}_p = \dot{Q}_s$) and achieve a linear curve with a slope of 1, and the measured results accuracy based on the deviation from the ideal slope. **Figure 4.1** shows the correlation between the energy transferred from the primary airflow and energy transferred to the secondary airstreams in heat exchanger models HX1 and HX2 under different test conditions. As shown in **Figure 4.1** the obtained experimental data energy balance analysis is satisfied within a reasonable accuracy of ±15%. Therefore, the experiment data can be treated as accurate.

4.5. Effects of air temperature on the HRV unit performance

Figure 4.2 shows the sensible efficiency (η_S) varied with the inlet temperature of the primary airflow under variable primary air velocity and constant primary air velocity of 2.6 ± 0.1 m/s, secondary air velocity of 2.75 ± 0.1 m/s and secondary air inlet temperature of 23.0 ± 0.6 °C. As shown in

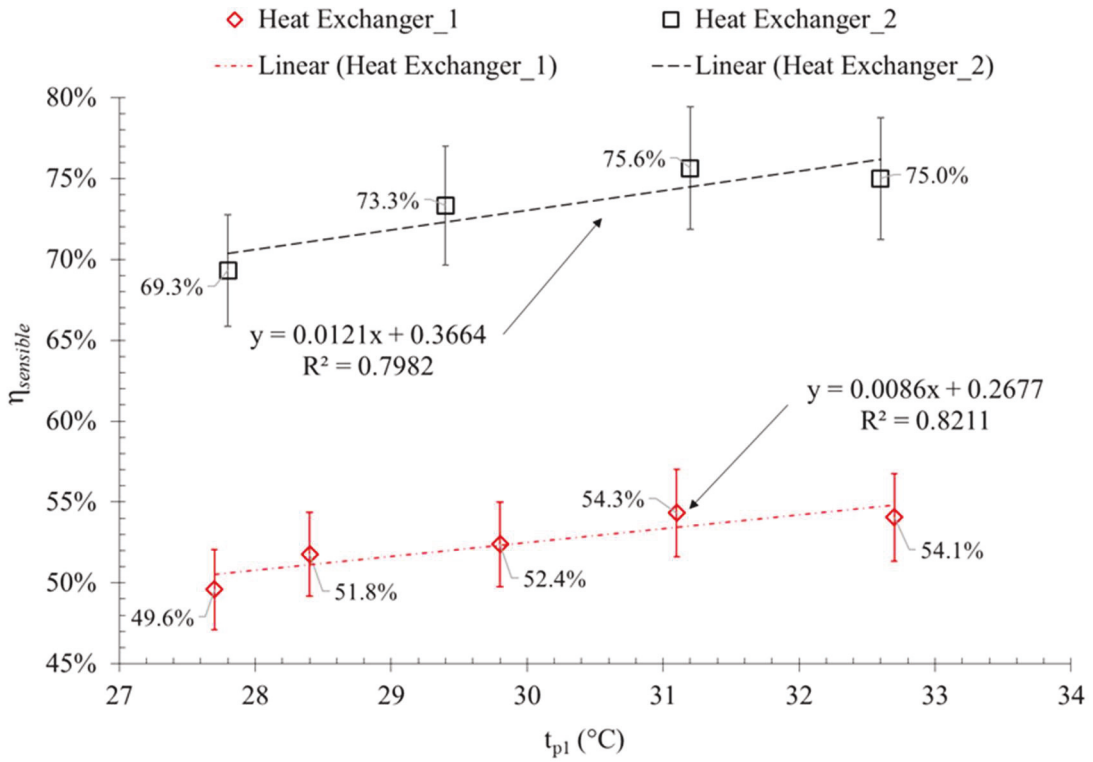

Figure 4.2 under all primary air inlet temperature values, the sensible efficiency of HX2 is about 20% greater than that of HX1. This is mainly due to the surface area increased and heat exchange enhanced by the surface geometry in HX2, compared with HX1. It also shows that sensible efficiency increases at a similar rate with the increase of the inlet temperature of the primary airflow in both heat exchangers.

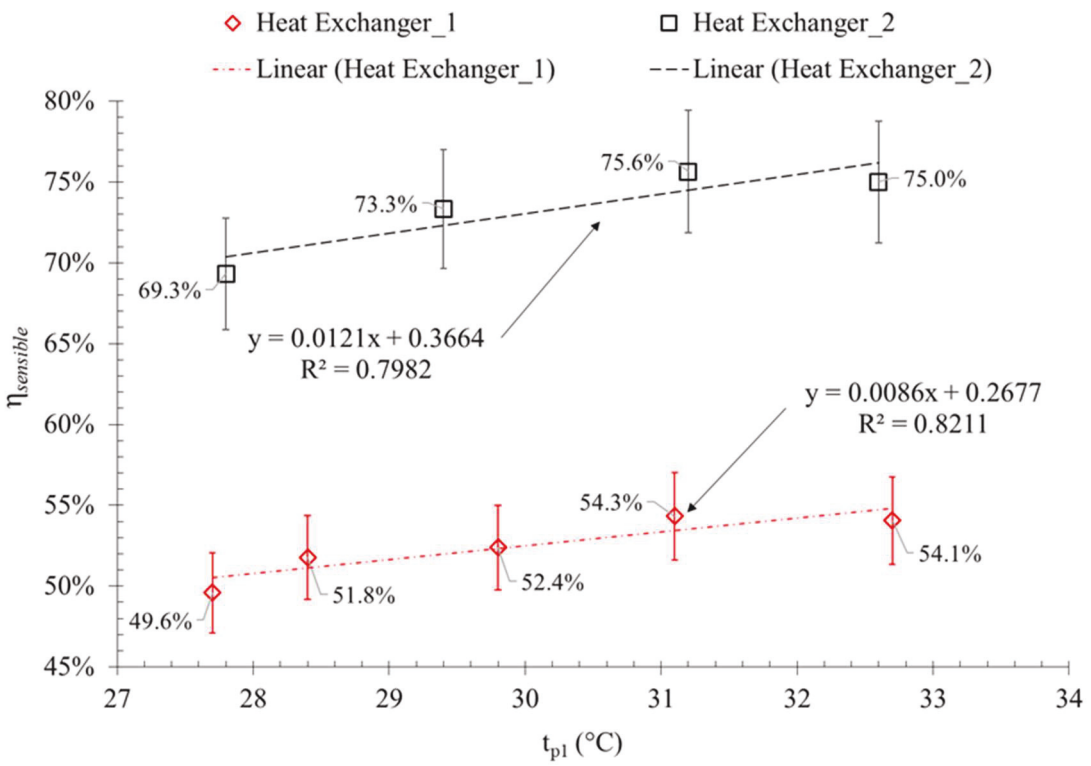

Figure 4.2. Effect of the inlet temperature of the primary airflow on sensible efficiency

As shown in

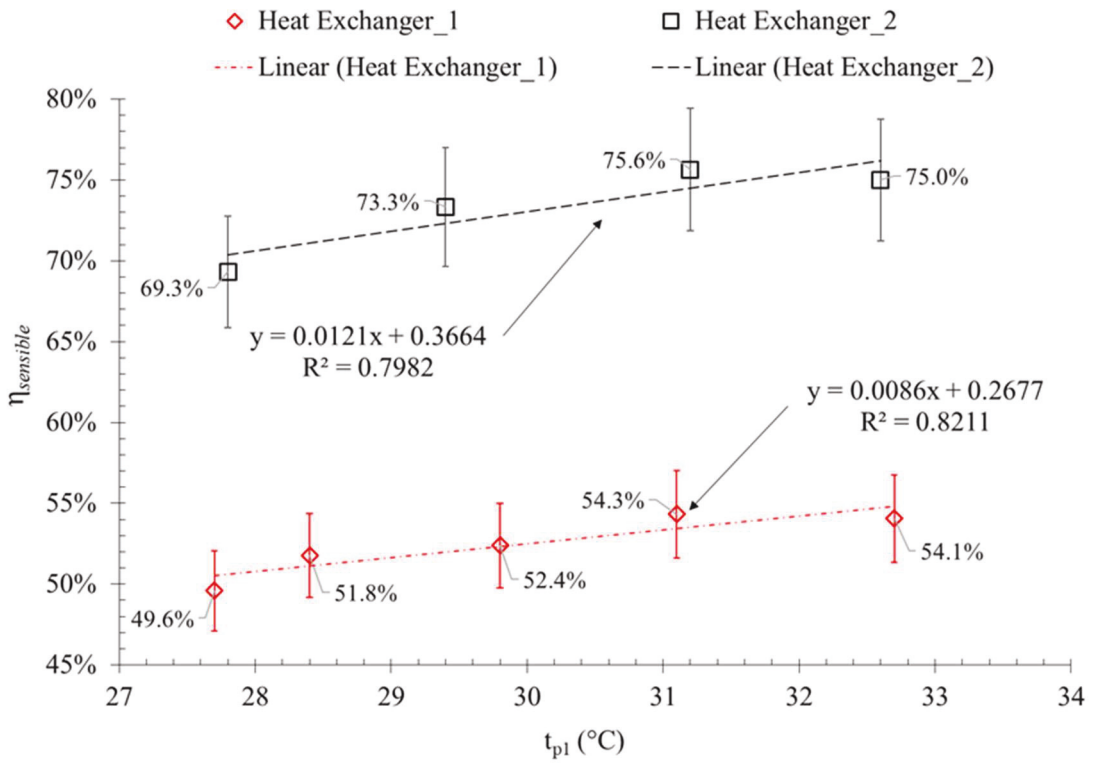

Figure *4.2* that inlet temperature of the primary airflow increasing by about 6.5 °C (from 27.7 °C to 32.7 °C) increases the sensible efficiency of HX1 by approximately 4.5% (from 49.6% to 54.1%). However, the sensible efficiency of the HX2 increased by 5.7% (from 69.3% to 75%) when the inlet temperature of the primary air was increased by 6.8 °C (from 27.8 °C to 31.2 °C). With further increase of the inlet temperature of the primary airflow from 31.2 to 32.8 °C, the sensible efficiency of HX2 slightly decreases. This mainly due to the plate material and geometry, allowing the plates to retain thermal energy at increased temperatures, causing a reduction of the sensible efficiency.

The main concept of the study is to make a comparison between the effects of the plate surface geometry. For the first point, the test temperature range: With reminding of the test rig range capacity (discussed in chapter 3), the temperature range of the primary air temperature can reach the maximum of 36 °C. However, it was noticed that the dimpled face heat exchanger is starts to store the heat in the plates as the temperature go above 34 °C.

The first-order regression models of the data shown in

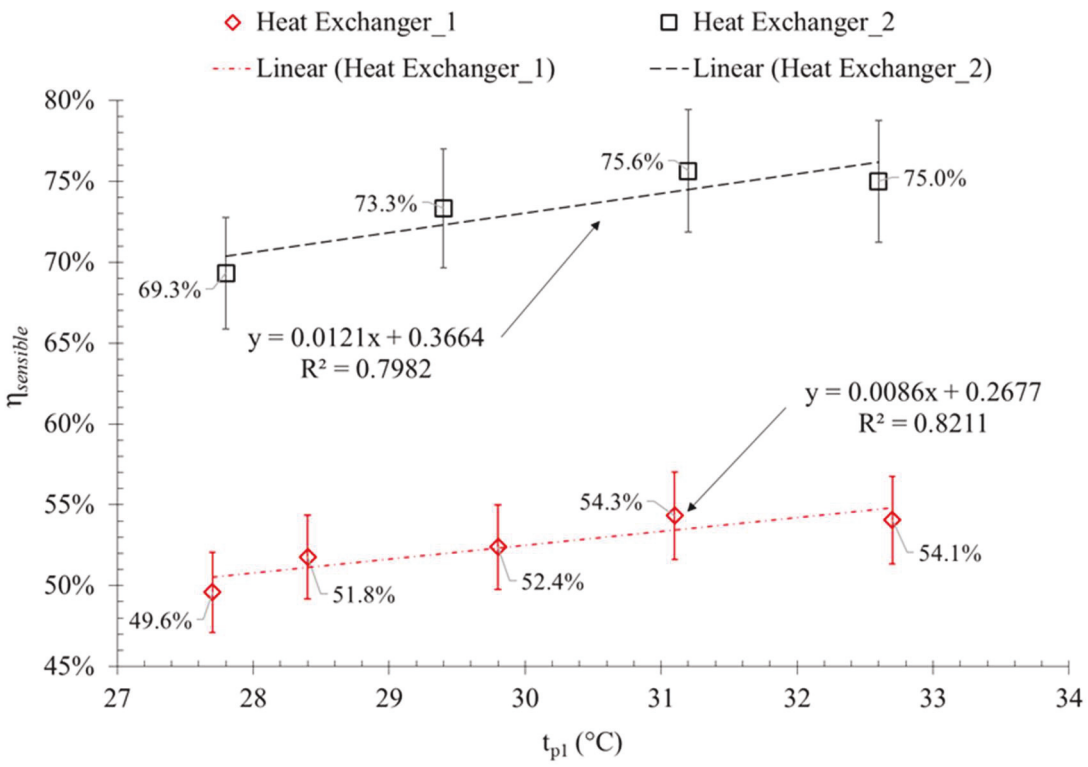

Figure *4.2* are:

$$\eta_S = 0.0086t_{p1} + 0.0.2677 \qquad \text{For HX\_1} \qquad \textbf{(4.9)}$$

$$\eta_S = 0.0121t_{p1} + 0.3664 \qquad \text{For HX\_2} \qquad \textbf{(4.10)}$$

The plate surface with dimpled geometry in HX2 resulted in a higher sensible efficiency than HX1 with the increase of the inlet temperature of the primary air. However, the material properties may result in a negative impact on the heat exchanger performance at a high inlet temperature of the primary airflow in HX2.

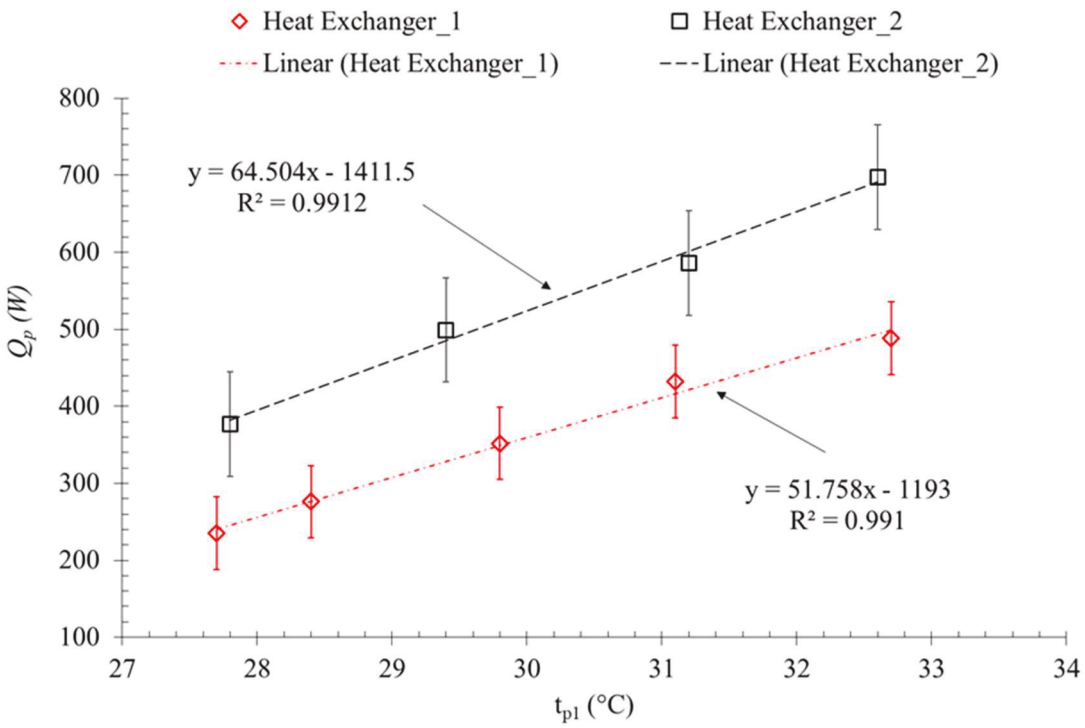

Figure 4.3. Effect of the inlet temperature of the primary airflow on cooling capacity

The variation of cooling capacity evaluated by the heat rejected by the primary airflow with the inlet temperature of the primary airflow. The heat rejected by the primary air, or the cooling capacity ($\dot{Q}_p$), were calculated by **Equation 4.4**. The effect of the inlet temperature of the primary airflow on cooling capacity is presented in

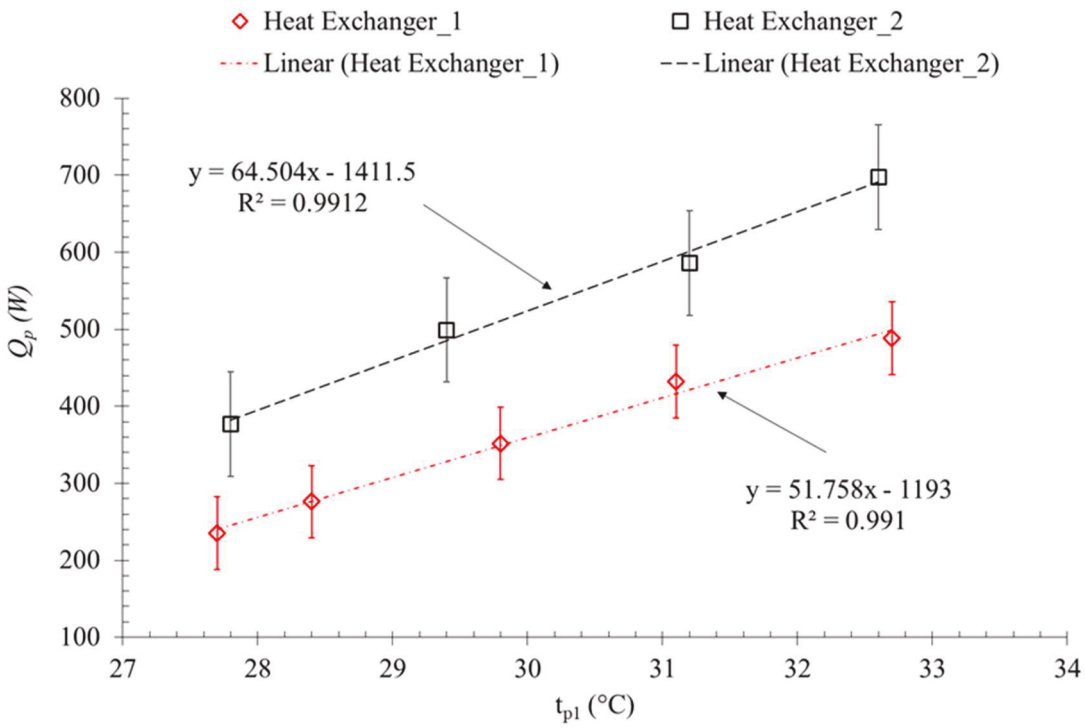

Figure *4.3* As shown in

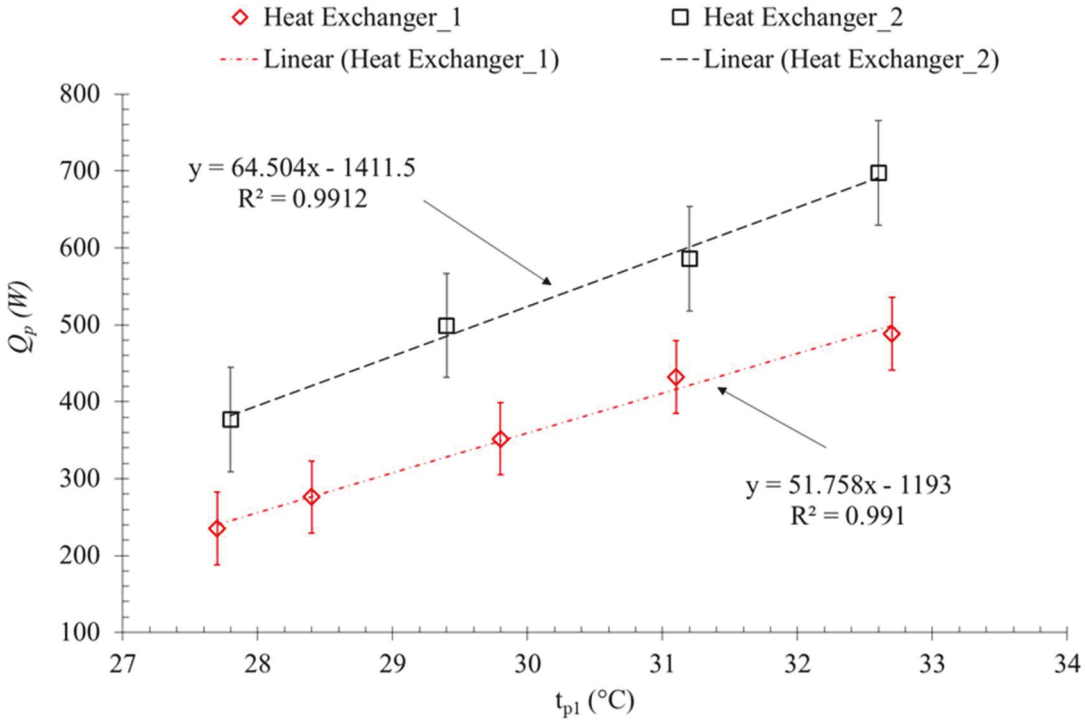

Figure *4.3*; the cooling capacity of HX1 is only 50-60% of that of HX2. In both heat exchangers, the cooling capacity is proportional to the inlet temperature of the primary airflow. For HX1, the cooling capacity was almost doubled from 235 W to 488 W when 5 °C increases the inlet temperature of the primary airflow from 27.7 °C to 32.7 °C.

Meanwhile, the primary air cooling capacity was increased significantly by 85% from 433 W to 820 W in HX2. Corresponding to the results of sensible efficiency,

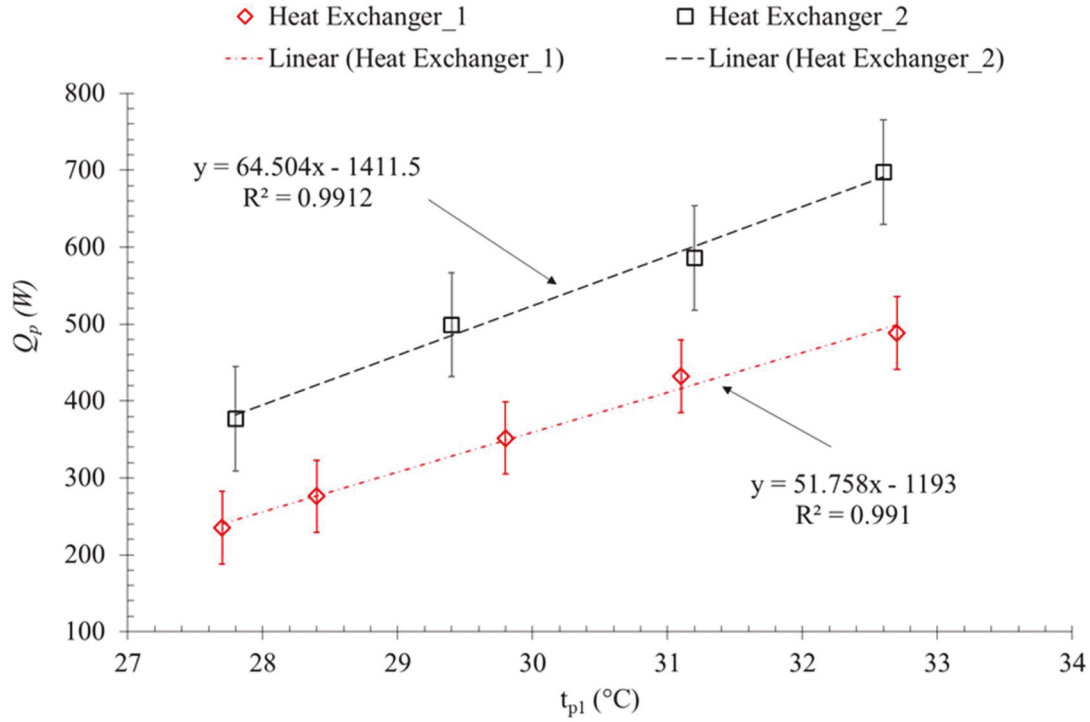

Figure *4.3* shows that the cooling capacity increases with the increase of the primary air inlet temperature, more quickly in HX2 than in HX1.

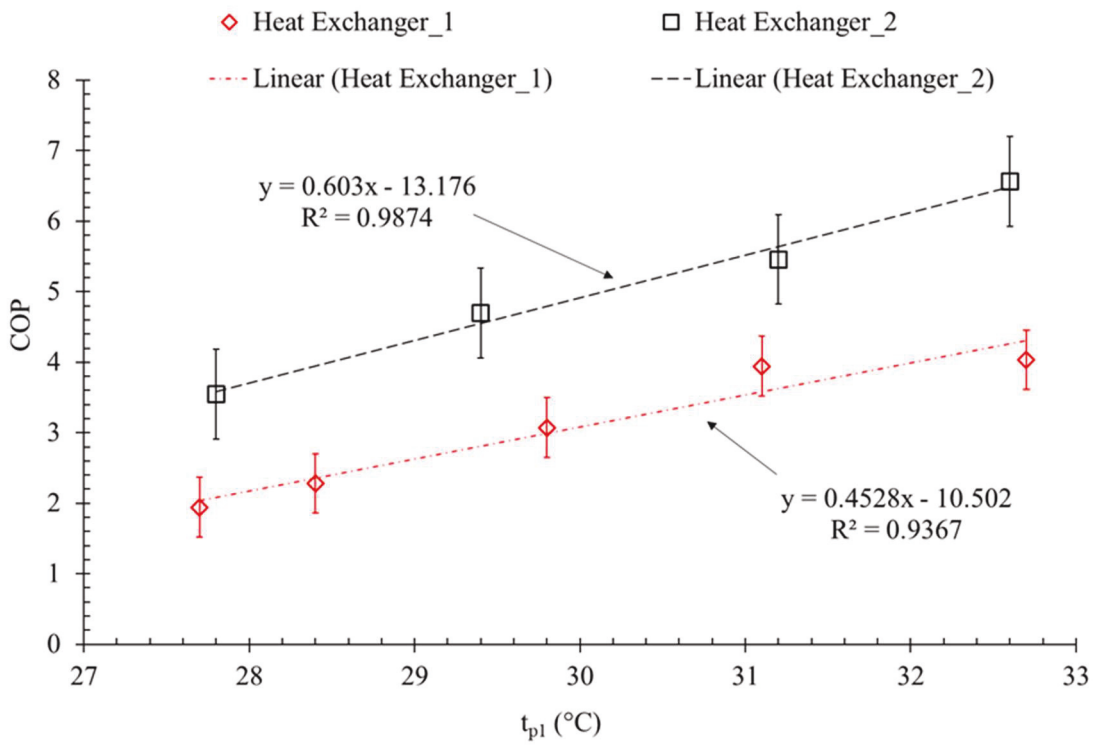

Figure 4.4. The variation of COP with the inlet temperature of the primary airflow

The primary air inlet temperature was found to have a positive impact on the heat exchangers cooling capacities. The inlet temperature variation at constant air velocities required no additional electrical power consumption by the system. Accordingly, at higher t_{p1} the systems performance increase as shown in **Figure 4.4**. The maximum COP value between the two systems was around 6.6 when HX2 operated at 32.6 ºC primary air inlet temperature with maximum fans speed. On the other side, the lowest COP was 1.9 for HX1 when the system operated at t_{p1} of 27.7 ºC.

As presented in **Figure 4.4**, the COPs values for HX1 increased from 1.9 at t_{p1} of 27.7 ºC to 4 as the temperature increased to 32.7 ºC. While HX2 COP increased from 3.5 at 27.8 ºC to 6.6 when t_{p1} increased to 32.6 ºC. From **Figure 4.4**, we can notice that the COP graph slopes for HX1 and HX2 were almost a tuned. The COPs for HX2 are higher despite the lower fans power consumption in HX1 system.

4.6. Effects of air velocity on the HRV unit performance

This section presents the comparison between the two heat exchangers performances under variable airflow velocity at fixed inlet parameters (t_{p1}= 29.3 ± 0.7 ºC, t_{s1}= 22.8 ± 0.5 ºC). The experimental results of the comparison are presented with a variation of both the primary air velocity v_{p1} and the secondary air v_{s1}.

The variation of the sensible efficiency, $\eta_{.S}$ with the inlet velocity of the primary airflow, v_{p1} shown in **Figure 4.5** In general, the sensible efficiency of HX2 is 8-10% higher than that of HX1. As discussed above, this is mainly because the complicated geometry in HX2 increases the surface area and generates more turbulent flow for enhancing the heat transfer.

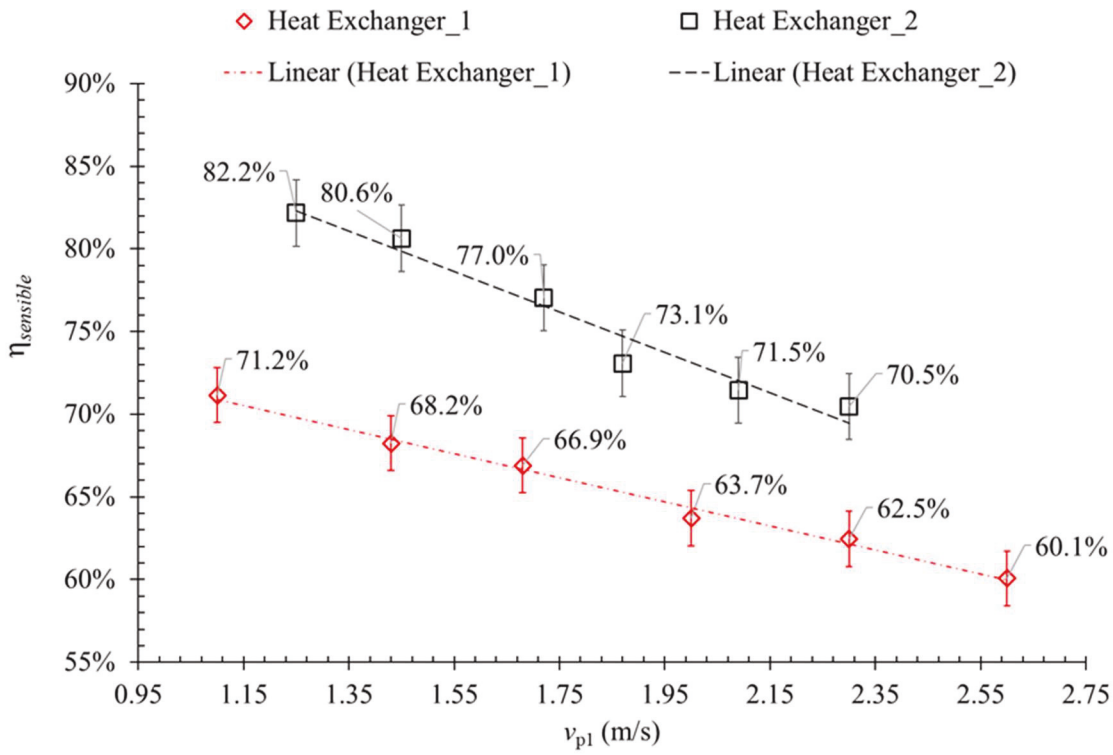

Figure 4.5. The inlet velocity of the primary air impact on the sensible efficiency

As shown in **Figure 4.5**, sensible efficiency reduces linearly with the increase of v_{p1}. The sensible efficiency of HX2 decreases by approximately 12.5% as the primary air inlet

velocity is increased from 1.25 m/s to 2.3 m/s. The highest $\eta_{.S}$ occurs at the lowest v_{p1}. In HX1, as v_{p1} is increased from 1.1 m/s to 2.6 m/s, the η_S of HX1 is reduced from 71.2% to 60.1%. That is easy to understand and explain, as the increased velocity of the airflow reduces the time for heat transfer in the heat exchanger. However, it also increases the Reynolds number and may generate a more turbulent flow.

Figure 4.6 shows the variation of sensible efficiency ($\eta_{.S}$) with the secondary airflow inlet velocity. As shown in **Figure 4.6**, that in contrast to the primary air velocity effect, the higher secondary air velocity, the higher system sensible efficiency. The HX1 sensible efficiency increased from 45.5% to 62.2% as the v_{s1} increased from 1.2 m/s to 2.8 m/s. The trend line slope for HX2 indicates that the change in velocities has a higher impact on the performance than in HX1. The HX2 sensible efficiency increased by approximately 20% as the velocity increased from 1.23 m/s to 2.29 m/s.

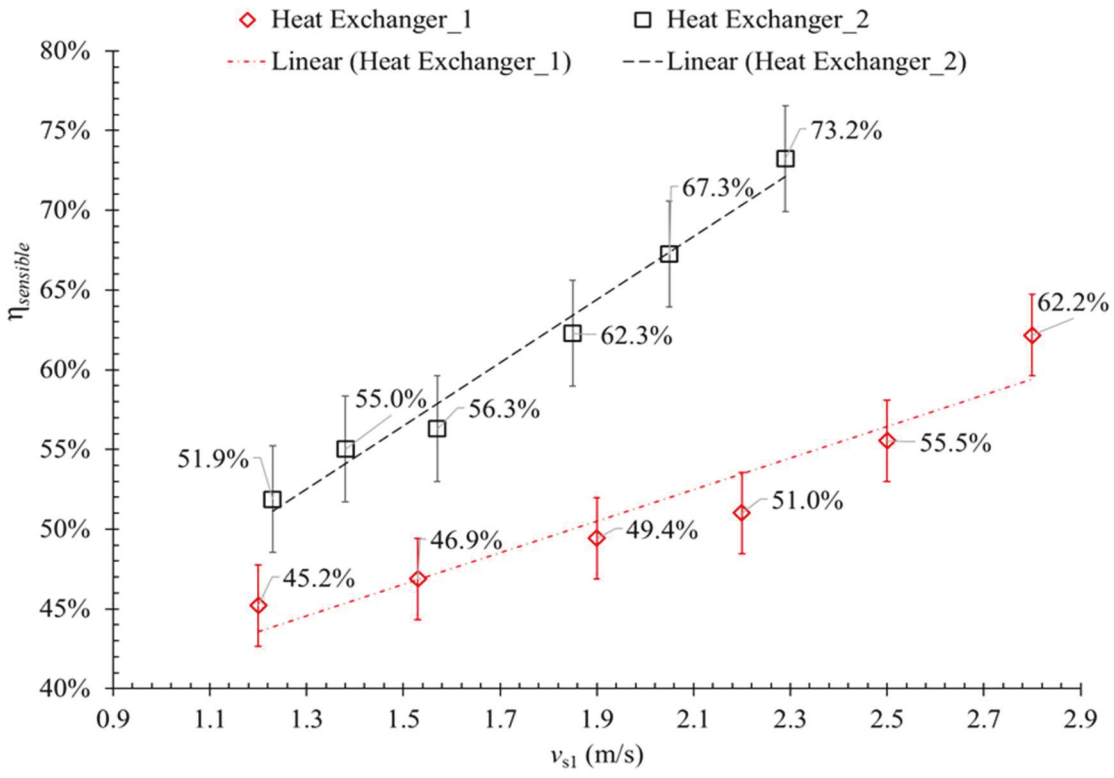

Figure 4.6. The inlet velocity of the secondary air impact on the sensible efficiency

The higher secondary air velocity effect in cooling mode is opposite to the case of HRV heating mode. In heating mode, where the secondary air is the hot stream, increasing the v_{s1} resulting in a decrease in the sensible efficiency of the HRV system (Liu et al. 2016). On contract in cooling mode the higher v_{s1} the higher $\eta_{.S}$ as investigated in this work and other references (Chen, Yang & Luo 2016a). Decreasing the secondary air velocity, will results in a lower turbulence inside the channels and increase the time required by the air to pass the channel, resulting in a poor convection heat transfer between the air stream and the plate surface. The HX2 performance response to the increased velocity at a higher rate due to the generation of vertices and higher Reynolds number (Dvořák & Vít 2015).

As described in the energy equations, the reduced difference between t_{p1} and t_{p2} or between h_{p1} and h_{p2} reduces the cooling capacity and the sensible efficiency. As cooling capacity is also dependent on the mass flow rate of the air, increasing the velocity of the airflow increases the mass flow rate, $\dot{m}$, of the air passing through the heat exchanger. Accordingly, increasing the primary air velocity will increase the primary air mass flow rate, $\dot{m}_P$ and consequently increasing the cooling capacity, $\dot{Q}_p$, based on the heat rejected by the primary airflow.

Figure 4.7 shows the linear function between the cooling capacity and the inlet velocity of the primary airflow (v_{p1}). As shown in **Figure 4.7**, the cooling capacity is increased by approximately 160 W from 227.1 W to 388.4 W when v_{p1} is increased from 1.1 m/s to 2.6 m/s in HX1, and $\dot{Q}_p$ is increased from 278.2 W to 411.8 W when v_{p1} is increased from 1.25 m/s to 2.3 m/s in HX2.

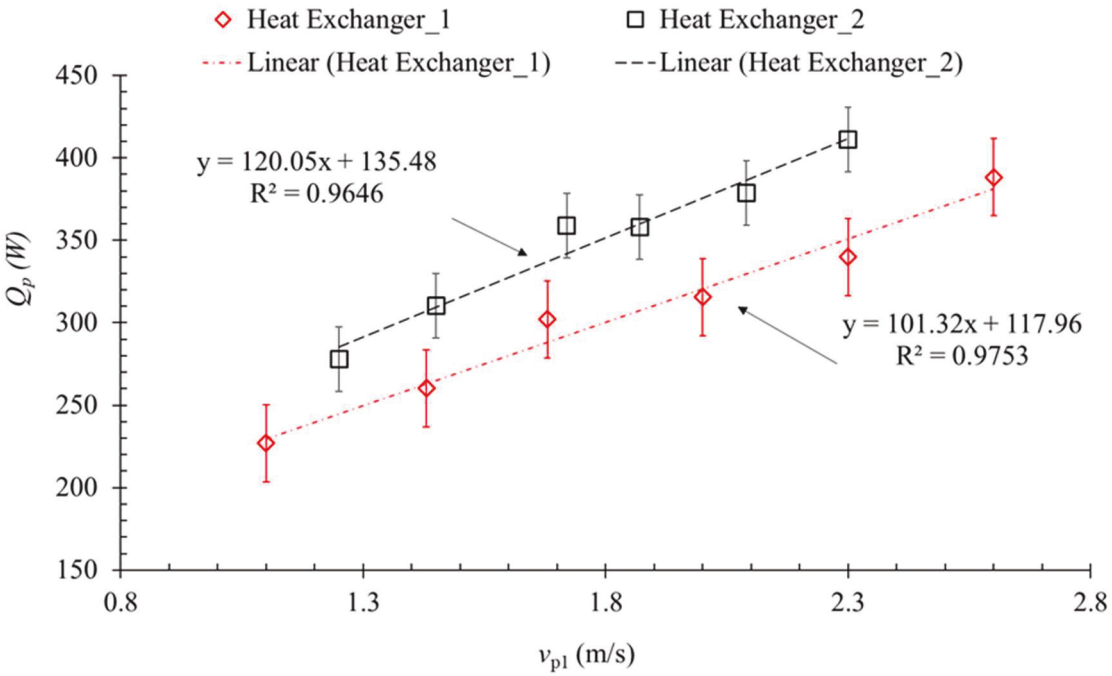

Figure 4.7. Effect of the inlet velocity of the primary airflow on cooling capacity

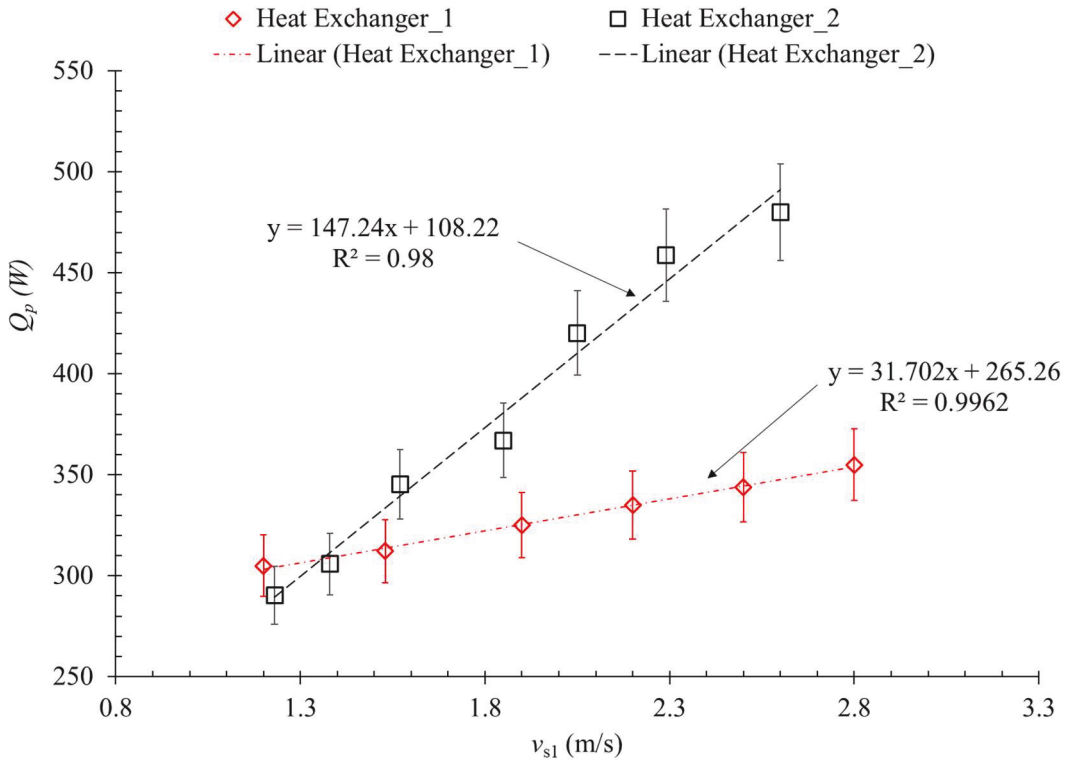

Figure 4.8. Effect of the inlet velocity of the secondary airflow on cooling capacity

The systems tested under constant v_{p1} and altered inlet secondary air velocity, v_{s1} values to study the influence on the cooling capacity. The results presented in **Figure 4.8** show insignificant effect of v_{s1} on the cooling capacity in HX1, with the only difference of 65 Watts between the maximum and minimum cooling capacity values (290.3 Watt at 1.2 m/s and 355.4 Watt at 2.8 m/s). However, with the same variation of v_{s1}, **Figure 4.8** shows the strong effect of v_{s1} on the cooling capacity in HX2, as the cooling capacity increased from 290.2 Watts to 458.7 Watts.

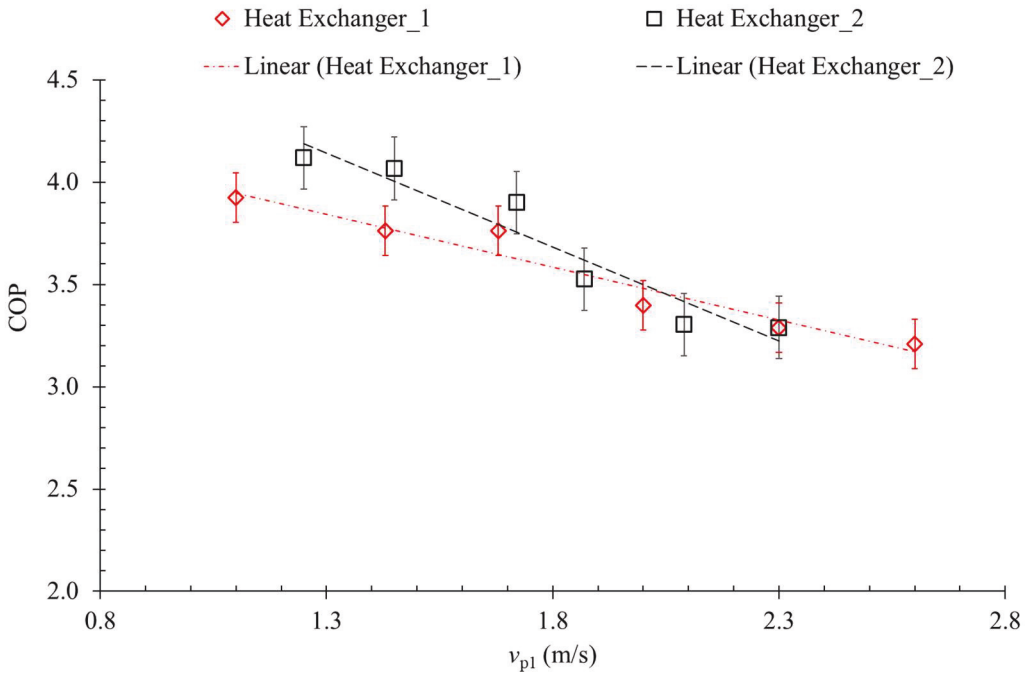

Figure 4.9. Variation of COP with the inlet velocity of the primary airflow

Figure 4.9 shows the variation of COP with the inlet velocity of the primary airflow, v_{p1}. As shown in **Figure 4.9**, the COP decreases with the increase of v_{p1} but linearly in HX1 and nonlinearly in HX2. As the cooling capacity is a linear function of v_{p1}, the nonlinear function between the COP of HX2 and v_{p1} is mainly due to the nonlinear variation of the primary fan power with v_{p1} in HX2 as shown in **Figure 3.19**.

Figure 4.9 also shows that the COP of HX2 is higher than that of HX1 when the v_{p1} is increased up to 1.8 m/s. With v_{p1} further increased to 2.1 m/s, the COP of HX2 is reduced to be 3.3, which is less than that of HX1. That is mainly due to the fan power increased more quickly in HX2 than that in HX1. Airflow more turbulent in HX2 may due to the resistance increase the higher fan power required by HX2 than that by HX1.

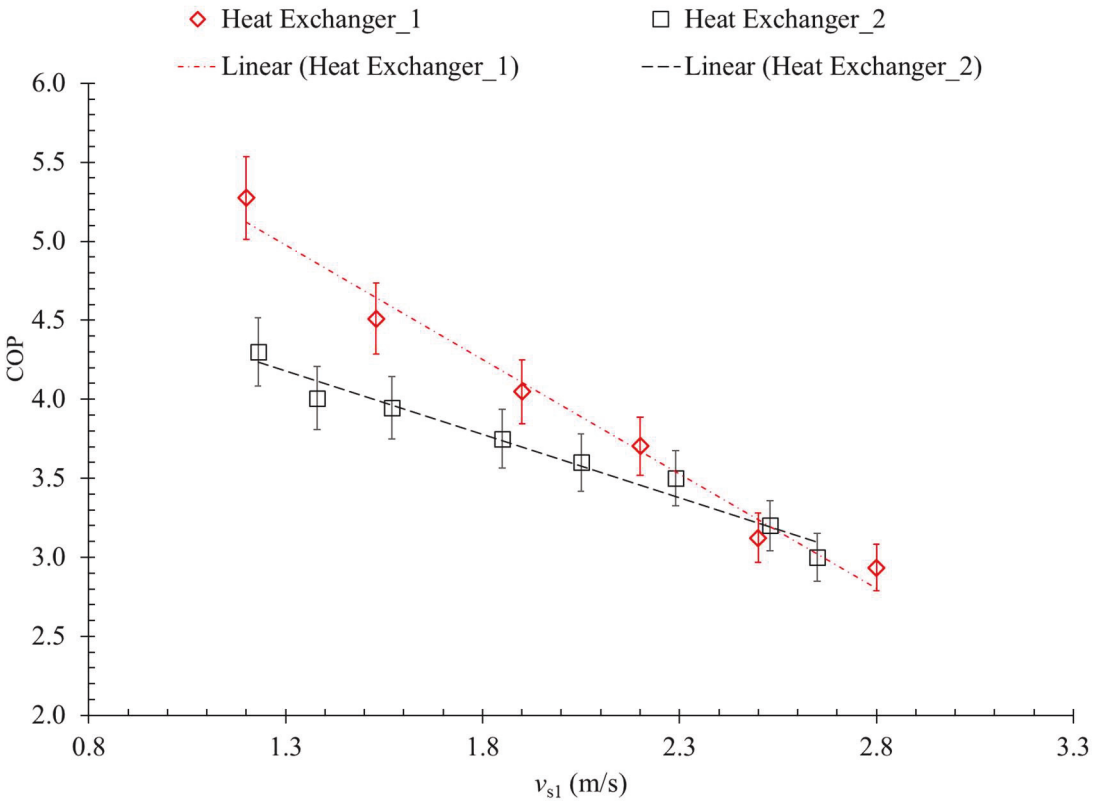

Figure 4.10. Variation of COP variation with the inlet velocity of the secondary airflow

Figure 4.10 shows the variation of COP with the velocity of the secondary airflow. As shown in **Figure 4.10**, as v_{s1} increase, the COP decreases linearly in HX1 and in HX2. **Figure 4.10** also shows that the HX1 COP is higher when the v_{p1} is less than 1.8 m/s. At v_{s1} of 1.2 m/s, the COP of HX1 was 5.3 compared to around 4.3 for HX2. As v_{s1} increases up to 2.2 m/s, the COP for two models becomes equal with around 3.5. As the velocity increased above 2.3 m/s the COP change performance lines for HX1 and HX2 becomes nearly tuned, although the cooling capacity of HX2 is higher at elevated v_{s1} and

that mainly due to the secondary fan power at higher v_{s1}. The secondary air velocity relatively lower influence of on the cooling capacity in HX1 (**Figure 4.8**) interpreted into lower COP at higher velocities.

4.7. Summary

Two fixed-plates heat exchangers with a flat surface and dimpled surface have been constructed and tested. The airflow arrangement was based on the hexagonal shape heat exchanger that provides a quasi-counter-flow over the plate surface. The novel design of the dimpled geometry was design to maximise the airflow turbulence and thus enhance the heat transfer rate across the plate. An experimental facility described in Chapter 3 was utilised to investigate the effect of the plate surface geometry on the heat exchanger performance as an HRV system in the cooling mode under varying inlet conditions.

The HRV system performance was highly influenced by the plate surface geometry. The effect of the dimples as turbulence generators has resulted as an increase of 20% in the sensible efficiency. The air inlet velocities effect on the HRV performance was investigated; it was found that sensible efficiency is proportional relative to the secondary air velocity. In contrast, the higher primary air velocity resulted in a drop in sensible efficiency.

Chapter 5

Experimental Study of a Novel Water-Spraying Configuration in Indirect Evaporative Cooling

5.1. Introduction

The literature review shows clearly a lack of research on water spraying systems and significant need for developing advanced water distribution systems in order to improve the IEC performance. Extensive studies are required to investigate the influence of nozzle angles, sprayer mass flow rate, spray angles, and water temperature on the overall performance of the IEC systems.

In order to meet the above needs, a novel water spraying arrangement was proposed in the present study. The HX1 described in section 3.4.B was employed as an IEC unit. The investigated system is an IEC with internally located nozzles for spraying water in multiple directions (vertically, horizontally and diagonally) within the wet channel to increase the wettability of the plates. Experimental results were analysed to compare the IEC performance under different climate conditions in three different water spray configurations: (1) external spraying mode, (2) internal spraying mode and (3) mixed spraying mode. The evaluation parameters adopted in this experiment were based on ANSI/ASHRAE Standard 143-2015 (ANSI/ASHRAE 2015) and references in the literature (Chen, Yang & Luo 2016b; Duan et al. 2016; Lin et al. 2017a).Chapter 5 presents the experimental results of an energy recovering ventilation IEC, promoting the novel internal spraying mode.

5.2. Data analysis and criteria for assessing the performance

Experiments were conducted using procedures specified in ASHRAE Standards. Four measuring stations as referenced in ASHRAE 84-2013 (ASHRAE 2013) are located at the heat exchanger entrances and exits to measure the dry bulb temperature, wet bulb temperature and air velocities. Air sampling devices measured air temperature (t_{DB} and t_{WB}). A variable speed controller was used to regulate the two centrifugal fans speed. A highly sensitive Testo-480 hot wire anemometer measured the velocity with a telescopic probe. The velocity measurements process was based on the Tchebycheff method (ASHRAE 2008).

The testing of different water distribution arrangements and varying the water mass flow rate are the main objectives of this experiment. A DC water pump with a variable controller was applied to control the water mass flow rate for fitting the capacities of the nozzles in the specified arrangements. The water mass flow rate was set to 23 g/s, 25 g/s and 50 g/s for the external spraying mode, internal spraying mode and the mixed spraying mode, respectively. The nozzles supplied water temperature was in the range of 19-22 °C through the experiment; the water temperature represents the sump water temperature, which is not a controlled parameter. The power consumption of the test facility was measured directly with a power meter.

The following parameters specified in the ANSI/ASHRAE Standard 143-2015 (ANSI/ASHRAE 2015) were measured and recorded at a sample rate of 0.1 Hz in the experiments. The following measurements were recorded:

1. Primary air:
    a. The dry-bulb temperature [°C] at the inlet and outlet of dry channels.
    b. The wet-bulb temperature [°C] at the inlet and outlet of dry channels.

2. Secondary air:
    a. The dry-bulb temperature [°C] at the inlet and outlet of the wet channel
    b. The wet-bulb temperature [°C] at the inlet and outlet of the wet channel.
3. Pump power consumptions [Watts].
4. The fan power consumption [Watts].
5. The water temperature [°C] at the water sump.

Unlike the dry mode ERV system, the sensible The wet-bulb efficiency under a non-condensation state of the primary air stream (ANSI/ASHRAE 2015) was calculated with the recorded temperature data. **Equation 5.1** defines the wet-bulb efficiency:

$$\eta_{WB} = \frac{t_{p1} - t_{p2}}{t_{p1} - t_{s1\_wb}} \quad \textbf{(5.1)}$$

Where $\eta_{.WB}$ is the wet-bulb efficiency, t_{p1} and t_{p2} are the primary air dry-bulb temperature at the inlet and the outlet, respectively, and t_{s1_wb} is the inlet secondary wet-bulb temperature.

The cooling capacity is a key factor in evaluating the performance of an IEC system. The sensible cooling capacity [$Q_{sensible}$] is defined by the sensible heat transformed from the primary airflow to the secondary airflow. We calculate the sensible cooling capacity:

$$Q_{sensible} = \dot{m}_p . c_{pa} . (t_{p1} - t_{p2}) \quad \textbf{(5.2)}$$

The total power consumption in an IEC system is the sum of the power supplied to the primary air fan [P_{fan_p}], secondary air fan [P_{fans}] and the water pump [P_{pump}]. The consideration of the power consumed by the instruments [$P_{instruments}$] in the IEC

analysis is recommended by the ASHRAE (ANSI/ASHRAE 2015) test procedure. The total power [P_{total}] is calculated with **Equation 5.3**:

$$P_{total} = P_{fan\_p} + P_{fan\_s} + P_{instruments} + P_{pump} \quad \textbf{(5.3)}$$

Where P_{fan_p} and P_{fan_s} are the power for driving the primary and secondary path fans, P_{pump} is the water pump power consumption and $P_{Instrument}$ is the power consumed by the sensors and data acquisition system. The power measurement method described in **Section 3.5.F**.

Equation 5.4 defines the coefficient of performance [COP]. The analysis of this work emphasises sensible cooling effectiveness.

$$COP = \frac{Q_{sensible}}{P_{total}} \quad \textbf{(5.4)}$$

Based on the supply duct cross-sectional area, air velocity [v] and the air density [ρ], the air volume flow rate [$\dot{V}$] and mass flow rate [$\dot{m}$] are calculated by **Equations 5.5** and **5.6**, respectively:

$$\dot{V} = v.A_D \quad \textbf{(5.5)}$$

$$\dot{m} = \dot{V}.\rho \quad \textbf{(5.6)}$$

An energy balance between the primary and secondary air was conducted to verify the accuracy and consistency of the experiment. The energy balance in the IEC systems is the comparison between the enthalpy changes in the primary air and secondary air obtained from **Equations 5.7** and **5.8** (Wang et al. 2017). **Figure 5.1** shows the percentage of energy changes in the two air streams is within 10%.

$$Q_p = \dot{m}_p(h_{p1} - h_{p2}) \quad \textbf{(5.7)}$$

$$Q_s = \dot{m}_s(h_{s2} - h_{s1}) \quad \textbf{(5.8)}$$

The experimental results will be presented and discussed to show the effects of three water spraying modes on the IEC performance, which is evaluated by the temperature drop of the primary airflow, wet-bulb efficiency [$\eta_{.WB}$], cooling capacity [$Q_{sensible}$], and the overall system COP at different inlet temperature and velocity of the primary airflow.

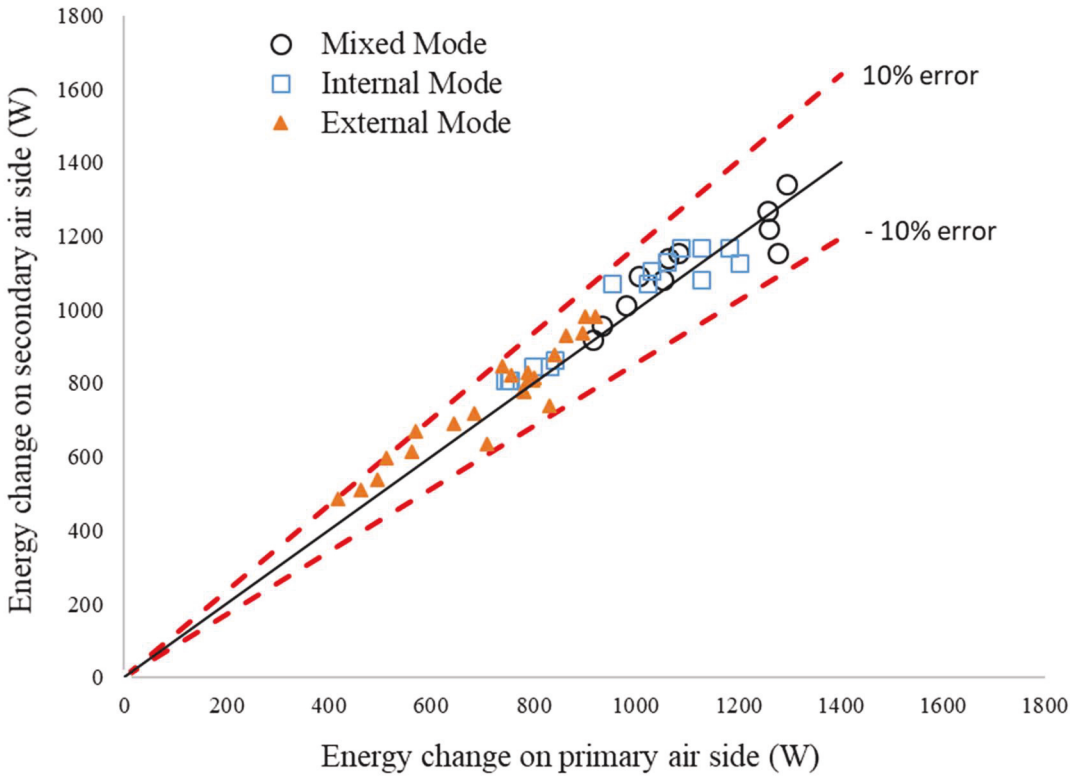

Figure 5.1. Energy balance for primary and secondary air streams

5.3. Effect of water spraying mode on IEC performance at varied primary air inlet temperature

The IEC unit was operated with the primary air inlet temperature t_{p1} varied from 26.9 °C to 36.6 °C to compare the effects of three water-spraying modes on the performance of IEC. **Figure 5.2** shows the water-spraying mode and the effect of the primary air inlet temperature on the primary air temperature drop [Δt_p]. In general, as shown in **Figure**

5.2, the t_{p2} and primary air temperature depression, $(t_{p1} - t_{p2})$ or Δt_p increases with the increased t_{p1}.

Figure 5.2 shows the linear regression fitting equations for the variation of Δt_p with t_{p1}. The correlation coefficients close to 1.0 confirms that the variation of Δt_p with t_{p1} is linear. The small differences in the coefficients for the slope, 0.7126, 0.7722 and 0.7727 show that the three fitting lines are almost in parallel. The mixed mode is most effective in cooling the primary airflow, and the external mode is least, as shown in **Figure 5.2**. Quantitatively the cooling effect represented by the temperature drop of the primary airflow in the mixed mode is 1.7 °C more than that in the internal mode and 2.85 °C more than that in the external mode.

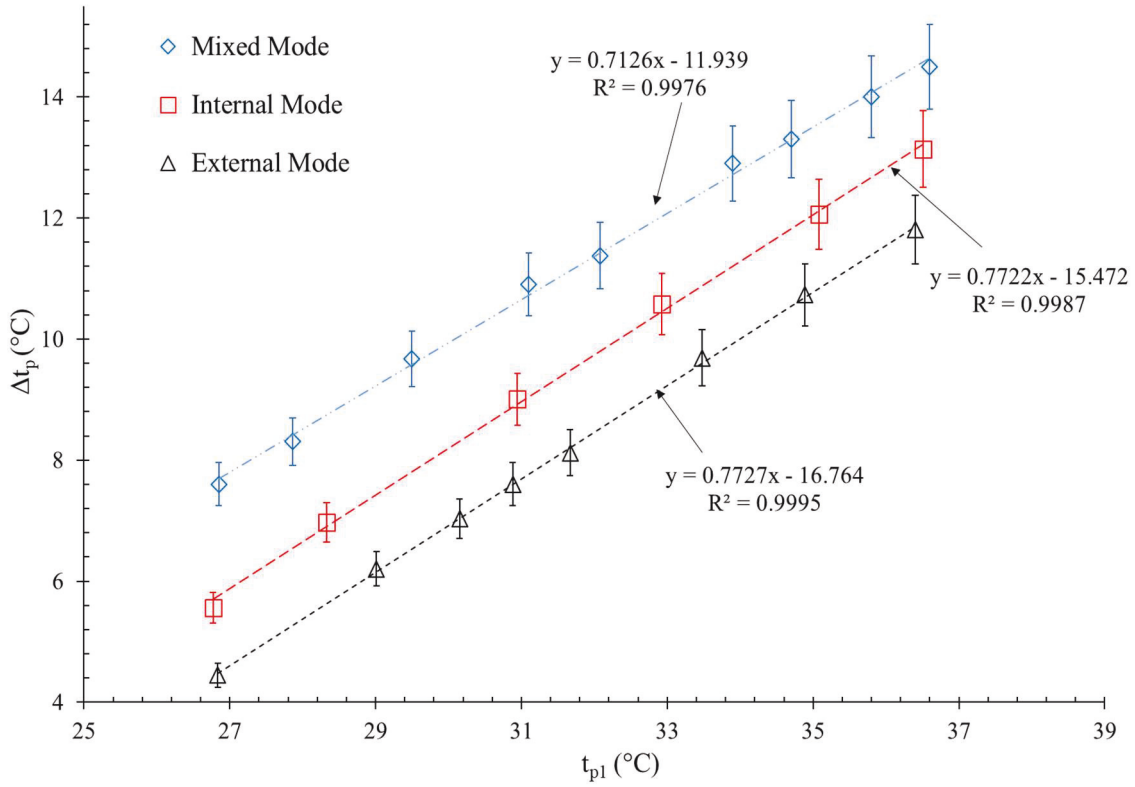

Figure 5.2. The water-spraying mode and primary air inlet temperature effect on the primary air temperature drop

In the comparison of the IEC system performance under the three operation modes, **Figure 5.2** shows that in the mixed mode the primary air temperature depression [Δt_p] is almost doubled from 7.1 °C to 13.9 °C as t_{p1} increased from 26.9 °C to 36.6 °C. Meanwhile, for the external mode, the Δt_p increased from around 5 °C to 12.6 °C as t_{p1} increased from 26.8 °C to 36.4 °C. The internal mode performed more efficiently in terms of Δt_p than the external mode, but less than the mixed mode.

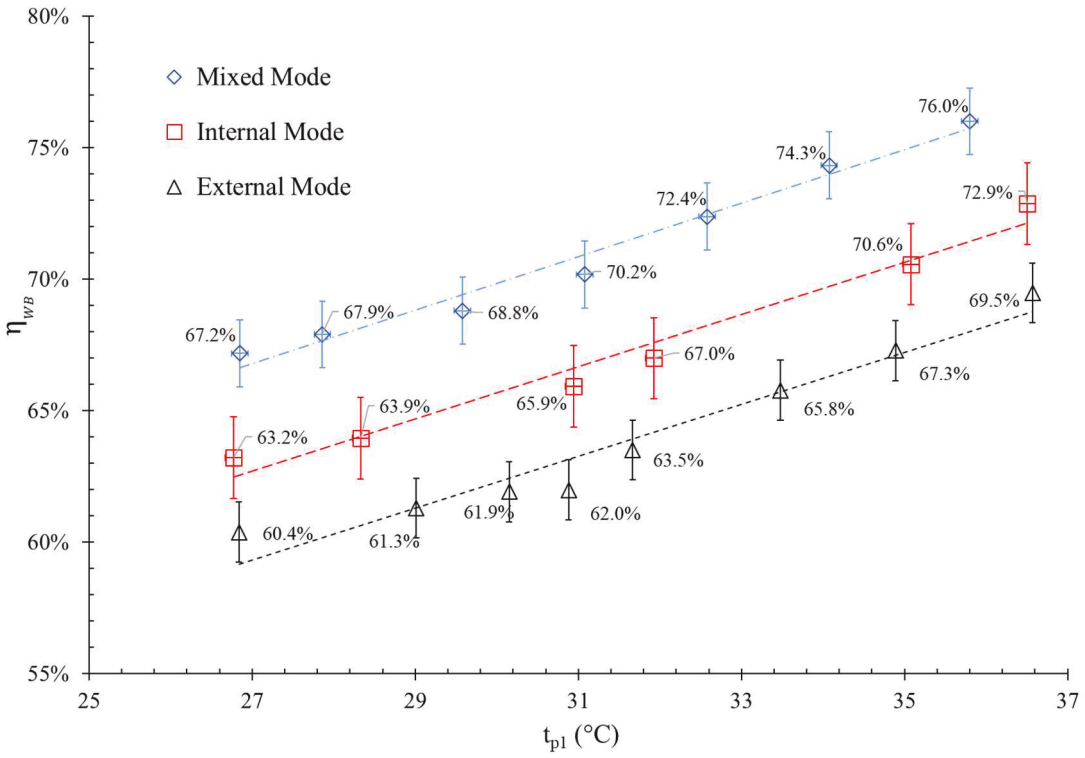

Figure 5.3. The water spraying mode and primary air inlet temperature effect on wet-bulb efficiency ($\eta_{\cdot WB}$)

In steady conditions of the secondary inlet airflow, t_{s1} and RH_{s1}, the air's temperature decrease Δt_p indicate an increase in the system wet-bulb efficiency [η_{WB}] calculated by Equation 5.1. As shown in **Figure 5.3**, the η_{WB} values at a primary air inlet temperature of about 27 °C are 60.0%, 63.0% and 67.0% in external mode, internal mode and mixed mode, respectively. As noticed in **Figure 5.3**, when the t_{p1} is increased from around 27 °C to approximately 31.0 °C, the η_{WB} efficiency is improved from 60.0% to 62% in

external mode, 63.2% to 65.9% in the internal mode and from 67.0% to 70.0% in the mixed mode correspondingly at t_{p1}= 31.0 °C. When t_{p1} is further increased to 36.0 °C, the η_{WB} is increased to 70% in the external mode, 73.0% in the internal mode and 76% in the mixed mode.

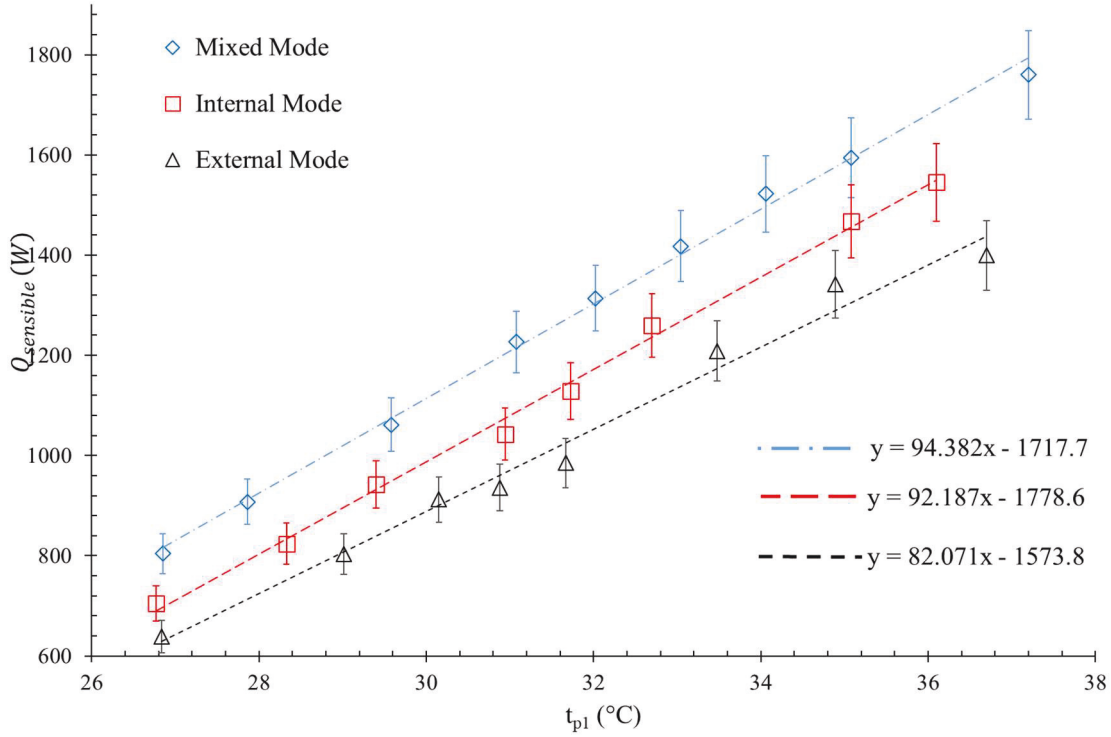

Figure 5.4. The water-spraying mode and primary air inlet temperature effect on sensible cooling capacity

Figure 5.4 shows the effect of three water spray modes on the sensible cooling capacity in the IEC system. As shown in **Figure 5.4**, in the internal mode the system cooling capacity is reduced from around 1.47 kW at t_{p1}= 35.1 °C to approximately 0.7 kW at t_{p1}= 26.8 °C. The cooling capacity of the internal mode is higher than that of the external nozzles spray arrangement at all t_{p1} values between 26 °C to 36 °C. As also presented in **Figure 5.4**, the mixed mode has the highest cooling capacity with a maximum cooling capacity of approximately 1.76 kW at t_{p1} of 37.2 °C and a minimum of 0.76 kW at t_{p1} of 26.9 °C. In summary, the highest cooling capacity values are 1.76 kW at t_{p1} of 37.2

°C for the mixed mode, 1.55 kW at t_{p1} of 36.1 °C for the internal mode, and 1.4 kW at t_{p1} of 36.7 °C for the external mode.

The COP calculated by Equation 5.4 is inversely proportional to the electrical power consumption of the system represented in **Equation 5.3**. The recorded data of electrical power were approximately 101 Watt for the mixed mode, 96 Watt for the internal mode and 94 Watt for the external mode. The different power consumption values were primarily caused by different pump power consumption required to circulate the water in each mode and the electrical power to drive the fans to keep constant velocity of the inlet airflow [v_{s1}].

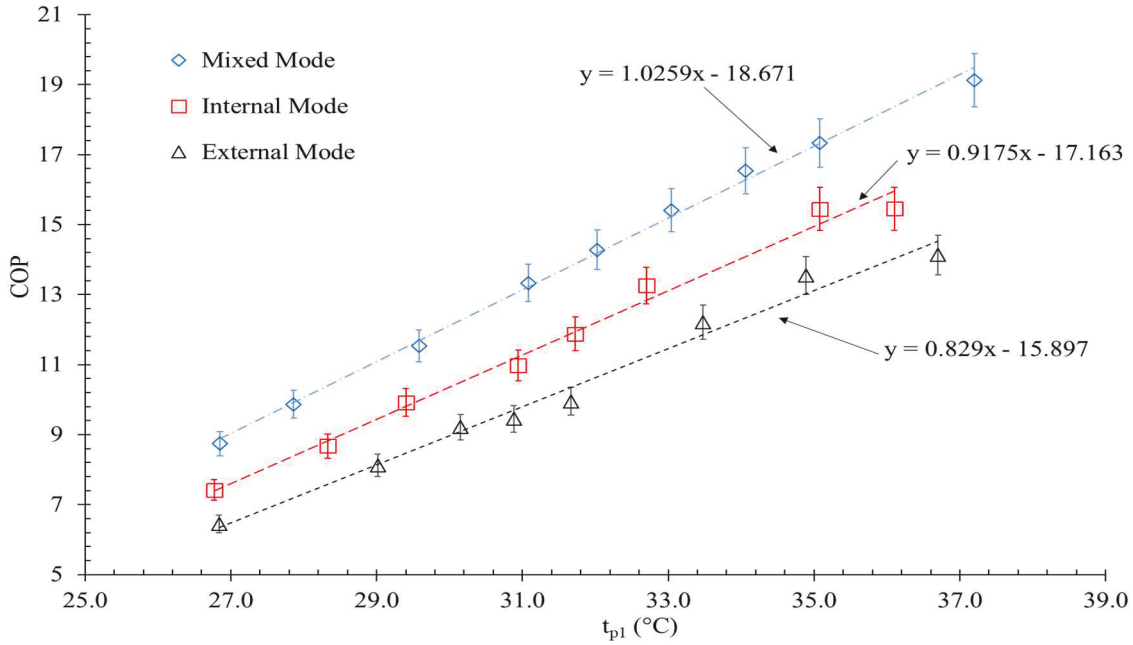

Figure 5.5. The water-spraying mode and primary air inlet temperature effect on IEC system COP

Figure 5.5 showed the COP of the IEC in the three modes of water spray when t_{p1} was varied from 26.9 °C to 36.6 °C. As shown in **Figure 5.5**, the COP of the IEC with the mixed mode is higher than that with the other two water spray modes. At t_{p1} of 35.1 °C, the COP with the mixed mode is 17.3; the internal mode is 15.4 and external mode is

13.5. The differences are mainly due to the differences in the cooling effect. The electrical power consumption of the mixed mode is the greatest, internal the second and external the least. Further increasing the t_{p1} to 37.2 °C, the COP of the IEC with mixed mode reached 19.2, indicating high cooling capacity of the experimental model.

5.4. Effect of water spray mode on IEC performance at a varied primary air velocity

The effect of the water spraying mode on IEC performance with a different primary air inlet velocity [v_{p1}] was investigated under a constant primary inlet temperature [t_{p1}] of 27.8 ± 1 °C, secondary air inlet temperature [t_{s1}] of 22.5 ± 0.7 °C, and secondary air inlet velocity [v_{s1}] of 2.68 ± 0.1 m/s. The primary air inlet velocity gradually reduced from the full speed of 2.85 m/s to around 1.5 m/s in five steps. The primary air temperature reduction [Δt_p] significantly increases with decreased primary air inlet velocity into the dry channels, as illustrated in **Figure 5.6**.

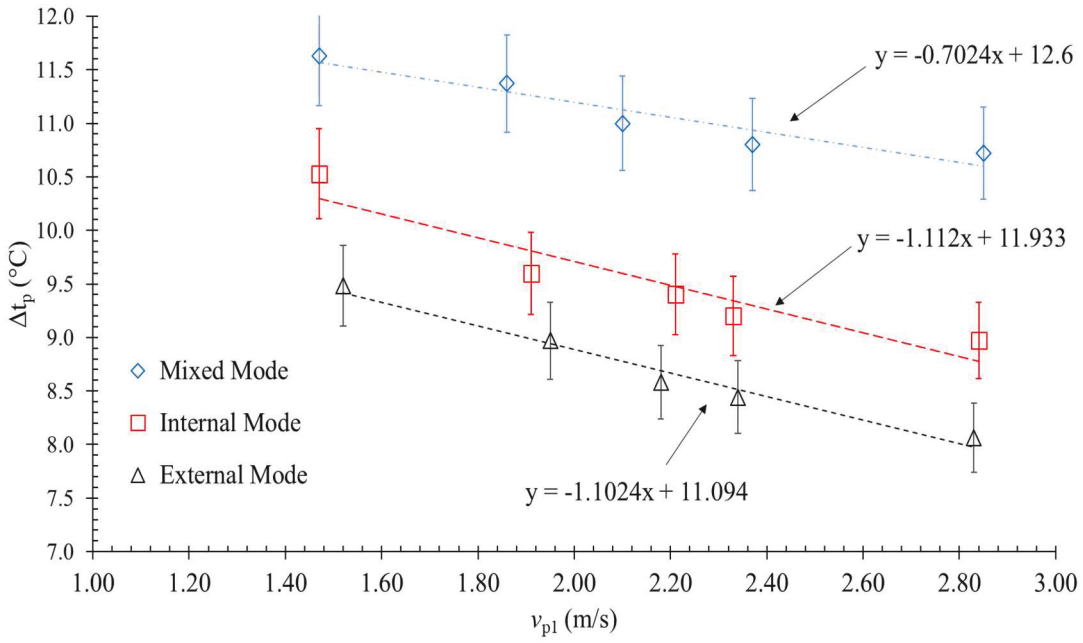

Figure 5.6. The water-spraying mode and primary air inlet velocity effect on the primary air temperature depression

As shown in **Figure 5.6**, Δt_p reduces from 11.7 °C to 10.7 °C as the velocity v_{p1} is increased from 1.47 m/s to 2.85 m/s in the mixed mode. Results of other modes show a stronger effect of the v_{p1} variation on Δt_p. The Δt_p decreases by 1.5 °C in the internal mode as the v_{p1} is increased from 1.47 m/s to 2.84 m/s and by 1.4 °C in the external mode as the v_{p1} is increased from 1.52 m/s to 2.83 m/s.

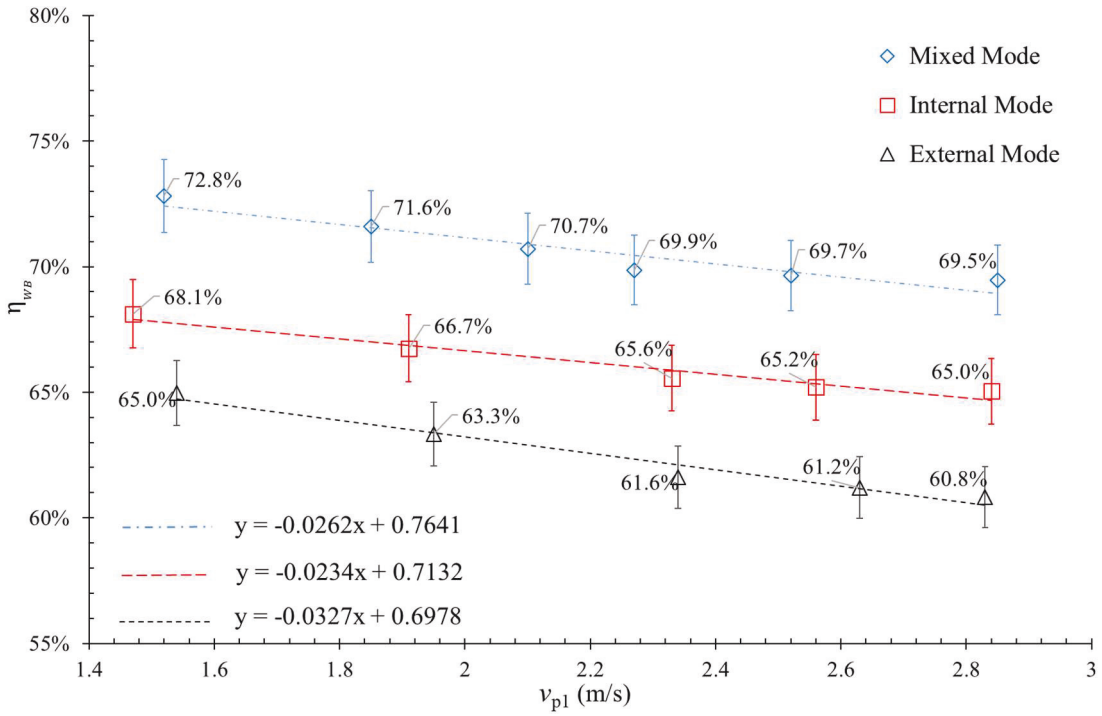

Figure 5.7. The water spraying mode and primary air inlet velocity effect on the wet-bulb efficiency (η_{WB})

Figure 5.7 shows the wet-bulb efficiency (η_{WB}) varied nonlinearly with the primary air velocity v_{p1} in three different water spray modes. As shown in **Figure 5.7**, the η_{WB} with the mixed mode is higher than that in the other two water spray modes. The η_{WB} with the external mode is the lowest, although the η_{WB} reduces with the increase of primary air velocity in all the three modes. That is mainly due to the reduction in the cooling effect per unit mass because of the increase in the primary air mass flow rate.

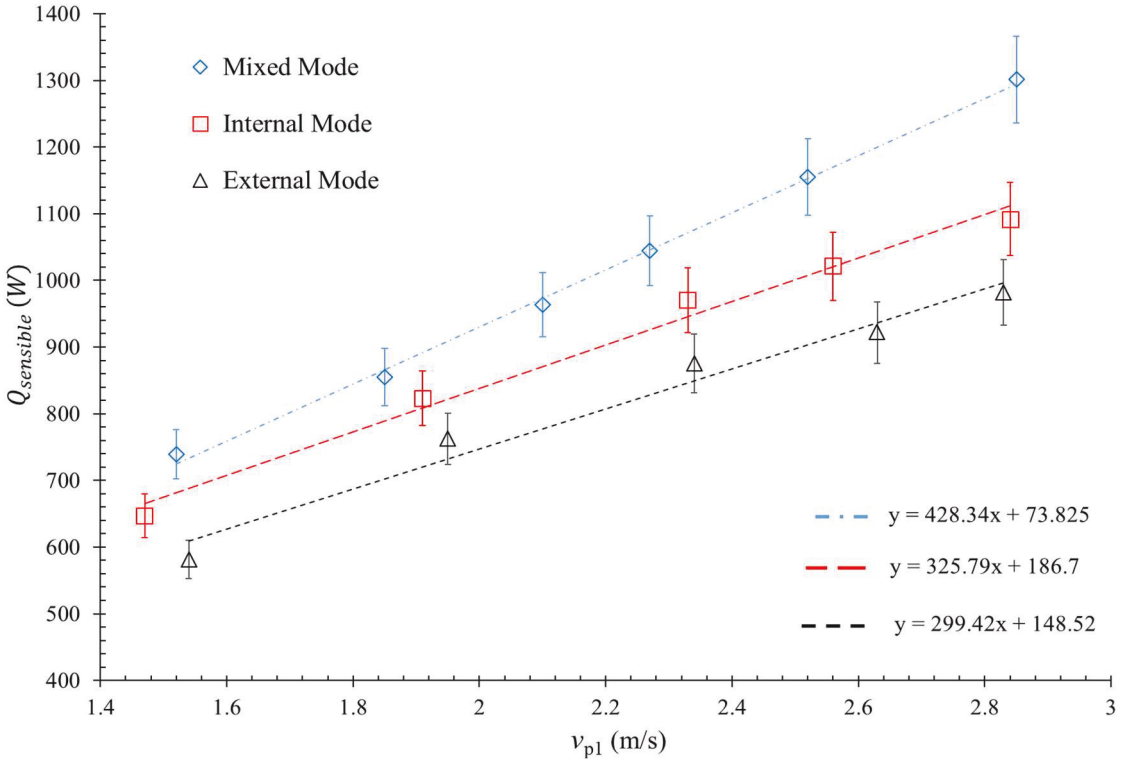

Figure 5.8. The water-spraying mode and primary air inlet velocity effect on the IEC cooling capacity

Figure 5.8 shows the sensible cooling capacity for three water spraying modes under variable primary air inlet velocity. This sensible cooling capacity represents the total cooling capacity of the IEC system because there is no latent heat transfer, as described previously. As shown in **Figure 5.8**, the higher primary air velocity results in higher volume flow rate at constant air inlet cross-sectional area, and that reflected as a higher cooling capacity at higher v_{p1} (refer to Equation 5.2). Increasing the v_{p1} caused a significant progression in the overall system cooling capacities.

Experimental results summarised in **Figure 5.8** reveal that in the mixed mode, increasing v_{p1} from around 1.45 m/s to 2.85 m/s caused an elevated cooling capacity of approximately 0.56 kW. This represents about 75% cooling capacity improvement compared to approximately 69% improvement in the two other operation modes (0.445 kW for the internal mode and 0.4 kW for external mode). The lower cooling capacity at

reduced v_{p1} values is linked to the principles of the convection heat transfer, where the convective heat transfer coefficient for air is proportional to the air velocity.

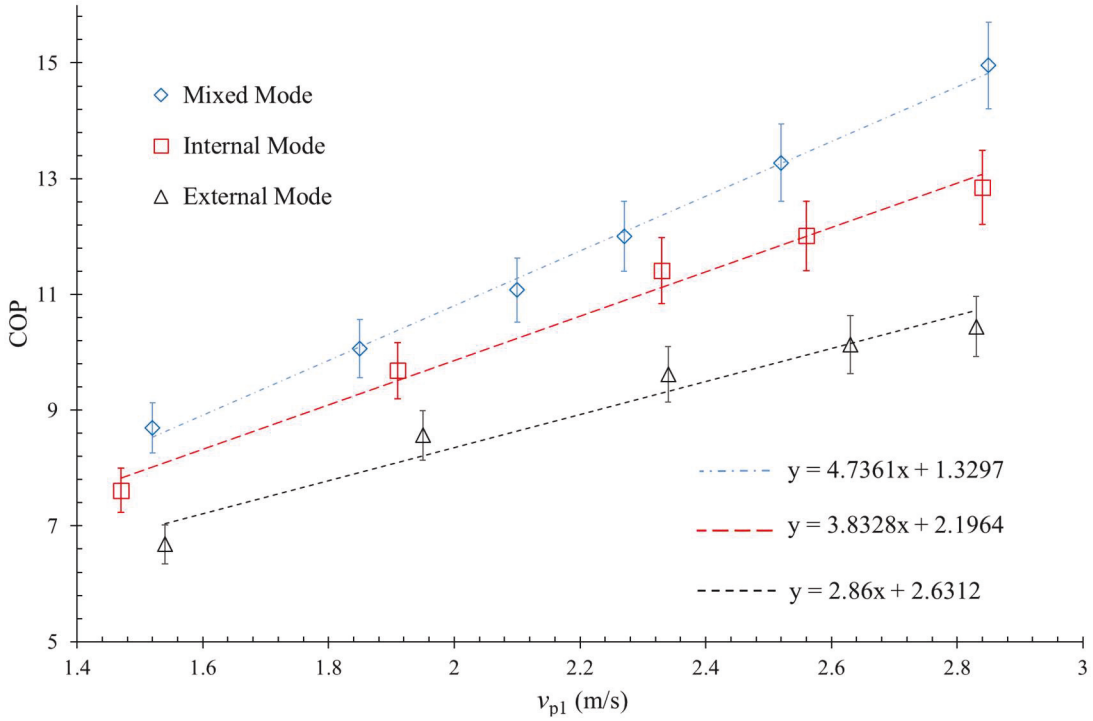

Figure 5.9. The water-spraying mode and the effect of primary air inlet velocity on the IEC system COP

As explained in section **3.8**, the power consumption is lower at lower fan speed and lower water pump flow rate, but this impact is irrelevant on the COP due to the high decrease in cooling capacity values. As indicated in **Figure 5.9**, the reduction in fan power consumption ran the system at close COP at lower fan speeds. In general, in the best case, the COP in the external mode decreased by more than 35% as the velocity v_{p1} reduced by approximately 1.45 m/s, while it declined by nearly 38% and 36% in mixed mode and internal mode, respectively. However, the COPs for the three different test modes were acceptable under most of the test conditions.

In summary, the changing of the primary air velocity v_{p1} had a significant effect on the IEC system performance. The system performance at higher v_{p1} was receded in terms of

absolute primary air temperature depression [Δt_p] and the wet-bulb efficiency [η_{WB}] but improved in terms of the sensible cooling capacity and COP. Decreasing the v_{p1} resulted in a significant drop in air mass flow rate, and that justify the decline in $Q_{sensible}$ despite the increase of Δt_p. Qualitatively, based on the performance indications, the mixed mode performance is optimal among the three operation modes.

5.5. Effect of water spray mode on IEC performance under varied secondary air velocity

The secondary air inlet velocity [v_{s1}] is a major parameter that effecting IEC performance. The increasing of the secondary air inlet velocity is expected to accelerate the water evaporation rate of the water film above the heat exchanger plate. To experimentally evaluate the three water spray modes effects on the IEC overall performance, the performance test parameters (i.e. primary air temperature depression, wet bulb efficiency, cooling capacity and coefficient of performance) inspected under four v_{s1} levels at constant v_{p1}, t_{p1} and t_{s1}. The v_{s1} is reduced from the full speed of approximately 2.7 m/s to around 1.25 m/s in four steps keeping the other operating conditions fixed at t_{p1}= 29.73 °C (Dry bulb), t_{p1wb} = 21.5 °C, t_{s1} = 23.1 °C and t_{s1wb} = 18.94 °C.

The effect of the water spray mode on primary air temperature depression at varied secondary air velocity is presented in **Figure 5.10**. As shown in **Figure 5.10**, Δt_p is increased from 10 °C to 10.7 °C as the velocity v_{s1} is increased from 1.29 m/s to 2.64 m/s in the mixed mode from 9.2 °C to 9.9 °C as the velocity v_{s1} is increased from 1.22 m/s to 2.63 m/s in the internal mode. Results of the external mode show that v_{s1} variation had less effect on Δt_p. The Δt_p is increased by 0.5 °C in the external mode as the v_{p1} is increased from 1.3 m/s to 2.7 m/s.

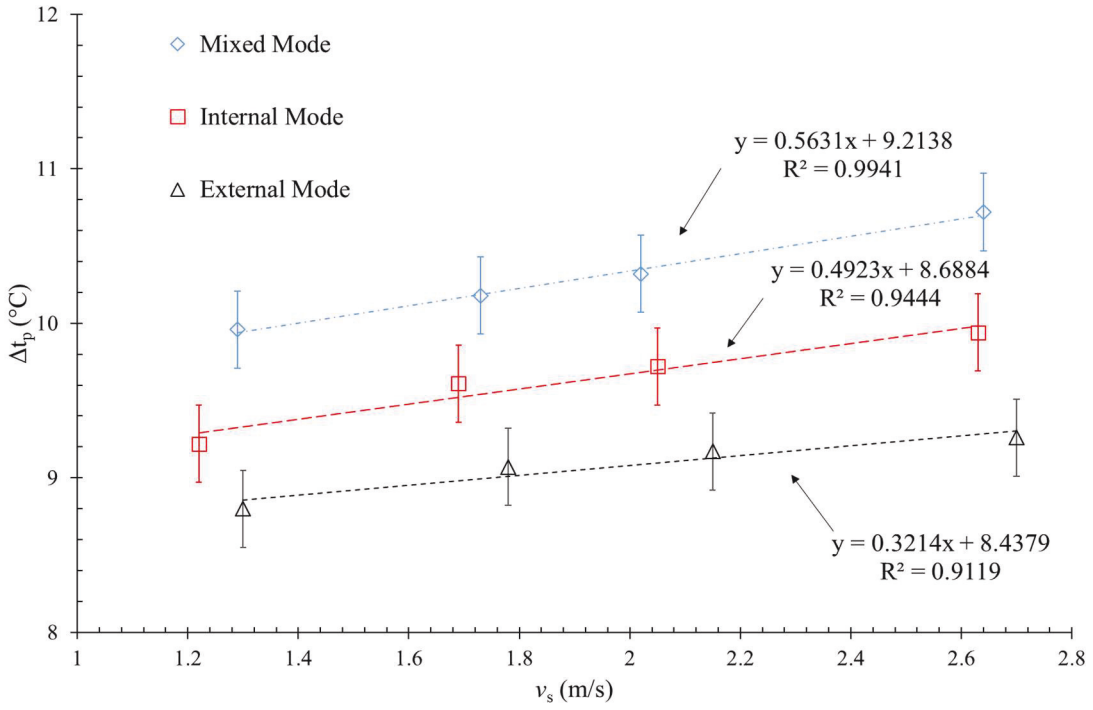

Figure 5.10. The water-spraying mode and secondary air inlet velocity effect on the primary air temperature depression

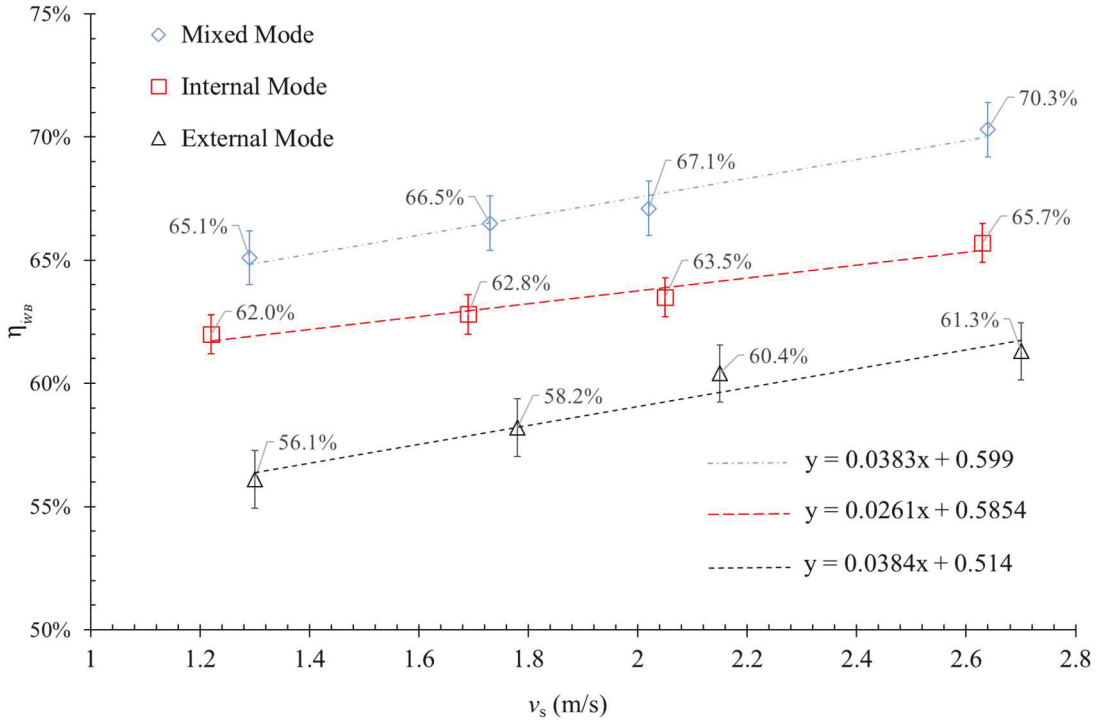

Figure 5.11. The water-spraying mode and secondary air inlet velocity effect on the IEC wet-bulb efficiency (η_{WB})

Figure 5.11 shows the wet-bulb efficiency (η_{WB}) with v_{s1} variation. As shown in **Figure 5.11**, the η_{WB} varied linearly with the secondary air velocity variation in the three water spray modes. In addition, **Figure 5.11** shows that the η_{WB} with the mixed mode is greater than that in the other two water spray modes. In addition, the η_{WB} with the external mode is found to be the lowest, although the η_{WB} was increased with the increasing of secondary air velocity v_{s1} in all the three modes. The effect of the increasing the v_{s1} was higher in both mixed mode and external mode over the internal mode. Also shown in **Figure 5.11**, that increasing the v_{s1} from 1.29 m/s to 2.64 m/s results in increasing the η_{WB} by 5.2% in the mixed mode and external mode respectively, while in internal mode, the η_{WB} increased by 3.7% as v_{s1} increased from 1.22 m/s to 2.63 m/s. The improvement of the IEC system performance at elevated v_{s1} is mainly due to the increase of the mass flow rate of the cooling media and thus increasing the secondary air cooling capacity and improving both evaporation rate and heat transfer (Anisimov et al. 2014; Duan et al. 2017).

Figure 5.12 shows the influence of water spraying mode and v_{s1} variation on the IEC cooling capacity. As shown in **Figure 5.12**, the IEC cooling capacity relatively increased by approximately 8.5% as v_{s1} was increased from the range of 1.2-1.25 m/s to around 2.68 m/s in all operating modes. The cooling capacity of the mixed mode increased by approximately 0.2 kW as the v_{s1} is increased from 1.29 m/s to 2.64 m/s, while the internal mode the increasing was 0.16 kW (1.22 m/s – 2.63 m/s) and the external mode increased by 0.15 kW with v_{s1} increased from 1.3 m/s to 2.7 m/s.

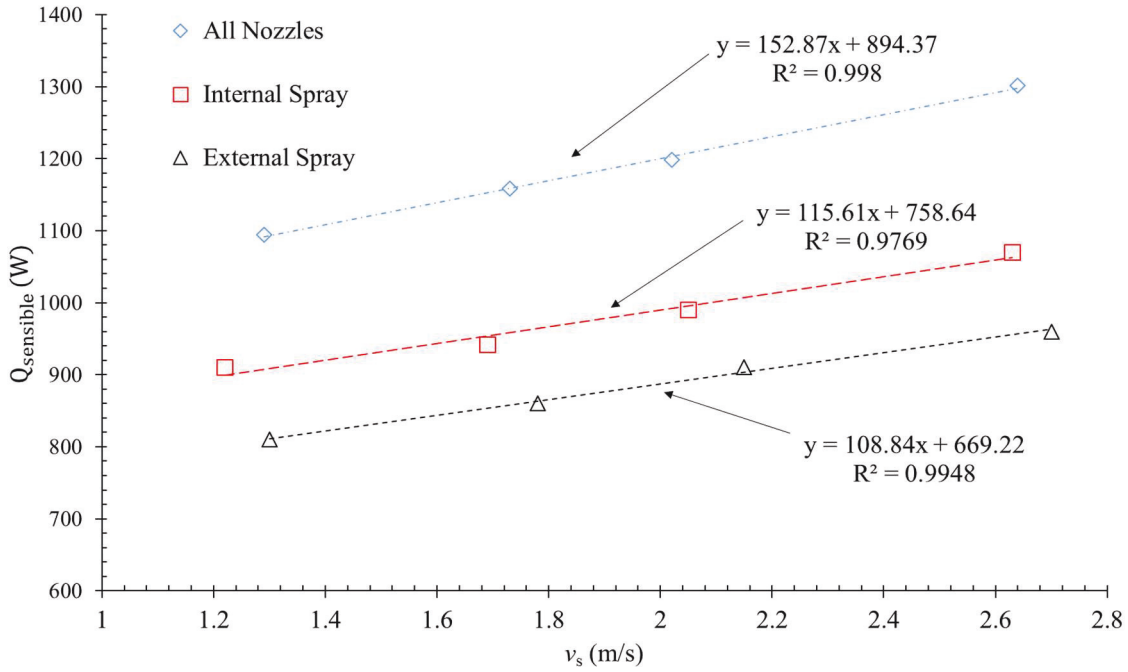

Figure 5.12. The water-spraying mode and secondary air inlet velocity effect on the IEC cooling capacity

The linear relationship in **Figure 5.12** represents the change in the cooling capacity with the variation in v_{s1}:

For external mode: $$Q_{sensible} = 107.46v_{s1} + 672.81 \quad \textbf{(5.18)}$$

For internal mode: $$Q_{sensible} = 116.52v_{s1} + 765.21 \quad \textbf{(5.19)}$$

And for mixed mode: $$Q_{sensible} = 157.98v_{s1} + 887.77 \quad \textbf{(5.20)}$$

Figure 5.13 shows the variation of the experimental IEC under the effect of the water-spraying mode and v_{s1} variation. In **Figure 5.13**, we can be perceived that the system COP variation with v_{s1} correlation is close to linear. The system COP is increased at higher v_{s1} as a result of increasing the sensible cooling capacity. The COP change with v_{s1} was found to be more significant than the cooling load change. In external mode, the COP value increased by approximately 10% as the v_{s1} increased from 1.3 m/s to 2.7 m/s.

In the internal mode, the COP increased by 10.5% as v_{s1} changed from 1.22 m/s to 2.63 m/s and COP changed by 11% in mixed mode.

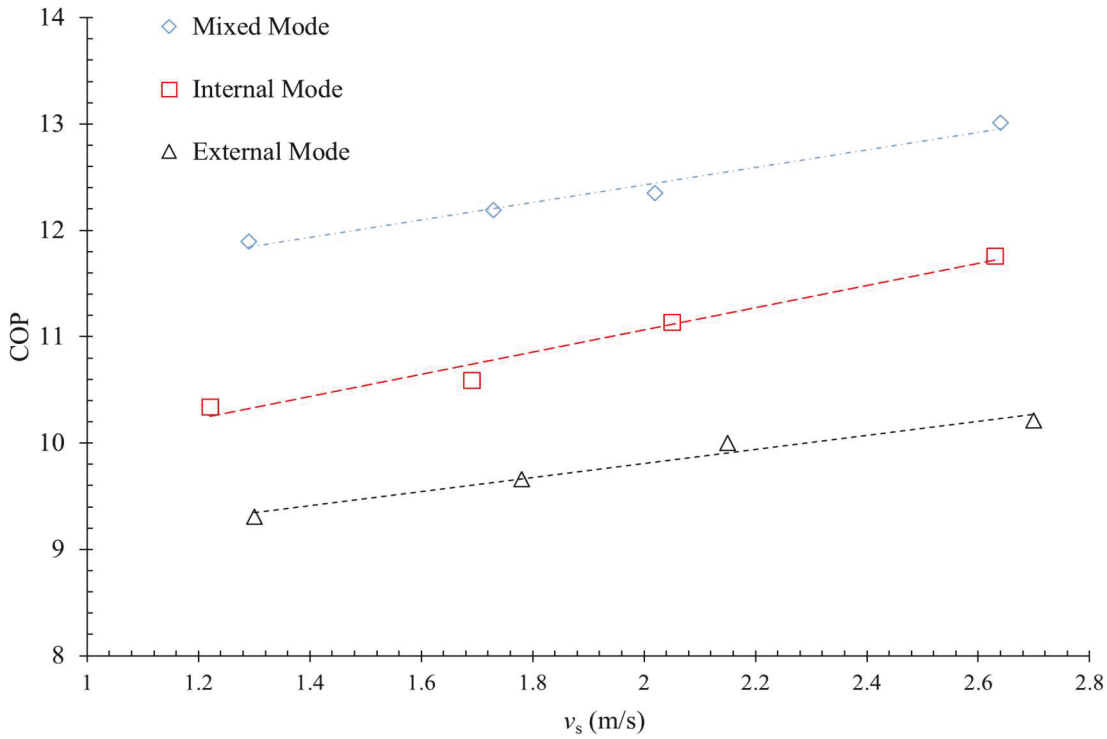

Figure 5.13. The water-spraying mode and secondary air inlet velocity effect on the IEC unit COP

The higher cooling capacities in both mixed mode and internal mode resulted in higher COPs with v_{s1} variation even though the pump consumed less power in the external mode. In summary, the secondary working air heat capacity and ability to absorb the water vapour from the water layer is a function of velocity. Accordingly, the IEC performance was found to be improved at higher v_{s1}. The IEC in mixed mode shows higher performance outputs over the internal and external modes under all v_{s1} variations and that potentially related to the increase in the water evaporation rate in two stages: pre-cooling with external spray mist and the cooling of the water film over the plate surface.

5.6. Effect of water spray mode on IEC performance under varied primary air humidity ratio

The primary air humidity ratio [ω_{p1}] effect on the IEC system performance was reported in previous works in the literature (Duan 2011; Xin 2015; Yi 2016). The indirect evaporative cooling is a sensible cooling process as described earlier, i.e. no moisture to be added to the primary air stream. However, the increase in the moisture contents of the primary air would increase the dew point temperature. Accordingly, condensation occurs during the process. The incidence of condensation results in a reduction in the humidity ratio of the outlet primary air. The effect of the humidity ratio of the primary air (moisture content) as a test parameter that effecting the IEC performance was investigated in this section.

To experimentally evaluate the three water spray modes effect on the IEC overall performance under elevated primary air moisture content, the performance test parameters (i.e. primary air temperature depression, wet bulb efficiency, cooling capacity and coefficient of performance) inspected under seven ω_{p1} levels at constant v_{p1}, t_{p1} and t_{s1}. The ω_{p1} was increased from 13.5 g/kg to 16.5 g/kg in seven steps keeping the other operating conditions fixed at t_{p1}= 27.6 °C (Dry bulb), t_{s1}= 22.4 °C and t_{s1wb} = 18.2 °C.

The effect of water spray mode on primary air temperature depression at varied primary air humidity ratio (ω_{p1}) is presented in **Figure 5.15**. As shown in **Figure 5.15**, the increase of ω_{p1} under contestant t_{p1} resulted in a reduction in Δt_p. The declining trend was uniformly in the case of the mixed mode and the external mode; nevertheless, a curved trend represents the Δt_p performance in the internal mode. In internal mode, the Δt_p shows some persistent as ω_{p1} increased from 13.45 g/kg to 14.92 g/kg. Further ω_{p1}

elevation resulted in a dramatic decline in Δt_p from 5.7 °C to 5.1 °C as ω_{p1} increased from 14.92 g/kg to 16.44 g/kg.

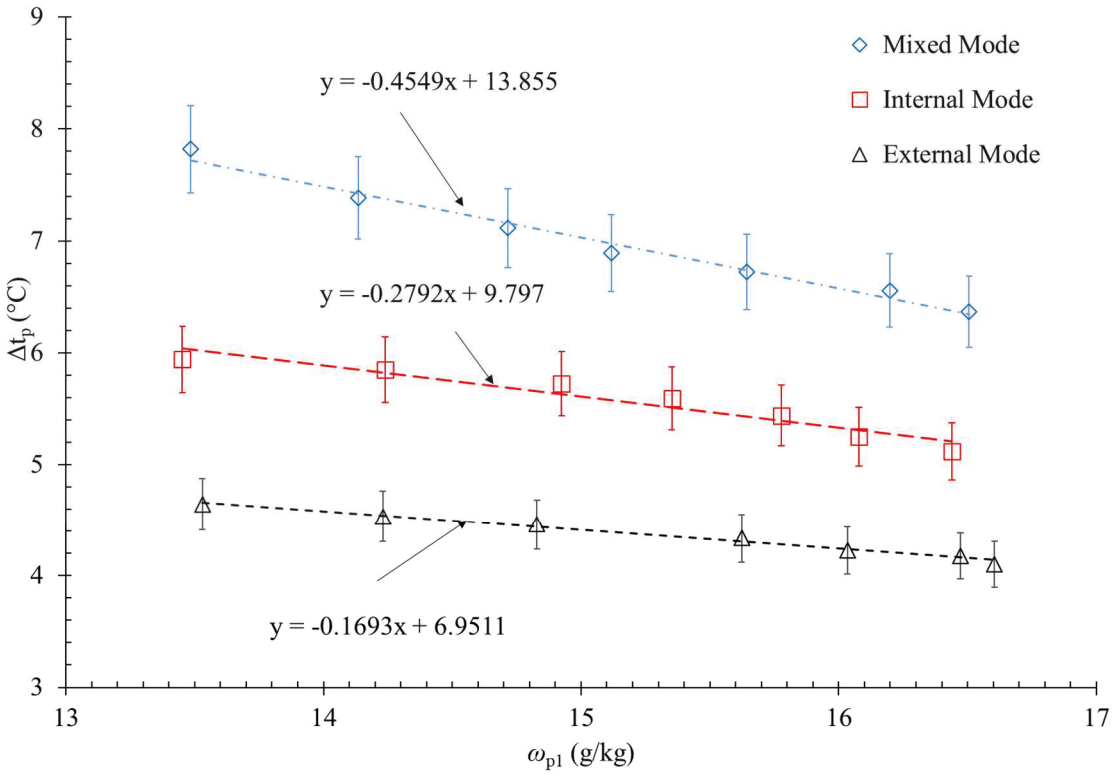

Figure 5.14. The water-spraying mode and the effect of primary air humidity ratio on the primary air temperature depression

The correlation shows more linearity in both mixed mode and external mode. As shown in **Figure 5.14**, the mixed mode performance shows a reduction in Δt_p is from 7.8 °C to 6.37 °C as the ω_{p1} is increased from 13.48 g/kg to 16.5 g/kg. In the external mode, the performance show more sustained outputs, the increase of ω_{p1} from 13.53 g/kg to 16.6 g/kg resulted in a reduction of Δt_p is from 4.65 °C to 4.1 °C.

The variation in the primary air temperature depression (Δt_p) with the variation in ω_{p1} is represented by the linear relationship in **Figure 5.14**:

For external mode: Δt_p = -0.1693 ω_{p1}+ 6.9511 **(5.21)**

For internal mode Δt_p = -0.2792 ω_{p1}+ 9.797 **(5.22)**

And for mixed mode: Δt_p = -0.4549 ω_{p1}+ 13.855 **(5.23)**

The IEC performance distinction between the internal mode and external mode tend to diminish at elevated ω_{p1}.

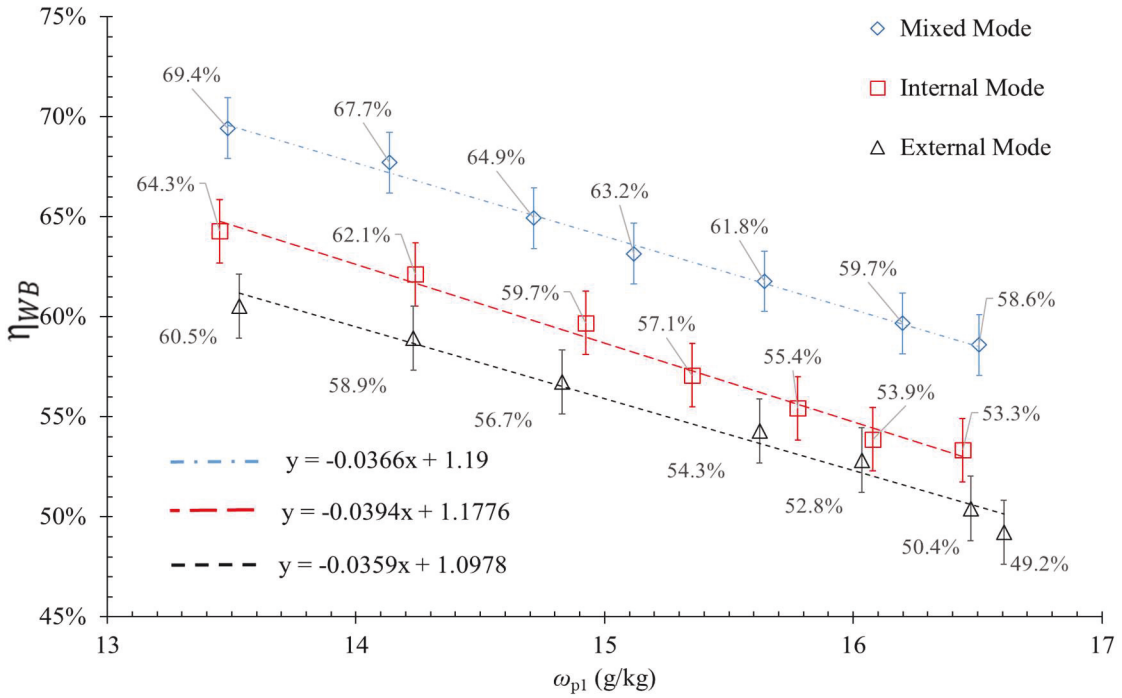

Figure 5.15. The water-spraying mode and primary air humidity ratio effect on the IEC wet-bulb efficiency (η_{WB})

The wet-bulb efficiency of IEC [η_{WB}] is a function of Δt_p (**Equation 6.1**); accordingly, the decrease of Δt_p against ω_{p1} increasing resulted in a simultaneous decrease in η_{WB}. **Figure 5.15** shows the water spraying mode and primary air humidity ratio [ω_{p1}] variation effect on the IEC wet-bulb efficiency [η_{WB}]. The performance curves in **Figure 5.15** show that a linear variation of η_{WB} with the primary air humidity ratio (ω_{p1}) air

velocity variation in the three water spray modes. In addition, **Figure 5.15** shows a perceptible regression in η_{WB} for the internal mode at higher ω_{p1} levels. The inversely proportional relationship shows that the η_{WB} increased from 53.3% to 64.3% as ω_{p1} dropped from 16.44 g/kg to 13.45 g/kg. The mixed mode performance was affected continuously by ω_{p1} variation. In mixed mode, the reduction in ω_{p1} from 16.5 g/kg to 13.48 g/kg resulted in 11.3% improvement in the system η_{WB} with a smooth curve of continuous uniform changes.

The performance of the external spray mode is showing a relative stability compared to the internal mode. In the external mode, the reduction in η_{WB} as the ω_{p1} increased from 13.53 g/kg to 14.23 g/kg was 1.6% compared to 2.2% in internal mode, with further increase in ω_{p1} up to 15.32 g/kg the η_{WB} dropped to 52.8 % compared to 53.9 % for the internal mode. These results show that the internal and external modes performed at the same level at elevated relative humidity.

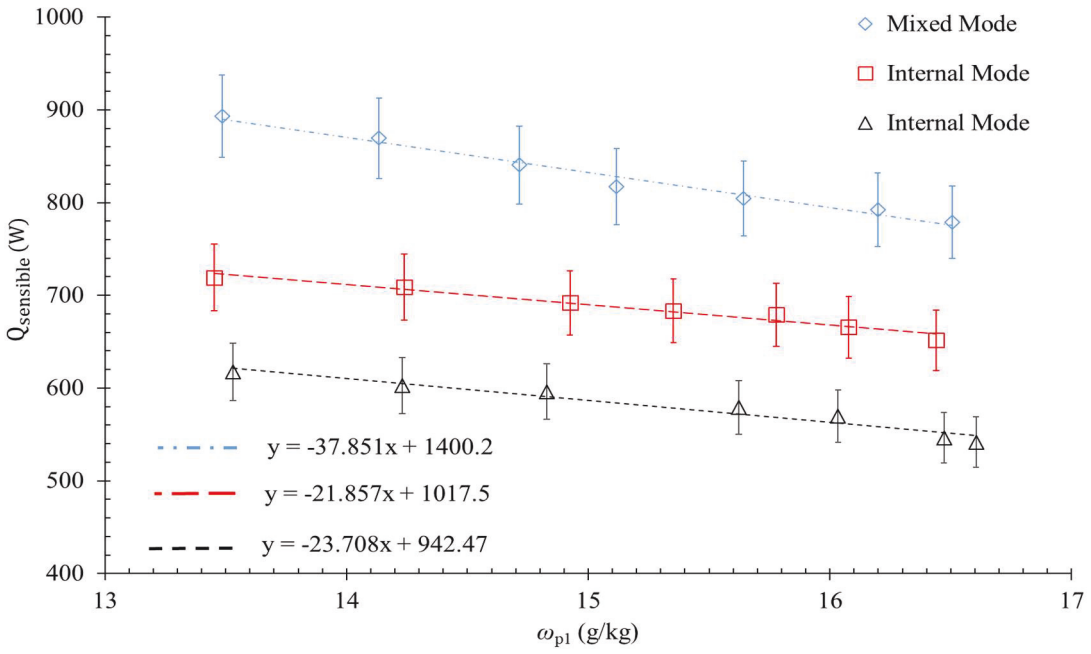

Figure 5.16. The water-spraying mode and primary air humidity ratio effect on the IEC sensible cooling capacity

The water-spraying mode and primary air humidity ratio (ω_{p1}) effect on the IEC cooling capacity is shown in **Figure 5.16**. As shown in **Figure 5.16**, the IEC cooling capacity in the external mode moderately decreased by approximately 75.8 Watt as ω_{p1} was increased from the range of 13.53 g/kg to 16.60 g/kg. The cooling capacity decreasing was more consistent in the internal mode with 67.8 Watt reduction for a similar increase in ω_{p1}.

The mixed mode performance variation with ω_{p1} increase shows a higher drop in sensible cooling capacity by approximately 114.22 Watt represents 12.3 % reduction (9.5% 12% for internal mode and external mode respectively). The linear relationship in **Figure 5.16** represents the change in the cooling capacity with the variation in ω_{p1}:

For external mode: $Q_{sensible}$ = -23.708 ω_{p1} + 1400.2 **(5.24)**

For internal mode: $Q_{sensible}$ = -21.857 ω_{p1} + 1017.5 **(5.25)**

And for mixed mode: $Q_{sensible}$ = -37.851 ω_{p1} + 942.47 **(5.26)**

The increase of the inlet primary air humidity ratio (ω_{p1}) resulted in a sensible reduction in the IEC system performance in terms of evaluation parameters: dry bulb temperature depression [Δt_p], wet bulb efficiency (η_{WB}) and the cooling load capacity [$Q_{sensible}$]. For example, it can be seen that the primary air temperature depression in the mixed mode operation dropped by approximately 17.8% and the sensible cooling capacity reduced by 12.8% when the ω_{p1} was increased from 13.48 g/kg to 16.5 g/kg. The reduction in the Δt_p, η_{WB} and $Q_{sensible}$ was combined with a reduction in the outlet primary air humidity ratio [ω_{p2}] due to the condensation process of the primary air. The condensation

process led to the decline in the sensible cooling process and increased the latent heat transfer on the other side.

The reduction in the IEC sensible cooling capacity was mainly related to the increase in the latent cooling capacity of the system. Explicitly, the condensed moisture increased the heat exchanger plate temperature on the dry channel side and slowing down the sensible cooling process across the plate. However, despite the reduction in sensible cooling, the condensation process can play an important role in both comfort cooling and energy saving.

5.7. Water evaporation rate

The R718 is the refrigerant in typical IEC systems. Unlike in vapour compression air conditioning systems, the refrigerant in IEC is continually evaporating, and continuous level make-up is required. Minimise water consumption is desirable, especially in regions where the water is scarce. The water consumption evaluation was presented in many previous works (De Antonellis et al. 2016; Duan et al. 2016; Zhao et al. 2009). The methodology adopted to determine the water evaporation rate in IEC unit is simply based on the comparison of the moisture level in the secondary air at inlet and outlet ports. The increase in the ω_s represents the amount of water carried out by the secondary air at the exit of the secondary channel.

To calculate the water evaporation rate per unit time (V_w), the amount of the moisture increase in the secondary air (g H_2O) is multiplying by the secondary air mass flow rate. Duan et al. (Duan et al. 2016) formula for the regenerative IEC unit can be modified to use for counter flow IEC as follows:

$$\dot{V}_w = \frac{1000\,\dot{V}_{s2}.\rho_{s2}}{\rho_w}.(\omega_{s2} - \omega_{s1}) \quad \textbf{(5.27)}$$

Where ω_{s1} and ω_{s2} are the secondary air humidity ratio (kg_{water}/kg_{air}) at the wet channel inlet and outlet, respectively, $\dot{V}_{s2}$ is the secondary air volume flow rate (m^3/hr), ρ_{s2} is the air density at the secondary channel outlet (kg/m^3), and ρ_w is the water film density (kg/m^3). The parameters are calculated based on the measured values of secondary air dry-bulb and wet-bulb temperatures at the wet channel inlet and outlet.

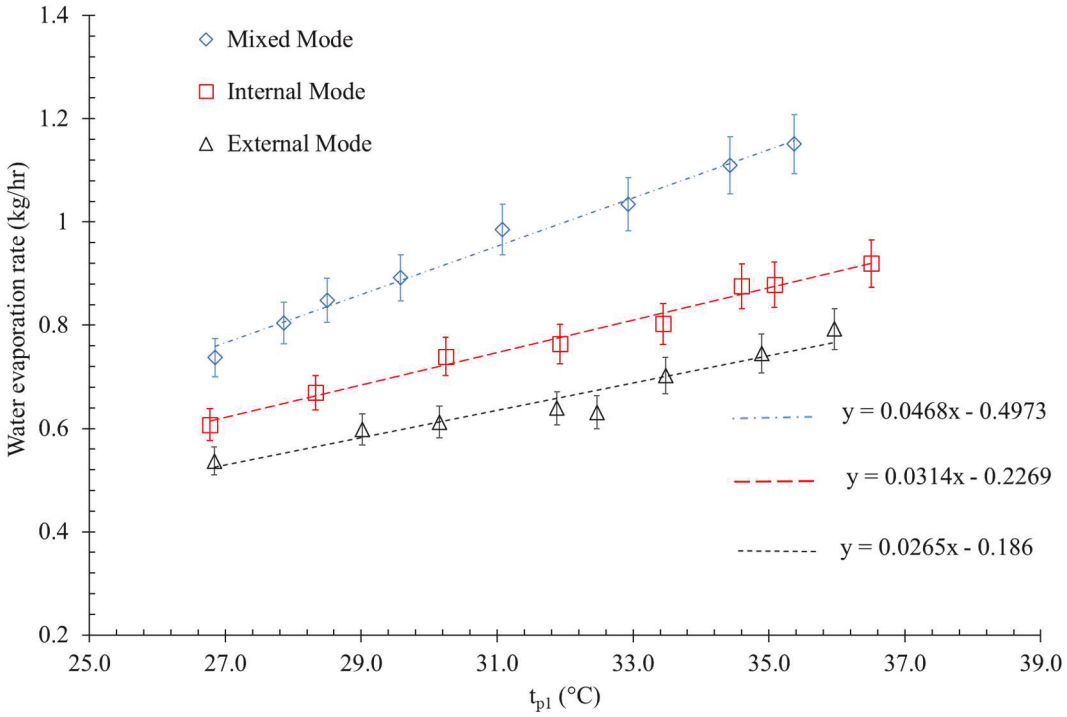

Figure 5.17. The water-spraying mode and primary air humidity ratio effects on the IEC water evaporation rate (constant secondary airflow rate of 256 m^3/hr)

The wet-bulb temperature of the primary air was neglected, as the working air is the secondary air stream with a constant wet-bulb temperature range of 16.9 – 17.8 °C. The other parameters for this test were at t_{p1} varied between 26.3 °C to 36.5 °C, t_{s1} of 21.4 - 22.5 °C, v_{p1} of 2.73 – 2.78 m/s and v_{s1} of 2.62 – 2.67 m/s.

Figure 5.18 presents the effect of water spraying mode on the water evaporation rate. As shown in **Figure 5.17**, the water evaporation rate increased linearly with the increased in the t_{p1} in the three spraying modes. The internal mode shows a higher water evaporation

rate than the external mode at the same operating conditions. As shown in **Figure 5.17**, at t_{p1} of 26.8 °C, t_{s1} of 22.1 °C, v_{p1} of 2.73 m/s and v_{s1} of 2.64 m/s, the evaporation rates were 0.6075 kg/hr in the internal mode and 0.537 kg/s in the external mode, respectively. The water evaporation rate increased as the t_{p1} increased. The internal mode water evaporation rate increased up to 0.88 kg/hr and 0.75 kg/hr in the external mode as the t_{p1} increased to around 35.1 °C.

The internal mode with multiple internal nozzles achieved a larger wetted surface area resulted in a higher water evaporation rate. Consequently, the water evaporation rate per unit time in the mixed mode is higher than both internal and external modes. The water evaporation rate in the mixed mode was 20% higher than the internal mode at t_{p1} of 26.75 °C and increasing gradually to exceed 1 kg/hr (1.045 kg/hr) as t_{p1} reach 32.9 °C and 1.15 kg/hr as t_{p1} = 35.4 °C.

The increase in water evaporation rate is an indication of the enhanced heat exchanger plate wettability in the internal and mixed mode over the external mode. The proposed water spraying system (internal system) is now validated as an effective method to improve the IEC performance.

Chapter 6

Thermal Modelling of the Indirect Evaporative Heat Exchanger

Numerical simulation was performed in order to understand and improve the performance of the indirect evaporative cooling (IEC) system with the mixed mode of spraying arrangement. This simulation extends the empirical results from Chapter 5 for heat exchanger with similar geometry and characteristics of HX1. This model is envisioned to evaluate the sensible cooling produced when forced air circulation and evaporation come into the process in the wet channels of IEC systems. Numerical methods, model verification and simulation results will be reported in this chapter.

6.1. Introduction

An analytical thermal analysis can extend the evaluation of the IEHX (Indirect Evaporative Heat Exchanger) with the opportunity of the testing parameters variation in an extensive range. Unlike the experimental work, the analytical method is not limited to the performance prediction with the temperature, airspeed and humidity variations, but also it can predict the effect of changing the heat exchanger geometrical characteristics (Alonso et al. 1998; Min, Chen & Yang 2019; Moshari & Heidarinejad 2017). Computational fluid dynamics [CFD] simulations are a powerful engineering numerical simulation tool used for the modelling of the flow conditions. CFD modelling applications are continuously developing and growing due to the increase in computer capacities and the number of research projects that apply CFD for the modelling of different flow types. With the continuous development of the CFD packages and the

numerical simulation hardware, 3-D CFD prediction capacity and accuracy are becoming more realistic and matching with the experimental results (Al-Waked et al. 2013; Montazeri, Blocken & Hensen 2015; Pakari & Ghani 2019; Yaïci, Ghorab & Entchev 2013). In comparison to numerical 1-D models, the most recent studies show the difference between the CFD simulation results and the experimental results are within 8.5% or less compared to 10% for the mathematical model simulation (Lin et al. 2017b; Pakari & Ghani 2019; Wan, Ren & Xing 2017).

In this chapter, the development of a 3-D CFD model of the IEHX will be reported. The Eulerian-Lagrangian model was aimed to replicate the actual IEHX presented in the experimental work with multiple water nozzles and variable locations. The CFD model can simulate the air-cooling process in the IEC through a test characteristic range with consideration of the complex water spraying and water droplet transportation and evaporation phenomena. Though it consumes more computational time and resources, a validated CFD model can provide a precise design tool that can deal with 3-D simulation conditions and analyse the complex heat and mass transfer process by solving the continuity, momentum, energy and species equations.

6.2. Mathematical Models

In order to understand the IEHX (Indirect Evaporative Heat Exchanger) performance, I need to understand the mathematical representation of the heat and mass transfer process in the indirect evaporative cooling system. As mentioned in Chapter 2, the mathematical analytical modelling of the IEC system can be traced to the early 1980s. The mathematical model presented by MacLaine-Cross and Banks from UNSW (Maclaine-cross & Banks 1981) is considered to be the earliest model designed for the analysis of the wet-plate performance in a regenerative IEHX with acceptable accuracy by solving a set of 8

differential equations. With the development of computational hardware, more advanced models followed, the principle design of these models are similar, but they differ in the operational assumptions, i.e. the Lewis number value, the water film temperature, the linearity of the moist water enthalpy, the plate surface wettability, etc. (Sadighi Dizaji, Hu & Chen 2018). Among these models, Stoitchkov and Dimitrov (Stoitchkov & Dimitrov 1998) modified MacLaine model for a cross-flow IEHX by considering the determination of mean surface temperature and presenting a correlation to estimate the barometric pressure. Chengqin and Hongxing (Chengqin & Hongxing 2006) designed a model in an attempt to avoid the solution inaccuracy resulting from simplifying assumptions. Their assumptions for achieving accurate solutions include more realistic consideration for the plate surface incomplete wettability, Lewis number, the water spray evaporation, water temperature variation and enthalpy change through the heat exchanger.

Other modelling methods based on the fundamental heat exchanger evaluation methods, Logarithmic mean temperature difference [LMTD] and Effectiveness-Number of Transfer Units [ε-NTU], were also presented (Cianfrini et al. 2014; Cui, Chua, Islam, et al. 2014; Heidarinejad & Moshari 2015; Liu, Allen & Modera 2013). Modified LMTD and ε-NTU methods can also predict the IEC performance in humid weather with consideration of condensation occurrence (Chen, Yang & Luo 2016b; Pandelidis et al. 2019). In their work, Sadighi, Hu and Chen (Sadighi Dizaji, Hu & Chen 2018) presented the IEHX mathematical modelling state of the art. Amongst all models, Pandelidies el al. (Pandelidis et al. 2019) described an analytical model that is most similar to the IEHX in our study, the quasi-counter-flow heat exchanger. The main differences between the IEHX model in this thesis and the prototype presented by Pandelidies are the heat exchanger orientation (Horizontal aginst a vertical installation in this study), and the water

spraying arrangement (Pandelidies model not considered the study of the nozzle arrangement). Pandelidies model was based on the ε-NTU method to analyse the mass and heat transfer in a hexagonal quasi-counter-flow IEHX. However, no analytical model was found in literal simulating the performance of IEHX with consider to the nozzles arrangement, as the case can not be simplified into a 2D case.

6.3. CFD Model

In this section, the development of the 3-D CFD simulation model is analysed in detail. The analysis of IEHX geometry, the software package and governing equations, followed by the initial settings of the problem and the boundary conditions are presented.

The water spray involves two-phase flow interface with a combination of heat, mass and momentum transfer when the droplets are injected into the air. The experimental analysis is limited to the parameter variation effects on the complicated two-phase phenomenon. However, CFD provides a simple way to analyse spray cooling. In our study, ANSYS FLUENT (versions 18.2-19.2) were selected as the CFD tools to explore spray nozzles arrangements for cooling the primary air flowing through IEHX wet channel and the plate surface. Trajectories of particles/droplets (discrete phase) are computed in a Lagrangian frame that exchange (couple) heat, mass, and momentum with Eulerian frame continuous gas phase.

Through literature, it was found that there is a research gap in the 3-D simulation of IEHX operates in discrete phase mode, i.e., with the simulation of water sprayer droplets. However, works simulated the performances of natural draft cooling towers covered this specific model. The PhD thesis of Alkhedair (Alkhedhair 2015) and Sun et al. (Sun et al. 2017) are the closest examples that can be used as a guide for the CFD numerical analysis of IEHX in discrete mode.

The 3-D model was simplified into an IEHX with single dry channel in between two wet channels to validate the numerical outputs with experimental results.

6.3.1. Numerical approach

The direct numerical simulation (DNS) has no averaging or approximation, and the instant turbulence quantities can be obtained directly; accordingly, it is considered as the most accurate approach to solving the conservation equations of turbulent flows. However, it requires intensive computational processing even for a simple flow configuration. Reynolds-averaged Navier-Stokes (RANS) is based on the averaging of the conservation equations to model the flow turbulence. The RANS is the commonly used method for solving the Navier-stokes equations of a turbulent fluid flow as it demands fewer computational resources compared to DNS.

The RANS is the most suitable approach to model the turbulent airflow with the presence of water droplets large geometries in the spray cooling system. However, turbulent stress and turbulent flux and other variables are introduced to the time-averaged Navier-Stokes equations due to Reynolds based averaging; therefore a new turbulence modelling described in section 6.3.2 is required when using the Reynolds-averaged Navier-Stokes (RANS) approach to model turbulent flow fields.

6.3.2. Turbulence modelling

The standard k-ε turbulence model is considered to be the second-most accurate turbulence model after the Reynolds stress models (RSM) to solve mist impinging jet-cooling applications (Wang & Dhanasekaran 2010). The standard k-ε turbulence model is simple, reasonably accurate with lower computational time, make it suitable in the simulation of engineering application that involves two-phase flow with a wide range of turbulence flows. The model was applied in the CFD simulation of indirect evaporative

cooling and heat recovery ventilation system, cooling towers, heat exchangers and air conditioning system with validated outcomes (Al-Waked et al. 2013; Alkhedhair 2015; Pakari & Ghani 2019; Saraireh 2012; Sun et al. 2017).

The IEHX flow is usually laminar or transitional flow (Alonso et al. 1998; Kettleborough, Waugaman & Johnson 1992); however, the presence of the multi-nozzles spray increases the turbulence within the wet channels. In this study, the standard k-ε turbulence model was adopted for its suitability for the turbulence level and the capability to solve the spray movement in the air.

6.3.3. Solver setting

Fluent is a CFD flow analysis system in the ANSYS software package. Fluent is a very common fluid flow analysis tool due to its flexibility, robustness and accuracy compared to other available CFD software packages (Greifzu et al. 2016; Zou, Zhao & Chen 2018). It was used for the analysis of the two-phase fluid flow and discrete mode (Alkhedhair 2015; Sun et al. 2017), accordingly, it was adopted in this study for the numerical analysis of the IEHX with multi-nozzles.

In this study, the ANSYS version 18.2 and later updated to version 19.1 was utilised to construct and modelling the 3-D computational model using the governing equations of the fluid flow with the finite-volume method. The Eulerian-Lagrangian approach was used to describe the continuous mode (Air), and the discrete mode (Water droplet) relations and the Reynolds-time averaged Navier-Stokes (RANS) conservation equations were used to describe the airflow field. The standard and Realizable k-ε turbulence mode with the scalable wall function was used to model the air turbulence model. The discrete phase modelling (DPM) in Fluent was used for the Lagrangian modelling of water droplets. The effect of the water droplet on the airflow is substantial; accordingly, the

"two-way coupling" approach was used to model the transport of the water droplets in the turbulent airflow within the wet channels.

6.3.4. Governing equations

A set of assumptions for the model are required (Pakari & Ghani 2019; Vali et al. 2015; Wan et al. 2018). These assumptions are:

1- A turbulent and steady airflow.

2- The air density and viscosity are constant.

3- The thermal conductivity is isotropic and constant.

4- Nozzles inject water continuously at a constant temperature, and the water film thickness is constant.

The governing equations for the air as a continuous flow modelled with RANS and standard k-ε turbulence mode are given in Eulerian modelling (Sun 2019). The general equation represents the model for airflow that consists of conversion equations for the mass, momentum, thermal energy and concentration for one continuous phase (Cui, Chua, Yang, et al. 2014):

$$\nabla.\left(\rho u\phi - \Gamma_{\varphi}\nabla\phi\right) = S_{\varphi} + S_{p\varphi} \qquad \textbf{(6.1)}$$

Where ϕ is the flow variable such as mean enthalpy, mean air velocity and mean water vapour concentration, Γ_{φ} is the diffusion coefficient, S_{φ} is the source term for the continuous phase and $S_{p\varphi}$ is the additional source due to the interaction between air and water droplets.

ANSYS FLUENT uses the Lagrangian frame to simulate and compute the trajectories of the discrete phase entities, the mass and heat transfer of the spherical particles water droplets.

6.3.5. Computational geometry

In order to study the analyse the complex heat and mass transfer process for the IEHX by solving the continuity, momentum, energy and species equations, a 3-D model of two pairs of the wet channels, one pair of the dry channel and four separation plates were built and simulated (**Figure 6.1**). The domain for the numerical analysis was based on the details of the flat surface hexagonal IEHX described in chapters 3, 4 and 5. The model dimensions are replication the actual heat exchanger channel geometry dimensions described in **Figure 3.9**; with extensions added to the channels inlets and outlets and included to the fluid domain to create more realistic flow paths. As shown in **Figure 6.2**, the total parts counting in the wet and dry channels pairs 3-D model including the extensions and plates were 13 bodies.

The total height of the heat exchanger channel is 600 mm, 300 mm width and 6 mm channel gap. The plates are 5 $x10^{-4}$ m thickness and 0.13 m^2 surface area, the fluid domain volume is 78.12 $x10^{-5}$ m^3 per channel. Three plates included in the 3-D numerical model to contain the fluid domains of the wet and dry channels.

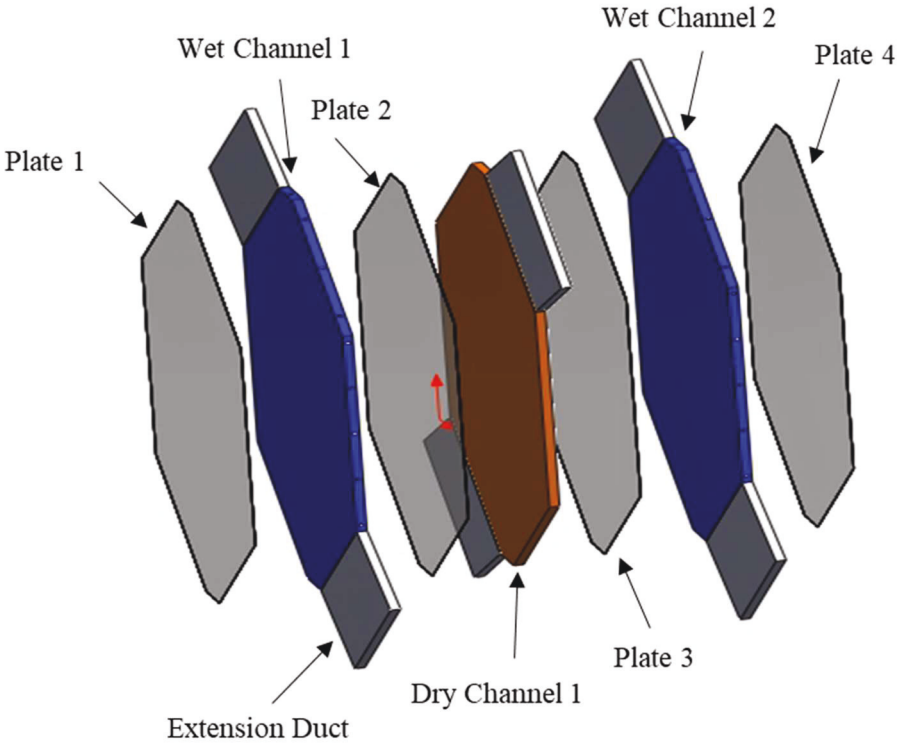

Figure 6.1. The exploded view of the 3-D CAD model

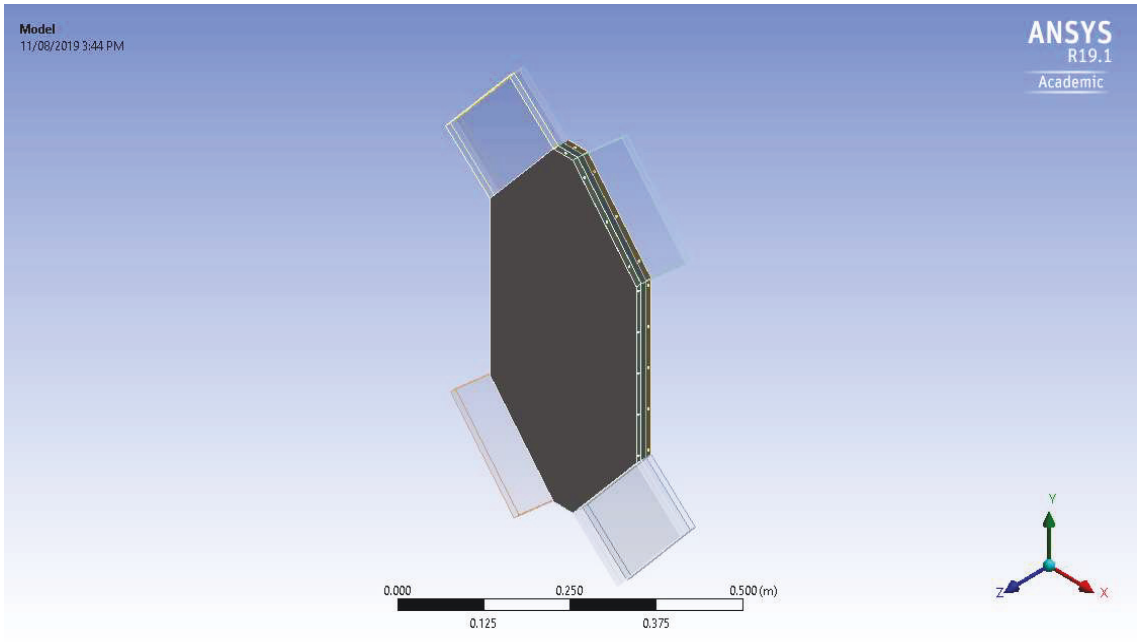

Figure 6.2. Fluid volume for the IEHX channels pair

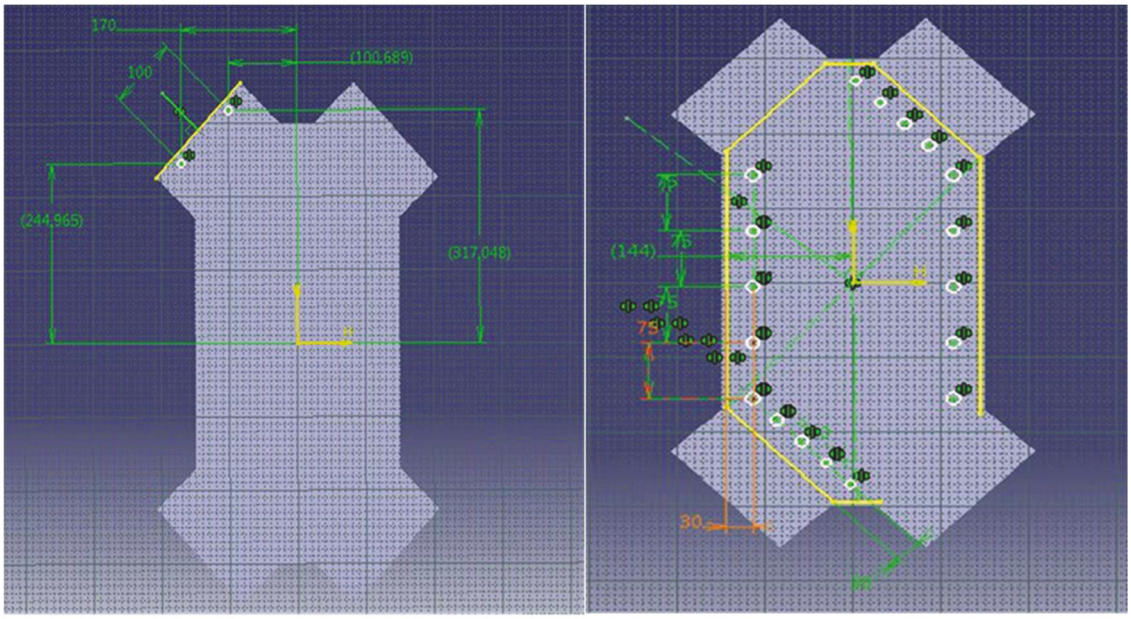

Figure 6.3. Water nozzles arrangement within the IEHX wet channel fluid domain

To study the water spraying effect on the IEHX performance, multiple spray nozzles with solid cones were simulated. As shown in **Figure 6.3**, the nozzles were distributed in the same pattern of the nozzles locations in the experimental model. The spray nozzles arrangement was designed to inject the water droplets in cross-flow against the airflow direction and aimed to cover the maximum area of the plate surface. The inlet airflow was set at a constant velocity for both channels.

6.3.6. Boundary and Operating Conditions

A- Gas phase (Air)

The main boundary conditions of the simulation domain considered in this study are shown in **Figure 6.4**. The boundary conditions for the air in the fluid domain was set as an ideal air mixture (containing Oxygen, Nitrogen and water vapour). The air inlets were set-up as velocity inlets. The velocity specified by a constant magnitude with profile flow normal to the inlet face boundary. The intensity and viscosity ratio turbulence specification method is used. The turbulence intensity was assumed as 5% and the

turbulence viscosity ratio of 10 for all the cases. The inlet air temperatures were based on the experimental test data. The species mass fractions were 0.23 for the Oxygen, 0.77 for the Nitrogen and variable mass fraction for the H_2O based on the air humidity ratio.

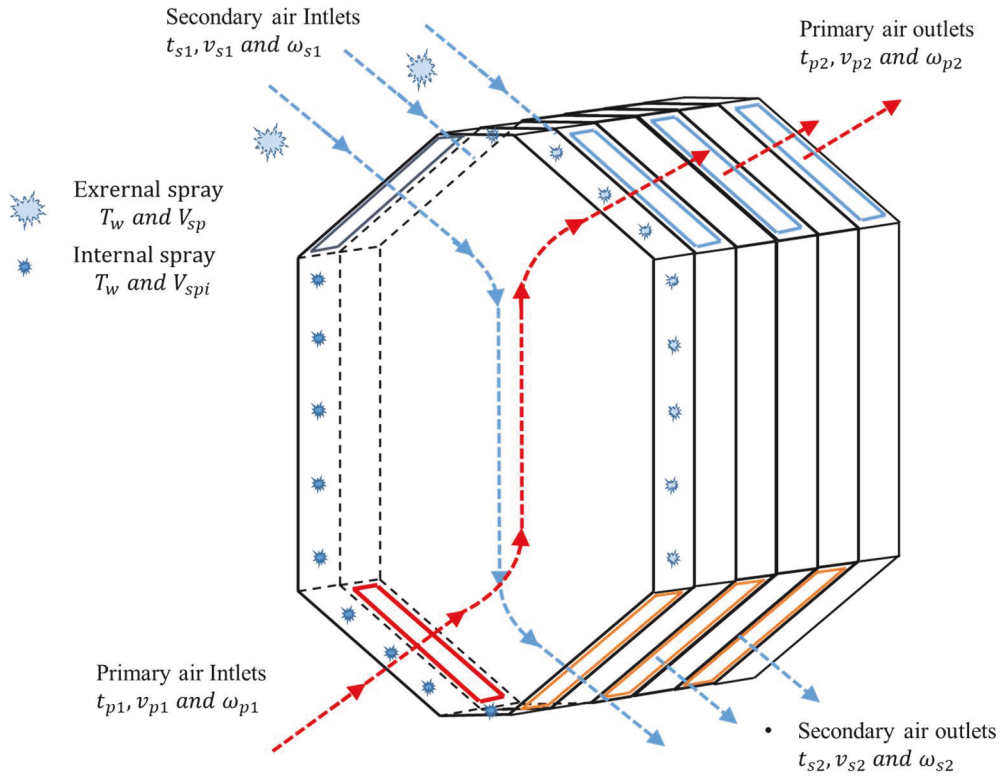

Figure 6.4. Boundary conditions for flow domain through the IEHX

B- Discrete Phase (Water)

In the discrete phase model, a solid-cone injection mode was selected with the spherical droplet particle type was assigned. The liquid phase material was selected as a pure water liquid that evaporates to H_2O vapour species. The injected water temperature was assigned to a parameter. In order to investigate the effect of the spray-water droplet temperature on the system performance. The wall DPM boundary conditions type was assigned as "trap" in order to build up a water film layer over the plate surface face.

Based on the water droplet thermal behaviour, it is not expected to achieve complete evaporation of the water droplet due to the short travelling distance and time. However,

partial evaporation and water liquid temperature drop are predicted. A smaller water droplet diameter will results in a higher evaporation rate (Al-Zubaydi, Dartnall & Dowd 2012). Accordingly and based on the nozzle specification (Siluan nozzle type AIC11004-VS) the solid-cone with a fine droplet size distribution of 30-50 µm was considered (very fine droplets). The water impact on plate's surface is modelled using eularian wall film method.

The operating conditions for the 3-D numerical method are listed in **Table 6.1**.

Table 6.1. Operating condition of the air and water droplet

Air (Continuous Eulerian phase)	Water droplet (Discrete Lagrangian phase)
Velocity: 2,2.2,2.4, 2.5 and 2,8 m/s Temperature: Primary airflow: 27,29,31 and 33 °C Secondary airflow: 23 °C Water content (kg_{water}/kg_{air}): Primary airflow: 0.009, 0.011 and 0.013 Secondary airflow: 0.009	Droplet diameter: 30, 40 and 50 µm Water Temperature: 19, 20 and 21 °C Velocity: 15 m/s Cone angle: 10° Flow rate (Kg/s): Internal nozzle (each): 0.0003 kg/s External nozzle (each): 0.001 kg/s

6.3.7. Mesh generation and Quality parameters check

The CFD model simulation requires the generation of the computational mesh from the fluid domain volume. The numerical model simulation accuracy is dependent on the mesh grid quality. The hexahedral elements were used to form the computational grid uniform mesh. The ANSYS Fluent meshing application (ANSYS 18.2) was used to build and generate computational domain grid mesh.

For the finest grid quality, the cell size should be small enough to capture high gradient change of calculated variables through the domain. The selection of grid size was defined in two stages: a dry fluid domain gird size and a spray implemented fluid domain. In the first stage, the stability of the results was achieved with cell size under 0.8 mm; accordingly, the maximum cell size for dry running continuous phase was set to 0.8 mm. With the introduction of the discrete mode and simulate with the presence of the multi injection water spraying, the grid size needed to refine further. After multiple attempts, it was found that the maximum grid size to obtain results consistency in the two-phase simulation must not exceed 4 mm. Accordingly, a 4 mm grid size was used for the simulation of discrete phase mode.

The independent mesh test was performed. The test result shows that 2,452,192 elements and 1,001,955 nodes count is sufficient to produce accurate simulation results (**Figure 6.5**). Further reduction of grid size (increasing elements counting) had no further significant effect on the simulation results.

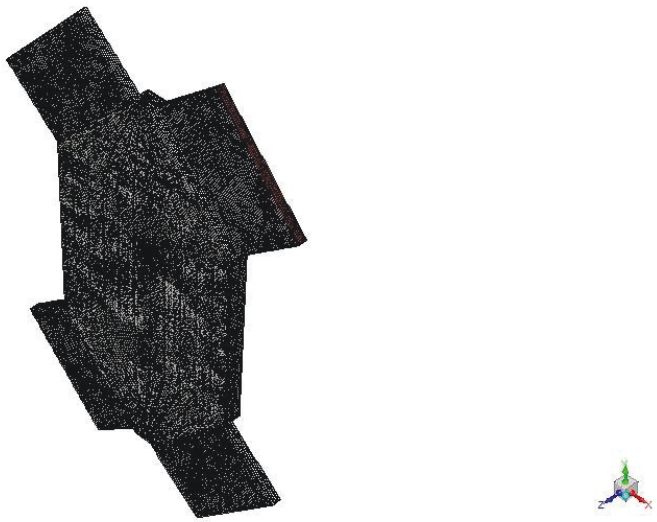

Figure 6.5. Meshes used for the fluid domain

6.3.8. Model verification

The 3-D numerical model was validated against the experimental data. I have carefully selected data from experimental results, simulation the CFD model using the same operation condition parameters and compared the outputs for the validation of the numerical model. The simulation results were mainly focused on the mixed-mode operation, with the variation of test parameters: t_{p1}, ω_{p1}, v_{p1}, t_{s1}, v_{s2} and ω_{s1}. The numerical model validation was based on the comparison of the predicted outlet conditions with the experimental measured outlet conditions of t_{p2} as shown in **Table 6.1**. Adopting the validation methodology represented by Cui et al (Cui, Chua, Yang, et al. 2014), the inconsistency was calculated by compare the primary air temperature depression $(\Delta t_p = t_{p1} - t_{p2})_{simulation}$ obtained from the simulation data with these measured from the experimental work $(\Delta t_p = t_{p1} - t_{p2})_{experimental}$. As listed in **Table 6.2** and shown in **Figure 6.6**, the maximum difference is 6.85%, and the minimum is 0.66% with an average of 2.5%. The inconsistency between the numerical and the experimental results are within the accepted range given in (Cui, Chua, Yang, et al. 2014; Pakari & Ghani 2019; Sun et al. 2017).

The validated 3-D numerical model can be used to predict the IEHX performance under variable operation parameter to optimise the system design. In addition, the numerical model can predict the airflow behaviour and distribution inside the IEHX channels and visualising the heat transfer, mass and pressure distribution contours. The main disadvantage is the high computational cost of the simulation process (Mixed-mode simulation time take up to 85 minutes for a channels pair and up to 8 hours for 1.5 channels pairs).

Table 6.2. Comparison between CFD model outputs and the experimental measurement

Test	Input data						Output data				Inconsistency
							Measured		Simulation		
	t_{p1} (°C)	ω_{p1} (g/kg)	v_{p1} (m/s)	t_{s1} (°C)	ω_{s2} (g/kg)	v_{s2} (m/s)	t_{p2} (°C)	Δt_p (°C)	t_{p2} (°C)	Δt_p (°C)	%
1	26.85	9.32	2.68	21.36	10.71	2.75	21.21	5.64	20.97	5.88	4.18
2	27.30	10.12	2.6	22.80	11.02	2.8	21.30	6.00	21.10	6.20	3.27
3	27.86	9.33	2.72	21.59	10.74	2.79	21.05	6.81	21.26	6.60	3.12
4	28.30	9.59	2.6	22.80	11.35	2.8	21.75	6.55	21.39	6.91	5.21
5	28.90	10.14	2.6	22.80	11.68	2.8	21.70	7.20	21.57	7.33	1.80
6	29.50	9.82	2.66	21.00	11.48	2.78	21.37	8.13	21.75	7.75	4.88
7	29.76	9.93	2.74	20.98	11.79	2.77	21.47	8.29	21.83	7.93	4.46
8	30.40	9.89	2.6	22.80	12.74	2.8	22.45	7.95	22.02	8.38	5.12
9	30.80	10.40	2.6	22.80	12.30	2.8	22.20	8.60	22.14	8.66	0.66
10	31.08	9.77	2.71	22.73	12.71	2.76	22.55	8.53	22.23	8.85	3.60
11	31.60	10.31	2.6	22.90	13.33	2.8	22.80	8.80	22.39	9.21	4.45
12	32.10	10.30	2.6	23.18	13.02	2.8	22.80	9.30	22.55	9.55	2.65
13	32.60	10.23	2.6	22.70	13.52	2.8	22.97	9.63	22.70	9.90	2.69
14	32.93	10.18	2.74	21.57	12.46	2.75	23.14	9.79	22.81	10.12	3.25
15	33.20	10.27	2.6	23.20	13.40	2.8	23.60	9.60	22.89	10.31	6.85

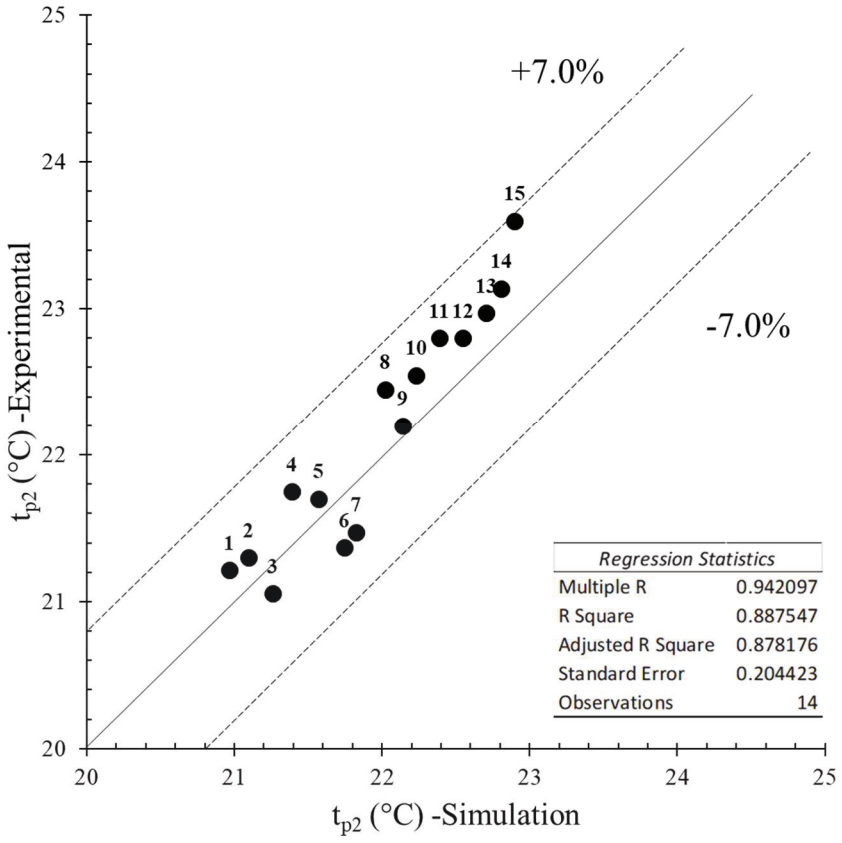

Figure 6.6. Comparison between the experimental and 3-D model primary air outlet temperature. The data points are labelled according to the test numbers in **Table 6.2.**

6.4. CFD simulation results and discussion

The 3-D verified CFD simulation model was used to predict the performance of the IEHX under variable testing parameters. The model simulated in the mixed spraying modes taking into consideration the experimental conditions practised in chapter 5. For the performance evaluation reported in section 5.2, accordingly, the IEHX test parameters are these specified in the ANSI/ASHRAE Standard 143-2015 (ANSI/ASHRAE 2015) mainly the:

1. Primary air: dry bulb temperature [°C], humidity ratio [kg/kg] and airflow velocity [m/s] at the dry channel inlet (Input).

2. Secondary air: dry bulb temperature [°C] humidity ratio [kg/kg] and airflow velocity [m/s] at the wet channel inlet (Input).
3. Primary air: dry bulb temperature [°C] and humidity ratio [kg/kg] at the dry channel exit (output).
4. Secondary air: dry bulb temperature [°C] and humidity ratio [kg/kg] at the wet channel outlet (output).

The evaluation parameters based on the simulation outputs are:

1. Primary air outlet temperature "t_{p2}" [°C].
2. Primary air temperature depression "Δt_p" [°C].
3. Wet-bulb efficiency "η_{WB}" [%].

Accordingly, we can calculate the primary air temperature depression "Δt_p" as the difference between the dry channels air temperatures at the heat exchanger inlet and outlet as expressed in the following equation:

$$\Delta t_p = t_{p1} - t_{p2} \quad \textbf{(6.2)}$$

Inlet the sensible wet-bulb efficiency under a non-condensation state of the primary air stream (ANSI/ASHRAE 2015) using the Input/output temperature data. Equation 6.3 defines the wet-bulb efficiency:

$$\eta_{WB} = \frac{t_{p1} - t_{p2}}{t_{p1} - t_{s1\_wb}} \quad \textbf{(6.3)}$$

Where $\eta_{.WB}$ is the wet-bulb efficiency, t_{p1} and t_{p2} are the primary air dry-bulb temperature at the inlet and the outlet respectively, and t_{s1_wb} is the inlet secondary wet-bulb temperature.

To analyse the effect of the water spray mode on the temperature and water distribution in IEHX channels, the 3-D simulation performed with the inlet inputs conditions of t_{p1} of 30 °C, t_{s1} of 23 °C and w_{p1}= w_{s1} = 0.09 kg_{water}/kg_{air}, the air velocity for primary and secondary air is 2.2 m/s, and the water temperature is 19.0 °C. The simulation results are presented in **Figure 6.7 – Figure 6.9**.

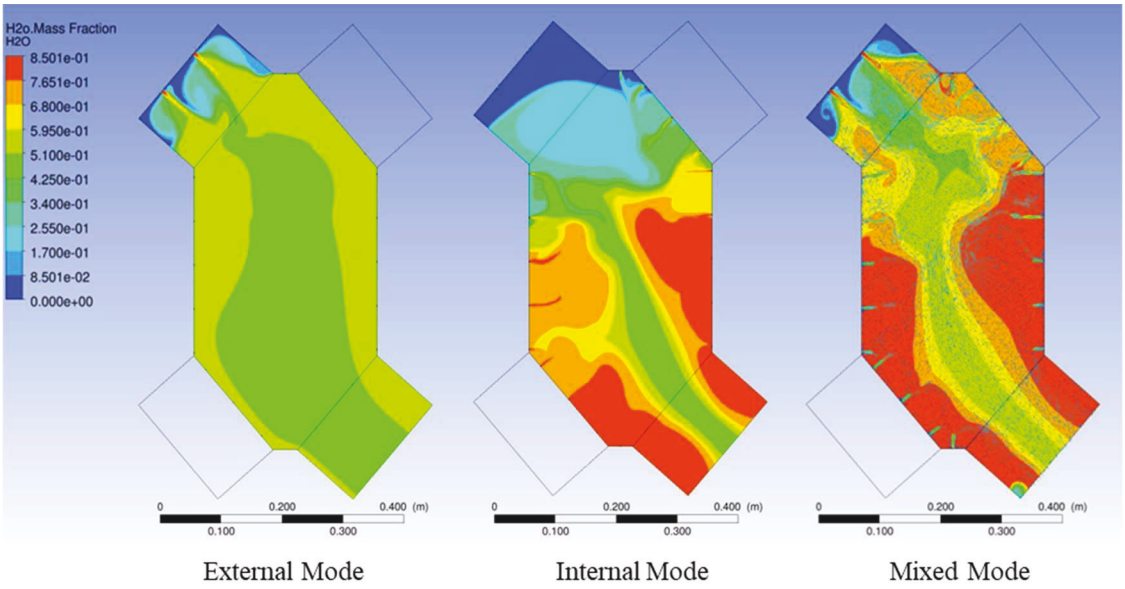

Figure 6.7. Secondary air H_2O mass fraction contours at a plane at the middle of the wet channel (z = 3 mm) at t_{s1} of 23 °C (296 K) and v_{s1} of 2.2 m/s, using the 3-D model

Figure 6.7 presents the secondary air H_2O mass fraction- ratio) distribution contours within the wet channel. As shown in **Figure 6.7**, the external mode increased the secondary air H2O mass fraction ratio from 0.09 kg_{water}/kg_{air} up to 0.68 kg_{water}/kg_{air} at the entrance of the IEHX. With the incident of the water droplets evaporation, the H2O mass fraction ratio within the secondary air reduced to the range of 0.44 in the centre area and 0.57 kg_{water}/kg_{air} on the sides.

The internal mode shows a higher capacity to increase the secondary air H2O mass fraction ratio with up to 0.81 kg_{water}/kg_{air} on the channel sides. However, the internal mode

insufficiently wetted the air at the entrance of the IEHX; also it can be noticed that the humidity ratio in most of the area opposite to the primary air entrance is dropped to 0.69 due to the high evaporation rate. The mixed mode contour in **Figure 6.7** shows that the spraying of water using all the nozzles simultaneously generated a better moisture content increment distribution in the secondary air stream. The mixed mode covered all the wet channel area with the minimum H2O mass fraction ratio of 0.49 kg_{water}/kg_{air} at the centre toward the exit and between 0.72-0.84 kg_{water}/kg_{air} on most of the channel area.

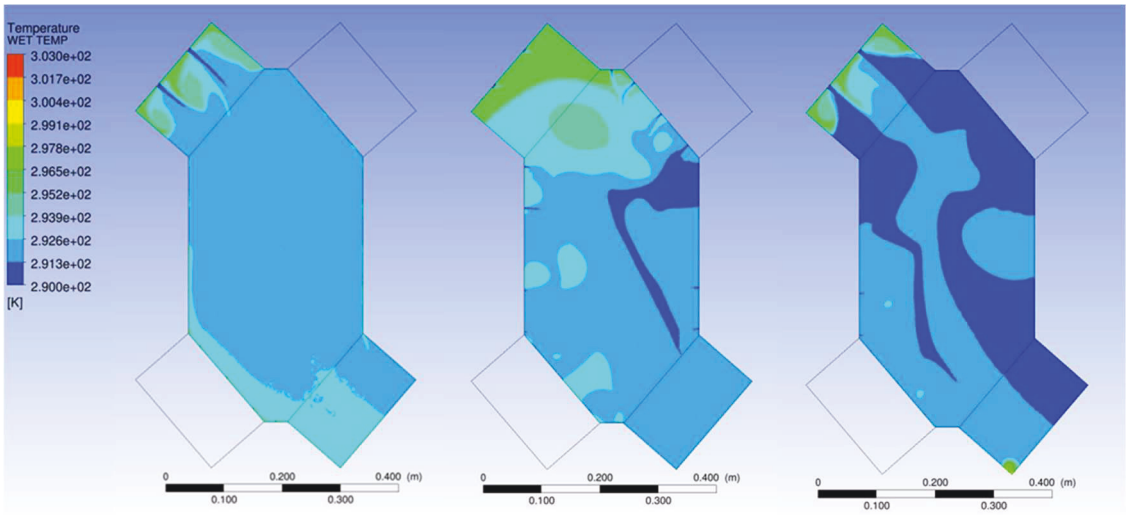

Figure 6.8. Temperature contours at a plane at the middle of the wet channel (z = 3 mm) at velocity of 2.2 m/s, using the 3-D model (temperature in Kelvin)

The air H2O mass fraction ratio distribution in the wet channel influences the temperature distribution within the heat exchanger. **Figure 6.8** presents the temperature contour of the secondary air stream in the wet channel. The comparison between the three modes temperature contours in **Figure 6.8** shows that the temperature distribution was optimised under the mixed mode. In the mixed mode, the secondary air temperature dropped to 291 K over more than 45% of the channel area and around 292 K in the remained area. The

internal mode temperature distribution was not as consistent as the external mode; however, the primary air temperature performance was enhanced in the internal mode.

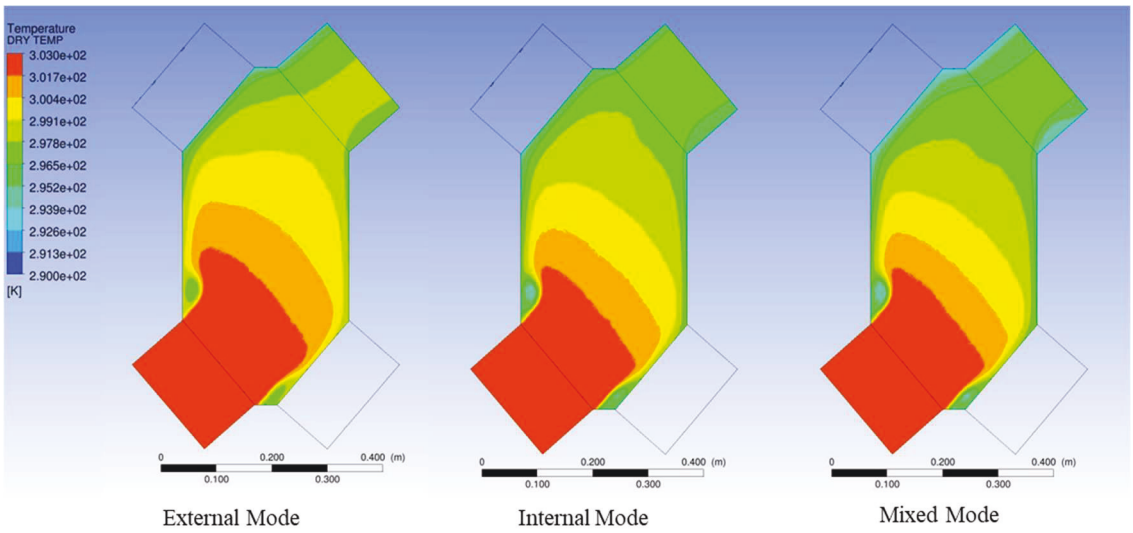

Figure 6.9. Temperature Contours at a plane at the middle of the dry channel (z = 3 mm) at velocity of 2.2 m/s, using the 3-D model (temperature in Kelvin)

The secondary air performance and distribution in the three modes reflected on the primary air temperature performance. As shown in **Figure 6.9**, the primary air was gradually cooled through the dry channel. The primary air was cooled by losing heat sensibly to the cold plate that in turn lose the heat to the water film in on the wet side. A comparison between the temperature contours in the three modes, it can be pointed out that the cooling rate is increased with the internal mode over the external mode. The hot zone area was minimised in the internal mode in comparison to the external mode, and that has resulted in a lower temperature supplied primary air. A further improvement achieved with the mixed mode with accelerated cooling rate and lower temperature product air compared to the other two modes.

6.4.1. Effect of primary air inlet temperature on the performance IEC with mixed-mode

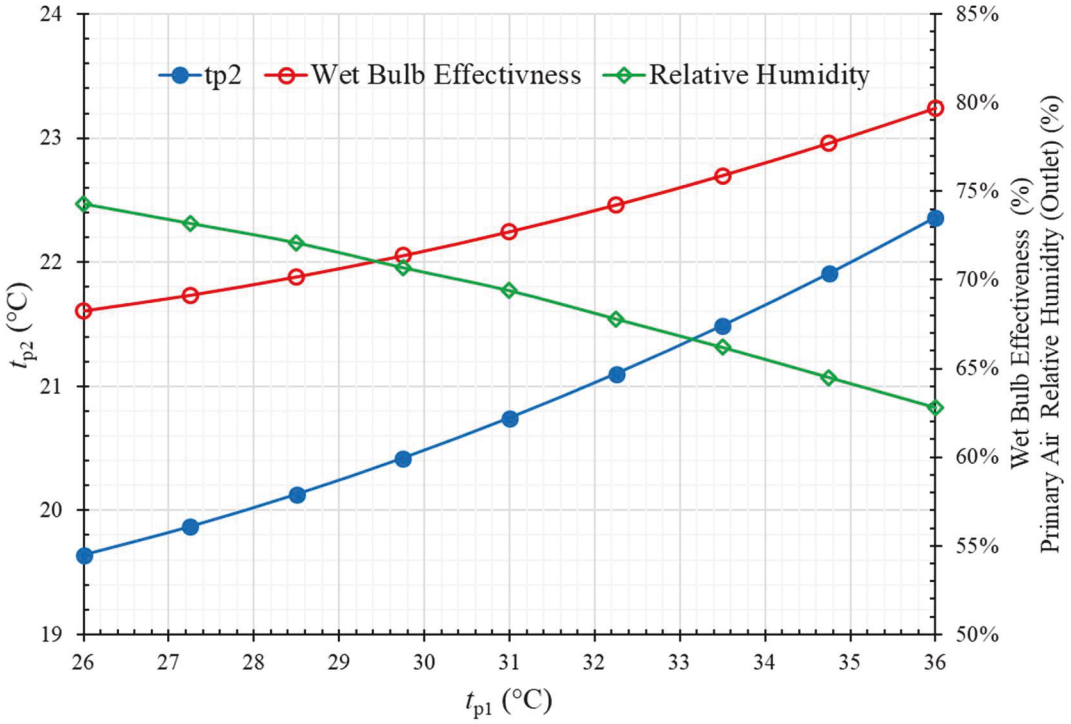

Figure 6.10. The effect of the primary air inlet temperature on the IEC performance parameters

The IEHX model in the "Mixed Mode" arrangement was simulated with the primary air inlet temperature t_{p1} varied from 26.0 °C to 36.0 °C to compare the effects of three water-spraying modes on the performance of IEC. Other simulation parameters were considered as a constant value including the primary air humidity ratio [$w_{p1} = 10$ g/kg], the primary air inlet velocity [$v_{p1} = 2.25$ m/s], the secondary air inlet temperature [$t_{s1} = 22.5$ °C], the secondary air humidity ratio [$w_{p2} = 11.07$ g/kg] and the secondary air inlet velocity [$v_{s1} = 2.25$ m/s]. **Figure 6.10** shows the primary air inlet temperature "t_{p1}" effect on the primary air outlet temperature "t_{p2}", the wet-bulb effectiveness [η_{WB}] and the outlet primary air relative humidity [RH]. In general, as shown in **Figure 6.10**, the t_{p2} is increasing as a function of t_{p1} and accordingly, the IEC wet-bulb effectiveness calculated

by **Equation (5.1)** increases as a result of the primary air temperature depression Δt_p increases with constant t_{s1_wb}.

As observed from **Figure 6.10**, the t_{p2} is increasing more rapidly as the t_{p1} increased between 31-36 °C. The maximum t_{p2} of 22.36 °C was predicted as the t_{p1} of 36 °C achieved. The η_{WB} curve trend in **Figure 6.10** is similar to the η_{WB} behaviour calculated from the experimental data (**Figure 5.3**). **Figure 6.10** also shows that the relative humidity [RH] of the outlet primary air decreases as a function of the t_{p1} with constant w_{p1}. The RH ranged between 74.3% when t_{p2} = 19.64 °C and 62.8% as the t_{p1} =36 °C.

6.4.2. Effect of primary air velocity on IEC performance

The effect of the water spraying mode on IEC model performance with a different primary air inlet velocity [v_{p1}] was considered under a constant primary inlet temperature [t_{p1}] of 30.0 °C, secondary air inlet temperature [t_{s1}] of 22.5 °C, and secondary air inlet velocity [v_{s1}] of 2.25 m/s.

Nine primary air inlet velocities between 1 m/s to around 3 m/s were used. The outlet primary air temperature reduction [t_{p1}] significantly increased as a function of the primary air inlet velocity into the dry channels, as illustrated in **Figure 6.11**. The behaviour is mainly related to the reduction of the contact time between the airflow and the plate surface in the dry channel resulted in the diminishing the heat transfer time across the plate. As a result of the t_{p2} increasing under the sensible heat conditions, the relative humidity of the supply air declined from 71% at v_{s1}= 1 m/s to 65% as v_{s1} raised to 3 m/s.

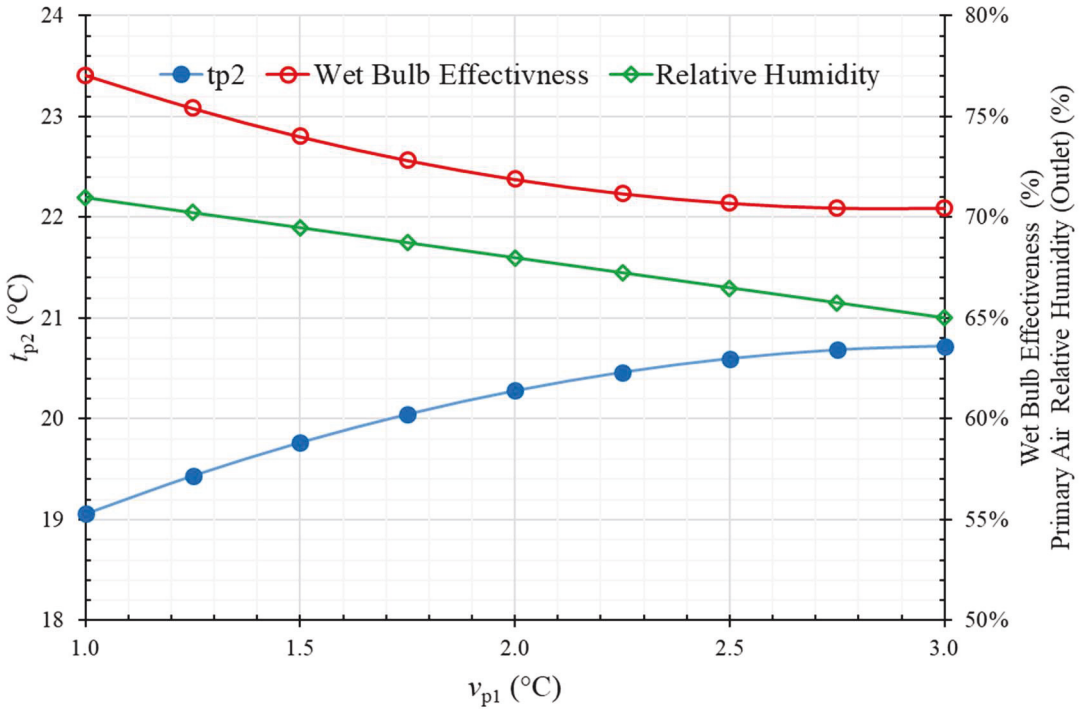

Figure 6.11. The effect of the primary air inlet velocity of the IEC performance

On the other side, **Figure 6.11** also shows that the wet-bulb efficiency η_{WB} declined as a result of the increase in the primary air velocity v_{p1}. This reduction is the result of the decrease in the Δt_p value that represents the numerator of **Equation 5.1** with constant dominator value of "$t_{p1} - t_{s1\_wb}$". Accordingly, the IEC efficiency was optimum at a lower primary air inlet velocity of 1 m/s and eventually dropped by approximately 6% as the v_{p1} was tripled to 3 m/s.

6.4.3. Effect of the primary air inlet humidity ratio on IEC performance

To study the IEC overall performance under high primary air humidity ratio, the CFD model simulated the evaluation parameters (i.e. outlet primary air temperature, wet bulb efficiency and relative humidity) under nine ω_{p1} levels at constant v_{p1}, t_{p1} and t_{s1}. The ω_{p1} was increased from 10.0 g/kg to around 14.8 g/kg in nine steps keeping the other inputs fixed at t_{p1}= 30.0 °C (Dry bulb), t_{s1}= 22.5 °C and t_{s1wb} = 17.25 °C.

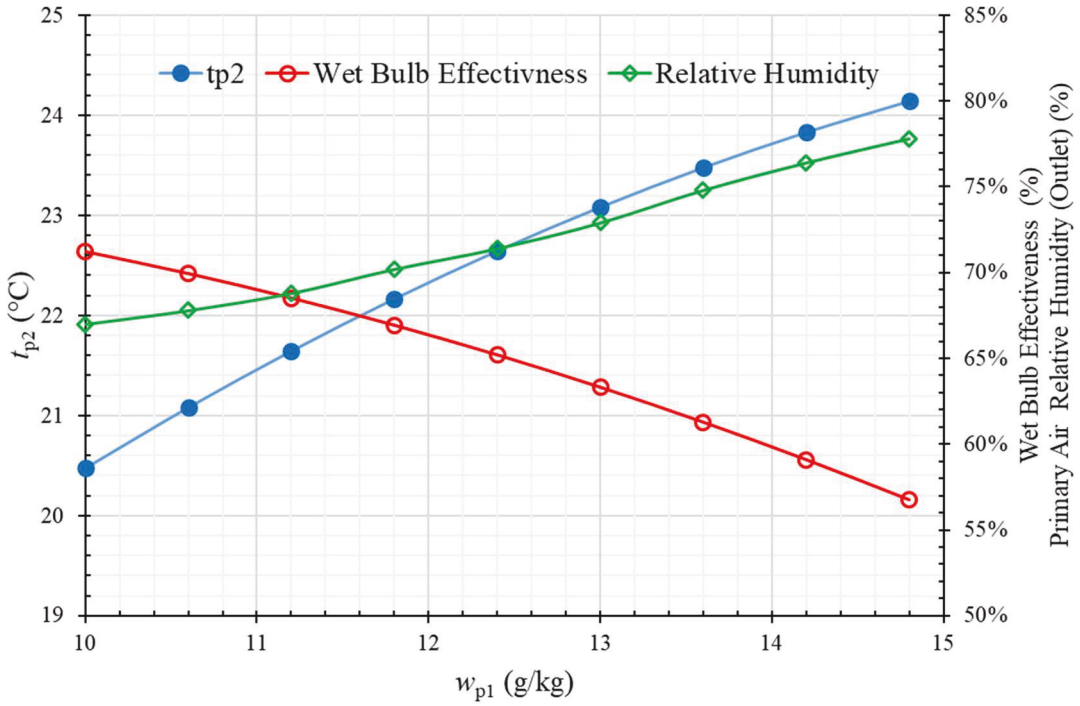

Figure 6.12. The effect of the primary air humidity ratio on the IEC performance

The simulation results are presented in **Figure 6.12**. As shown in **Figure 6.12**, the outlet primary airflow relative humidity was increased proportionally to the increase in the ω_{p1} under constant t_{p1}. However, it can be observed that the relationship is not perfectly linear, i.e. $\omega_{p2} \neq \omega_{p1}$, due to the possible presence of condensation through the dry channel. Accordingly, the IEC RH was increased from 66.3% (ω_{p2}= 9.987 g/kg) to 71.5% (ω_{p2}= 12.34 g/kg) as the ω_{p1} increased from 10.0 g/kg to 12.40 g/kg, and further 6.3% as the ω_{p1} increased to 14.8 g/kg.

The primary air outlet temperature [t_{p2}] is increased as ω_{p1} is increased. t_{p2} progressively increased from 20.47 °C to 24.14 °C as the ω_{p1} increased by 4.8 g/kg from 10 g/kg to 14.8 g/kg. This raise resulted in a 9.4% reduction in the η_{WB} from 71.2% at ω_{p1}=10.00 g/kg to 61.8% as ω_{p1} increased to 14.8 g/kg. The negative impact of the primary air moisture on the is mainly related to the presence of the latent heat transfer in

the dry channel due to the moisture content. The moisture content increases the plate surface temperature in the dry channel by releasing latent heat that negatively affects sensible heat transfer.

Chapter 7

Conclusions and Suggestions to Future Work

Experiments and numerical simulations have been conducted to investigate two types of heat exchangers which will be applied to recovering the energy of exhaust air and ultimately to reduce the energy consumption and increase the energy efficiency in HVAC systems. In the HRV, an air-to-air heat exchanger, the effect of plate shape on heat exchange was investigated. In the IEC with water spray to enhance the cooling effect, three modes of water spray were investigated. Conclusion will be drawn in 7.1, 7.2 and 7.3.

7.1. Experimental study on HRV

The sensible efficiency [$eff._S$] is increased with the increase of the inlet temperature of the primary airflow [t_{p1}]. The sensible efficiency of HX2 is increased from 69.3% to 75.6% when t_{p1} is increased from 27.8-31.2 °C, and then slightly decreased when t_{p1} is further increased from 31.2 to 32.8 °C. The sensible efficiency of HX1 is increased from 49.6% to 54.1% when t_{p1} is increased from 27.7 to 32.7 °C. In comparison, the sensible efficiency of HX2 is 20±1% greater than that of HX1, mainly due to the plate surface more complicated in HX2 than that in HX1. The cooling capacity [$\dot{Q}_p$] is proportional to the primary air inlet temperature [t_{p1}], primary air inlet velocity [v_{p1}] and the inlet velocity of the secondary airflow [v_{s1}]. $\dot{Q}_p$ is higher in HX2 than that in HX1 due to the heat transfer enhanced by the surface geometry in HX2 more complicated than that in HX1.

The $eff._S$ increases nonlinearly with v_{s1}, but reduces linearly with v_{p1} in both heat exchangers. The effect of the air velocity on $eff._S$ is stronger in HX2 than that in HX1 due to the turbulence generated by the dimpled surface of the plate in HX2. The COP of HX2 is higher than that of HX1, except at v_{p1} higher than 1.8 m/s. The maximum COP of HX2 is 6.6 at v_{p1} of 2.6 m/s, v_{s1} of 2.7 m/s and t_{p1} of 32.6°C. The maximum COP of HX1 is 5.3 at v_{p1} of 2.6 m/s, v_{s1} of 1.2 m/s and t_{p1} of 27.5°C.

Based on the above conclusions, it is recommended to use the dimpled face heat exchanger for heat recovery purposes in conditions of that the temperature difference between t_{p1} and t_{s1} is big enough to achieve a high cooling capacity [$\dot{Q}_p$] which offsets the fan power consumption.

7.2. Experimental study on IEC

In comparison with the classic external water spray for IEC, the internal water spray improved the IEC system performance in terms of product air temperature difference, wet-bulb efficiency, cooling capacity and coefficient of performance under all tested conditions. The performance of the IEC with the mixed water spray mode was better than that of the other two modes, with greater water flow rates. The wet-bulb efficiency (η_{WB}) of the IEC under the experimental three modes were compared. The η_{WB} varies in a wide range under the different operating modes and experimental parameters variation. The heights η_{WB} of 76% achieved by the IEC operating in the mixed mode at t_{p1}= 36.1 °C, t_{s1}= 22.7 °C, v_{p1}= 2.76 m/s and v_{s1}= 2.67 m/s. The minimum η_{WB} of 56.1% achieved by the IEC operating in the external mode at t_{p1}= 31.2 °C, t_{s1}= 22.5 °C, v_{p1}= 2.83 m/s and v_{s1}= 1.32 m/s. Most of the η_{WB} values are within the acceptable range (above 60%) in the three water spray modes.

The wet-bulb efficiency [η_{WB}] of the IEC under the experimental three modes were inversely proportional to the primary air inlet velocity [v_{p1}] and positively proportional to the increase in the secondary air velocity [v_{s1}]. In all spraying modes, the wet-bulb efficiency increases with the decrease of the primary air velocity, due to the increased contact time between the primary air and the plates. The internal spray mode improved the η_{WB} in the range of 3.5-5.2% compared to the external spray mode. The maximum sensible cooling capacity $Q_{sensible}$ = 1.76 kW (0.5 Refrigeration Ton) was achieved with the mixed water spray mode at t_{p1}= 37.2 °C, t_{s1}= 22.8 °C, v_{p1}= 2.76 m/s and v_{s1}= 2.67 m/s. On the other side, the minimum $Q_{sensible}$ of 0.58 kW was in the condition with the external water spray mode at t_{p1}= 27.1 °C, t_{s1}= 22.1 °C, v_{p1}= 1.54 m/s and v_{s1}= 2.665 m/s.

The system cooling capacity increases linearly with the increase of the air mass flow rate. Independent of the water spray mode, decreasing the primary air velocity, negatively affected the system performance, such as reducing the cooling capacity and coefficient of performance. Increasing t_{p1} and t_{s1} or decreasing t_{s1} and v_{p1} resulted in increasing the IEC cooling capacity. The maximum cooling capacity was achieved when the IEC operated at maximum possible v_{p1} and v_{s1}, with consideration of the water spray presentation within the wet channels resulted in a substantial boost in IEC performance.

In conclusion, the experimental work presented in Chapter 5 shows that the IEC units in mixed mode performed much better than the other two modes (External and internal). The optimum performance was achieved at higher primary air inlet temperatures. The primary air temperature depression [Δt_p] of 13.9 °C and COP of 17.3 were achieved at t_{p1} of 36.6 °C. The air inlet velocity can also optimize the system performance, whereby the higher primary air inlet velocity resulted in lower sensible air effectiveness of 69.5%,

while the higher secondary air velocity resulted in an increase in all performance evaluation parameters.

The IEC unit performance was negatively affected by the primary air humidity ratio. The lowest sensible effectiveness of 58.6% for the IEC was presents as ω_{p1} increased up to 16.44 g/kg. However, the experimental IEC performed in an acceptable performance at elevated humidity ratio of 13.45 g/kg.

7.3. IEHX CFD simulation

Understanding the performance of the IEHX employing the three water spraying modes requires in-depth knowledge of the temperature and moisture distribution in the heat exchanger. Therefore, part of this research was to perform numerical simulation modelling study using a Computational Fluid Dynamics (CFD) package, FLUENT. However, the available CFD packages such as FLUENT has some limitations when it comes to modelling evaporation and condensation conditions simultaneously. However, but the FLUENT has the advantage of simulating an IEHX heat and mass transfer performance with a realistic 3-D environment. The CFD model simulation was advantageous to study the water and temperature distribution within the heat exchanger.

The performance of the counter flow indirect evaporative cooler heat exchanger has been numerically studied. The CFD model was developed to investigate the effect of the input parameter on the system performance operating with the mixed mode spraying arrangement. The validation of the model simulation outputs against the experimental data shows an agreement within ±7.5 %.

In order to study the impact of the primary air conditions on the IEHX performance, the primary air outlet temperature and wet-bulb efficiency are applied as the performance indicators. The primary air supply temperature and the wet-bulb efficiency of the IEHX

were dependent on the primary air input parameters: t_{p1} , v_{p1} and w_{p1}. In order to achieve a lower primary air supply temperature [t_{p2}], the primary air inlet parameters need to be at lower values. To achieve the the primary air outlet temperature below 20 °C, the primary air inlet conditions requirements are: (1) Primary air inlet temperature less than 28 °C; (2) the primary air inlet velocity to be kept less than 1.7 m/s; and (3) the primary air humidity ratio to be less than 9 g/kg. The humidity ratio, amongst the test parameters, was the most negatively effective factor. The increase in the humidity ration from 10 g/kg to 14.9 g/kg resulted in a 20% drop in the IEHX wet-bulb efficiency and a 17.5% increase in the primary air outlet temperature.

7.4. Recommendations and future work

7.4.1. Development on the IEHX

The basic IEHX prototype employed in this study requires some fundamental improvements. The further improvements on the IEHX will result in a higher in the system cooling capacity. It is recommended to study the effect of IEHX geometry modifications and the effect of the ribs and air guides on the performance of the IEHX. The CFD model can be used to perform further study through the flexibility to varying the heat exchanger design parameters such in order to achieve higher effectiveness values. However, pressure drop effect has to be investigated using CFD modelling.

CFD modelling can also be used to study the effect of different boundary conditions on the heat exchanger performance, including varying the IEHX plates material and varying the operating conditions such as the humidity ratio gradient and between the two inlet streams and the velocities of the primary and secondary.

7.4.2. Development of water spraying systems

In this thesis, the concept of improving the IEHX performance by modifying the water spraying arrangement was approved. However, it is recommended to study further innovate water distribution arrangements that could improve the cooling capacity in the IHEX system. The CFD model presented in this study can be used as a benchmark model for future proposed developments.

7.4.3. Economic and energy analysis of IEC performance

The IEC technology can save a substantial energy consumption when applied as a standalone unit or as an HRV to the existence HVAC system. It is recommended to study, evaluate and compare the IEC system with the conventional cooling system in terms of energy, economic and environmental aspects. The simulation tools, such as TRNSYS or EnergyPlus, can provide a full year simulation of the system application in different locations. The simulation results can be studies to evaluate the IEC technology feasibility in real live applications.

Chapter 7: Conclusions and Suggestions to Future Work

References

AHRI 2014, *ANSI/AHRI Standard 1060: 2014 Standard for Performance Rating of Airto-Air Exchangers for Energy Recovery Ventilation Equipment*, AHRI Air-Conditioning, Heating and Refrigeration Institute.

Al-Waked, R., Nasif, M.S., Morrison, G. & Behnia, M. 2013, 'CFD simulation of air to air enthalpy heat exchanger', *Energy Conversion and Management*, vol. 74, pp. 377-85.

Al-Zubaydi, A.Y.T., Dartnall, J. & Dowd, A. 2012, 'Design, construction and calibration of an instrument for measuring the production of chilled water by the combined effects of evaporation and night sky radiation', *ASME Paper No. IMECE2012-85645*.

Al-Zubaydi, A.Y.T. & Hong, G. 2018, 'Experimental investigation of counter flow heat exchangers for energy recovery ventilation in cooling mode', *International Journal of Refrigeration*, vol. 93, pp. 132-43.

Al-Zubaydi, A.Y.T. & Hong, G. 2019, 'Experimental study of a novel water-spraying configuration in indirect evaporative cooling', *Applied Thermal Engineering*, vol. 151, pp. 283-93.

Al-Zubaydi, A.Y.T., Hong, G. & Dartnall, W.J. 2016, 'CFD Modelling and Analysis of Different Designs Plate Heat Exchangers', *10th Australasian Heat & Mass Transfer Conference*, Brisbane, QLD.

Alkhedhair, A.M. 2015, 'Modelling and Experimental Study of Spray Cooling Systems for Inlet Air Pre-Cooling in Natural Draft Dry Cooling Towers', The University of Queensland.

References

Alonso, J.S.J., Martinez, F.R., Gomez, E.V. & Plasencia, M.A.-G. 1998, 'Simulation model of an indirect evaporative cooler', *Energy and Buildings*, vol. 29, no. 1, pp. 23-7.

Anisimov, S. & Pandelidis, D. 2015, 'Theoretical study of the basic cycles for indirect evaporative air cooling', *International journal of heat and mass transfer*, vol. 84, pp. 974-89.

Anisimov, S., Pandelidis, D. & Danielewicz, J. 2015, 'Numerical study and optimization of the combined indirect evaporative air cooler for air-conditioning systems', *Energy*, vol. 80, pp. 452-64.

Anisimov, S., Pandelidis, D. & Jedlikowski, A. 2015, 'Performance study of the indirect evaporative air cooler and heat recovery exchanger in air conditioning system during the summer and winter operation', *Energy*, vol. 89, pp. 205-25.

Anisimov, S., Pandelidis, D., Jedlikowski, A. & Polushkin, V. 2014, 'Performance investigation of a M (Maisotsenko)-cycle cross-flow heat exchanger used for indirect evaporative cooling', *Energy*, vol. 76, pp. 593-606.

Anisimov, S., Pandelidis, D. & Maisotsenko, V. 2016, 'Numerical study of heat and mass transfer process in the Maisotsenko cycle for indirect evaporative air cooling', *Heat Transfer Engineering*, no. just-accepted, pp. 1-40.

ANSI/ASHRAE 2015, 'ANSI/ASHRAE Standard 143-2015, Method of test for rating indirect evaporative coolers', Washington: American Standards Committee Press.

ASHRAE 2008, *ANSI/ASHRAE Standard 111-2008, Measurement, Testing, Adjusting, and Balancing of Building HVAC Systems*, American Society of Heating, Refrigerating and Air-Conditioning Engineers, Inc., 1791 Tullie Circle NE, Atlanta, GA 30329.

References

ASHRAE 2012, '2012 ASHRAE Handbook - Heating, Ventilating, and Air-Conditioning Systems and Equipment (SI Edition)', American Society of Heating, Refrigerating and Air-Conditioning Engineers, Inc., <http://app.knovel.com/hotlink/toc/id:kpASHRAEA2/ashrae-handbook-heating/ashrae-handbook-heating>.

ASHRAE 2013, *ANSI/ASHRAE Standard 84-2013 - Method of Testing Air-to-Air Heat/Energy Exchangers*.

ASHRAE 2014, *Guideline 2-2010 (RA 2014) -- Engineering Analysis of Experimental Data*.

Bolotin, S., Vager, B. & Vasilijev, V. 2015, 'Comparative analysis of the cross-flow indirect evaporative air coolers', *International journal of heat and mass transfer*, vol. 88, pp. 224-35.

BOM 2019, *State of the climate 2018*, Bureau of Metrology, viewed 20 May 2019, <http://www.bom.gov.au/state-of-the-climate/>.

Bravo, G. & González, E. 2013, 'Thermal comfort in naturally ventilated spaces and under indirect evaporative passive cooling conditions in hot–humid climate', *Energy and Buildings*, vol. 63, pp. 79-86.

Bruno, F. & Liu, M.M. 2009, 'Technical background research on evaporative air conditioners and feasibility of rating their water consumption'.

Burillo, D., Chester, M.V., Pincetl, S., Fournier, E.D. & Reyna, J. 2019, 'Forecasting peak electricity demand for Los Angeles considering higher air temperatures due to climate change', *Applied Energy*, vol. 236, pp. 1-9.

Caliskan, H., Hepbasli, A., Dincer, I. & Maisotsenko, V. 2011, 'Thermodynamic performance assessment of a novel air cooling cycle: Maisotsenko cycle', *International Journal of Refrigeration*, vol. 34, no. 4, pp. 980-90.

CEPEZED 2017, *SmartBox*, <https://www.cepezed.com >.

References

Chang, C.-C., Chen, S.-L., Lin, T.-Y. & Chiang, Y.-C. 2017, 'Experimental and theoretical investigation of regenerative total heat exchanger with periodic flow for air-conditioning systems', *International Journal of Refrigeration*, vol. 81, pp. 123-33.

Chen, J., Brager, G.S., Augenbroe, G. & Song, X. 2019, 'Impact of outdoor air quality on the natural ventilation usage of commercial buildings in the US', *Applied energy*, vol. 235, pp. 673-84.

Chen, Y., Yan, H. & Yang, H. 2018, 'Comparative study of on-off control and novel high-low control of regenerative indirect evaporative cooler (RIEC)', *Applied Energy*, vol. 225, pp. 233-43.

Chen, Y., Yang, H. & Luo, Y. 2016a, 'Experimental study of plate type air cooler performances under four operating modes', *Building and Environment*, vol. 104, pp. 296-310.

Chen, Y., Yang, H. & Luo, Y. 2016b, 'Indirect evaporative cooler considering condensation from primary air: Model development and parameter analysis', *Building and Environment*, vol. 95, pp. 330-45.

Chen, Y., Yang, H. & Luo, Y. 2017, 'Parameter sensitivity analysis and configuration optimization of indirect evaporative cooler (IEC) considering condensation', *Applied Energy*, vol. 194, pp. 440-53.

Chengqin, R. & Hongxing, Y. 2006, 'An analytical model for the heat and mass transfer processes in indirect evaporative cooling with parallel/counter flow configurations', *International journal of heat and mass transfer*, vol. 49, no. 3-4, pp. 617-27.

Cianfrini, C., Corcione, M., Habib, E. & Quintino, A. 2014, 'Energy performance of air-conditioning systems using an indirect evaporative cooling combined with a cooling/reheating treatment', *Energy and Buildings*, vol. 69, pp. 490-7.

Coleman, H.W. & Steele, W.G. 2009, *Experimentation, Validation, and Uncertainty Analysis for Engineers*, 3rd Edition edn, John Wiley & Sons, Inc.

Costelloe, B. & Finn, D. 2003, 'Indirect evaporative cooling potential in air–water systems in temperate climates', *Energy and Buildings*, vol. 35, no. 6, pp. 573-91.

Cui, X., Chua, K., Islam, M. & Yang, W. 2014, 'Fundamental formulation of a modified LMTD method to study indirect evaporative heat exchangers', *Energy Conversion and Management*, vol. 88, pp. 372-81.

Cui, X., Chua, K., Yang, W., Ng, K., Thu, K. & Nguyen, V. 2014, 'Studying the performance of an improved dew-point evaporative design for cooling application', *Applied Thermal Engineering*, vol. 63, no. 2, pp. 624-33.

Dartnall, W.J., University of Technology Sydney 2015, *Counter-flow heat exchanger and method for manufacture*.

De Antonellis, S., Joppolo, C.M. & Liberati, P. 2019, 'Performance measurement of a cross-flow indirect evaporative cooler: Effect of water nozzles and airflows arrangement', *Energy and Buildings*, vol. 184, pp. 114-21.

De Antonellis, S., Joppolo, C.M., Liberati, P., Milani, S. & Molinaroli, L. 2016, 'Experimental analysis of a cross flow indirect evaporative cooling system', *Energy and Buildings*, vol. 121, pp. 130-8.

De Antonellis, S., Joppolo, C.M., Liberati, P., Milani, S. & Romano, F. 2017, 'Modeling and experimental study of an indirect evaporative cooler', *Energy and Buildings*, vol. 142, pp. 147-57.

Delfani, S., Esmaeelian, J., Pasdarshahri, H. & Karami, M. 2010, 'Energy saving potential of an indirect evaporative cooler as a pre-cooling unit for mechanical cooling systems in Iran', *Energy and Buildings*, vol. 42, no. 11, pp. 2169-76.

DOEE 2019, *Australian Greenhouse Emissions Information System*, Australian Goverment - Department of Enviromental and Energy, Australia, viewed 17

May 2019, <http://www.environment.gov.au/climate-change/climate-science-data/greenhouse-gas-measurement/ageis>.

Duan, Z. 2011, 'Investigation of a Novel Dew Point Indirect Evaporative Air Conditioning System for Buildings', University of Nottingham, United Kingdom.

Duan, Z., Zhan, C., Zhang, X., Mustafa, M., Zhao, X., Alimohammadisagvand, B. & Hasan, A. 2012, 'Indirect evaporative cooling: Past, present and future potentials', *Renewable and Sustainable Energy Reviews*, vol. 16, no. 9, pp. 6823-50.

Duan, Z., Zhan, C., Zhao, X. & Dong, X. 2016, 'Experimental study of a counter-flow regenerative evaporative cooler', *Building and Environment*, vol. 104, no. Supplement C, pp. 47-58.

Duan, Z., Zhao, X., Zhan, C., Dong, X. & Chen, H. 2017, 'Energy saving potential of a counter-flow regenerative evaporative cooler for various climates of China: Experiment-based evaluation', *Energy and Buildings*, vol. 148, pp. 199-210.

Dvořák, V. & Vít, T. 2015, 'Numerical Investigation of Counter Flow Plate Heat Exchanger', *Energy Procedia*, vol. 83, pp. 341-9.

ebm-papst 2016, *ebm-papst*, "ebm-papst Mulfingen GmbH & Co KG", viewed Septemper 27 2017, <http://www.ebmpapst.com/en/>.

Erens, P. & Dreyer, A. 1993, 'Modelling of indirect evaporative air coolers', *International journal of heat and mass transfer*, vol. 36, no. 1, pp. 17-26.

Fernández-Seara, J., Diz, R., Uhía, F.J., Dopazo, A. & Ferro, J.M. 2011, 'Experimental analysis of an air-to-air heat recovery unit for balanced ventilation systems in residential buildings', *Energy Conversion and Management*, vol. 52, no. 1, pp. 635-40.

References

Field, C. 2015, 'Acoustic design criteria for naturally ventilated buildings – unnecessarily stringent?', *EcoLibrium*, no. 2.

Foster, R.E. 1998, 'Evaporative Air-Conditioning Contributions to Reducing Greenhouse Gas Emissions and Global Warming', *Proceedings of American Society of Heating, Refrigerating and Air-Conditioning Engineers, Toronto, Canada*.

Fucci, F., Perone, C., La Fianza, G., Brunetti, L., Giametta, F. & Catalano, P. 2016, 'Study of a prototype of an advanced mechanical ventilation system with heat recovery integrated by heat pump', *Energy and Buildings*, vol. 133, pp. 111-21.

Gillan, L.E., Maisotsenko, V., Gillan, A.D. & Gillan, R.J. 2010, 'Fabrication materials and techniques for plate heat and mass exchangers for indirect evaporative coolers', Google Patents.

Gómez, E.V., González, A.T. & Martínez, F.J.R. 2012, 'Experimental characterisation of an indirect evaporative cooling prototype in two operating modes', *Applied Energy*, vol. 97, pp. 340-6.

Gough, H.L., Luo, Z., Halios, C.H., King, M.-F., Noakes, C.J., Grimmond, C.S.B., Barlow, J.F., Hoxey, R. & Quinn, A.D. 2018, 'Field measurement of natural ventilation rate in an idealised full-scale building located in a staggered urban array: comparison between tracer gas and pressure-based methods', *Building and Environment*, vol. 137, pp. 246-56.

Greifzu, F., Kratzsch, C., Forgber, T., Lindner, F. & Schwarze, R. 2016, 'Assessment of particle-tracking models for dispersed particle-laden flows implemented in OpenFOAM and ANSYS FLUENT', *Engineering Applications of Computational Fluid Mechanics*, vol. 10, no. 1, pp. 30-43.

Guo, X. & Zhao, T. 1998, 'A parametric study of an indirect evaporative air cooler', *International communications in heat and mass transfer*, vol. 25, no. 2, pp. 217-26.

References

Hasan, A. 2012, 'Going below the wet-bulb temperature by indirect evaporative cooling: Analysis using a modified ε-NTU method', *Applied Energy*, vol. 89, no. 1, pp. 237-45.

Heidarinejad, G., Bozorgmehr, M., Delfani, S. & Esmaeelian, J. 2009, 'Experimental investigation of two-stage indirect/direct evaporative cooling system in various climatic conditions', *Building and Environment*, vol. 44, no. 10, pp. 2073-9.

Heidarinejad, G. & Moshari, S. 2015, 'Novel modeling of an indirect evaporative cooling system with cross-flow configuration', *Energy and Buildings*, vol. 92, pp. 351-62.

Hettiarachchi, H.M., Golubovic, M. & Worek, W. 2007, 'The effect of longitudinal heat conduction in cross flow indirect evaporative air coolers', *Applied Thermal Engineering*, vol. 27, no. 11, pp. 1841-8.

Hobo Data Loggers,

Huang, S., Li, W., Lu, J. & Li, Y. 2017, 'Experimental study on two type of indirect evaporative cooling heat recovery ventilator', *Procedia Engineering*, vol. 205, pp. 4105-10.

Hunn, B.D. & Peterson, J.L. 1996, *Cost-effectiveness of indirect evaporative cooling for commercial buildings in Texas*, 0001-2505, American Society of Heating, Refrigerating and Air-Conditioning Engineers ….

IEA 2018, *Air conditioning use emerges as one of the key drivers of global electricity-demand growth*, International Energy Agency, viewed 20 May 2019, <https://www.iea.org/newsroom/news/2018/may/air-conditioning-use-emerges-as-one-of-the-key-drivers-of-global-electricity-dema.html>.

Jaber, S. & Ezzat, A.W. 2017, 'Investigation of energy recovery with exhaust air evaporative cooling in ventilation system', *Energy and Buildings*, vol. 139, pp. 439-48.

References

Jradi, M. & Riffat, S. 2014, 'Experimental and numerical investigation of a dew-point cooling system for thermal comfort in buildings', *Applied Energy*, vol. 132, pp. 524-35.

Kabeel, A.E. & Abdelgaied, M. 2016, 'Numerical and experimental investigation of a novel configuration of indirect evaporative cooler with internal baffles', *Energy Conversion and Management*, vol. 126, pp. 526-36.

Kettleborough, C., Waugaman, D. & Johnson, M. 1992, 'The Thermal Performance of the Cross-Flow Three-Dimensional Flat Plate Indirect Evaporative Cooler', *Journal of Energy Resources Technology*, vol. 114, no. 3, pp. 181-6.

Kim, H.-J., Ham, S.-W., Yoon, D.-S. & Jeong, J.-W. 2017, 'Cooling performance measurement of two cross-flow indirect evaporative coolers in general and regenerative operation modes', *Applied Energy*, vol. 195, pp. 268-77.

Kim, M.-H., Jeong, D.-S. & Jeong, J.-W. 2015, 'Practical thermal performance correlations for a wet-coil indirect evaporative cooler', *Energy and Buildings*, vol. 96, pp. 285-98.

Kragh, J., Rose, J., Nielsen, T.R. & Svendsen, S. 2007, 'New counter flow heat exchanger designed for ventilation systems in cold climates', *Energy and Buildings*, vol. 39, no. 11, pp. 1151-8.

Lecamwasam, L., Wilson, J. & Chokolich, D. 2012, *Guide to Best Practice Maintenance & Operation of HVAC Systems for Energy Efficiency*, Department of Climate Change and Energy Efficiency, Australia.

Lee, J., Choi, B. & Lee, D.-Y. 2013, 'Comparison of configurations for a compact regenerative evaporative cooler', *International Journal of Heat and Mass Transfer*, vol. 65, pp. 192-8.

Lee, J. & Lee, D.-Y. 2013, 'Experimental study of a counter flow regenerative evaporative cooler with finned channels', *International Journal of Heat and Mass Transfer*, vol. 65, pp. 173-9.

Lin, J., Bui, D.T., Wang, R. & Chua, K.J. 2018, 'The counter-flow dew point evaporative cooler: Analyzing its transient and steady-state behavior', *Applied Thermal Engineering*, vol. 143, pp. 34-47.

Lin, J., Thu, K., Bui, T.D., Wang, R.Z., Ng, K.C., Kumja, M. & Chua, K.J. 2016, 'Unsteady-state analysis of a counter-flow dew point evaporative cooling system', *Energy*, vol. 113, pp. 172-85.

Lin, J., Wang, R.Z., Kumja, M., Bui, T.D. & Chua, K.J. 2017a, 'Modelling and experimental investigation of the cross-flow dew point evaporative cooler with and without dehumidification', *Applied Thermal Engineering*, vol. 121, pp. 1-13.

Lin, J., Wang, R.Z., Kumja, M., Bui, T.D. & Chua, K.J. 2017b, 'Multivariate scaling and dimensional analysis of the counter-flow dew point evaporative cooler', *Energy Conversion and Management*, vol. 150, pp. 172-87.

Liu, P., Justo Alonso, M., Mathisen, H.M. & Simonson, C. 2016, 'Performance of a quasi-counter-flow air-to-air membrane energy exchanger in cold climates', *Energy and Buildings*, vol. 119, pp. 129-42.

Liu, Z., Allen, W. & Modera, M. 2013, 'Simplified thermal modeling of indirect evaporative heat exchangers', *HVAC&R Research*, vol. 19, no. 3, pp. 257-67.

M.F., Z. & A., M. 2016, 'Experimental investigation on the performance of an air-to-air energy recovery for building applications in hot-humid climate', *Journal of Mechanical Engineering and Sciences (JMES)*, vol. 10, no. 1, p. 8.

Maclaine-cross, I.L. & Banks, P.J. 1981, 'A General Theory of Wet Surface Heat Exchangers and its Application to Regenerative Evaporative Cooling', *Journal of Heat Transfer*, vol. 103, no. 3, pp. 579-85.

Maheshwari, G., Al-Ragom, F. & Suri, R. 2001, 'Energy-saving potential of an indirect evaporative cooler', *Applied Energy*, vol. 69, no. 1, pp. 69-76.

Mahmood, M.H., Sultan, M., Miyazaki, T., Koyama, S. & Maisotsenko, V.S. 2016, 'Overview of the Maisotsenko cycle – A way towards dew point evaporative cooling', *Renewable and Sustainable Energy Reviews*, vol. 66, pp. 537-55.

Maisotsenko, V., Gillan, L.E., Heaton, T.L. & Gillan, A.D. 2004, 'Method and apparatus for dew point evaporative product cooling', Google Patents.

Maisotsenko, V., Gillan, L.E., Heaton, T.L. & Gillan, A.D. 2007, 'Method and plate apparatus for dew point evaporative cooler', Google Patents.

Manz, H. & Huber, H. 2000, 'Experimental and numerical study of a duct/heat exchanger unit for building ventilation', *Energy and Buildings*, vol. 32, no. 2, pp. 189-96.

Mardiana-Idayu, A. & Riffat, S.B. 2012, 'Review on heat recovery technologies for building applications', *Renewable and Sustainable Energy Reviews*, vol. 16, no. 2, pp. 1241-55.

McNab, J.L. 1990, 'Indirect air conditioning system', Google Patents.

Meng, D., Lv, J., Chen, Y., Li, H. & Ma, X. 2018, 'Visualized experimental investigation on cross-flow indirect evaporative cooler with condensation', *Applied Thermal Engineering*, vol. 145, pp. 165-73.

Min, Y., Chen, Y. & Yang, H. 2019, 'Numerical study on indirect evaporative coolers considering condensation: A thorough comparison between cross flow and counter flow', *International Journal of Heat and Mass Transfer*, vol. 131, pp. 472-86.

Montazeri, H., Blocken, B. & Hensen, J.L.M. 2015, 'Evaporative cooling by water spray systems: CFD simulation, experimental validation and sensitivity analysis', *Building and Environment*, vol. 83, pp. 129-41.

References

Moshari, S. & Heidarinejad, G. 2015, 'Numerical study of regenerative evaporative coolers for sub-wet bulb cooling with cross- and counter-flow configuration', *Applied Thermal Engineering*, vol. 89, pp. 669-83.

Moshari, S. & Heidarinejad, G. 2017, 'Analytical estimation of pressure drop in indirect evaporative coolers for power reduction', *Energy and Buildings*, vol. 150, no. Supplement C, pp. 149-62.

Munters 2017, *Thermo-Z*, 2017, <https://www.munters.com/en/munters/products/energy-recovery/thermo-z/>.

Nasif, M., Al-Waked, R., Morrison, G. & Behnia, M. 2010, 'Membrane heat exchanger in HVAC energy recovery systems, systems energy analysis', *Energy and Buildings*, vol. 42, no. 10, pp. 1833-40.

Nasif, M.S. 2008, 'Analysis and Modelling of Membrane Heat Exchanger in HVAC Energy Recovery Systems ', The University of New South Wales, Sydney, Australia.

NGER 2017, *National Greenhouse and Energy Reporting NGER*, <http://www.cleanenergyregulator.gov.au/NGER>.

Nie, J., Yuan, S., Fang, L., Zhang, Q. & Li, D. 2018, 'Experimental study on an innovative enthalpy recovery technology based on indirect flash evaporative cooling', *Applied Thermal Engineering*, vol. 129, pp. 22-30.

O'Connor, D., Calautit, J.K.S. & Hughes, B.R. 2016, 'A review of heat recovery technology for passive ventilation applications', *Renewable and Sustainable Energy Reviews*, vol. 54, pp. 1481-93.

P.A.Hilton 2018, *A660 Air Conditioning Laboratory Unit*.

Pakari, A. & Ghani, S. 2019, 'Comparison of 1D and 3D heat and mass transfer models of a counter flow dew point evaporative cooling system: Numerical and experimental study', *International Journal of Refrigeration*, vol. 99, pp. 114-25.

References

Pandelidis, D. 2016, 'Mathematical modeling of the M-Cycle heat and mass exchanger used in air conditioning systems', Wroclaw University.

Pandelidis, D. & Anisimov, S. 2016, 'Numerical study and optimization of the cross-flow Maisotsenko cycle indirect evaporative air cooler', *International Journal of Heat and Mass Transfer*, vol. 103, pp. 1029-41.

Pandelidis, D., Anisimov, S., Rajski, K., Brychcy, E. & Sidorczyk, M. 2017, 'Performance comparison of the advanced indirect evaporative air coolers', *Energy*, vol. 135, pp. 138-52.

Pandelidis, D., Anisimov, S. & Worek, W.M. 2015, 'Performance study of counter-flow indirect evaporative air coolers', *Energy and Buildings*, vol. 109, pp. 53-64.

Pandelidis, D., Cichoń, A., Pacak, A., Anisimov, S. & Drąg, P. 2019, 'Performance comparison between counter- and cross-flow indirect evaporative coolers for heat recovery in air conditioning systems in the presence of condensation in the product air channels', *International Journal of Heat and Mass Transfer*, vol. 130, pp. 757-77.

Pescod, D. 1968, 'Unit air cooler using plastic heat exchanger with evaporatively cooled plates', *Australian refrigeration, Air conditioning and heating*, vol. 22, no. 9, pp. 22-6.

Pescod, D. 1979, 'A heat exchanger for energy saving in an air conditioning plant', *ASHRAE Transactions*, vol. 85, no. 2, pp. 238-51.

Pescod, D. & Prudhoe, R. 1980, 'Application of CSlRO Plate Heat Exchangers for Low Energy Cooling of Telecom Buildings', *Engineering Conference 1980: Engineering in the 80s; Conference Papers, The*, Institution of Engineers, Australia, p. 117.

References

Porumb, B., Ungureşan, P., Tutunaru, L.F., Şerban, A. & Bălan, M. 2016, 'A Review of Indirect Evaporative Cooling Technology', *Energy Procedia*, vol. 85, pp. 461-71.

Ray, W.T. 1935, 'Conditioning liquids and air and other gases', Google Patents.

Riangvilaikul, B. & Kumar, S. 2010, 'Numerical study of a novel dew point evaporative cooling system', *Energy and Buildings*, vol. 42, no. 11, pp. 2241-50.

Sadighi Dizaji, H., Hu, E.J. & Chen, L. 2018, 'A comprehensive review of the Maisotsenko-cycle based air conditioning systems', *Energy*, vol. 156, pp. 725-49.

Saraireh, M. 2012, 'Heat Transfer and Condensation of Water Vapour from Humid Air in Compact Heat Exchangers', Victoria University, Melbourne, Australia

Shallcross, D. 2012, *Handbook of Psychrometric Charts: Humidity diagrams for engineers*, Springer Science & Business Media.

Sohani, A., Sayyaadi, H. & Hoseinpoori, S. 2016, 'Modeling and multi-objective optimization of an M-cycle cross-flow indirect evaporative cooler using the GMDH type neural network', *International Journal of Refrigeration*, vol. 69, pp. 186-204.

Stoitchkov, N.J. & Dimitrov, G.I. 1998, 'Effectiveness of crossflow plate heat exchanger for indirect evaporative cooling: Efficacité des échangeurs thermiques à plaques, à courants croises pour refroidissement indirect évaporatif', *International Journal of Refrigeration*, vol. 21, no. 6, pp. 463-71.

Sun, Y. 2019, 'Numerical and experimental study on spray cooling system design for cooling performance enhancement of natural draft dry cooling towers'.

Sun, Y., Guan, Z., Gurgenci, H., Li, X. & Hooman, K. 2017, 'A study on multi-nozzle arrangement for spray cooling system in natural draft dry cooling tower', *Applied Thermal Engineering*, vol. 124, pp. 795-814.

Svedeman, S.J. 1981, 'The design evaluation of an improved indirect evaporative cooling system', Texas Tech University.

Vali, A., Ge, G., Besant, R.W. & Simonson, C.J. 2015, 'Numerical modeling of fluid flow and coupled heat and mass transfer in a counter-cross-flow parallel-plate liquid-to-air membrane energy exchanger', *International Journal of Heat and Mass Transfer*, vol. 89, pp. 1258-76.

Vera, M. & Quintero, A.E. 2015, 'Wall Conduction Effects in Laminar Counterflow Parallel-Plate Heat Exchangers with Small-Scale Wall Corrugations', in S.N. Kazi (ed.), *Heat Transfer Studies and Applications*, InTech, Rijeka, p. Ch. 01.

Vorayos, N., Katkhaw, N., Kiatsiriroat, T. & Nuntaphan, A. 2016, 'Heat transfer behavior of flat plate having spherical dimpled surfaces', *Case Studies in Thermal Engineering*, vol. 8, pp. 370-7.

Wan, Y., Lin, J., Chua, K.J. & Ren, C. 2018, 'Similarity analysis and comparative study on the performance of counter-flow dew point evaporative coolers with experimental validation', *Energy Conversion and Management*, vol. 169, pp. 97-110.

Wan, Y., Ren, C. & Xing, L. 2017, 'An approach to the analysis of heat and mass transfer characteristics in indirect evaporative cooling with counter flow configurations', *International Journal of Heat and Mass Transfer*, vol. 108, pp. 1750-63.

Wang, F., Sun, T., Huang, X., Chen, Y. & Yang, H. 2017, 'Experimental research on a novel porous ceramic tube type indirect evaporative cooler', *Applied Thermal Engineering*, vol. 125, pp. 1191-9.

Wang, T. & Dhanasekaran, T. 2010, 'Calibration of a computational model to predict mist/steam impinging jets cooling with an application to gas turbine blades', *Journal of Heat Transfer*, vol. 132, no. 12, p. 122201.

Wang, T.A. & Reid, R.L. 1996, 'Surface wettability effect on an indirect evaporative cooling system ', *ASHRAE Transactions*, vol. 102 (Part1.) pp. 427-33.

Watt, J. 2012, *Evaporative air conditioning handbook*, Springer Science & Business Media.

Xin, C. 2015, 'Compressor-less Water-Based Green Air-Conditioning System', National University of Singapore, Sigapore.

Xu, P., Ma, X., Zhao, X. & Fancey, K. 2017, 'Experimental investigation of a super performance dew point air cooler', *Applied Energy*, vol. 203, pp. 761-77.

Xu, P., Ma, X., Zhao, X. & Fancey, K.S. 2016, 'Experimental investigation on performance of fabrics for indirect evaporative cooling applications', *Building and Environment*, vol. 110, pp. 104-14.

Yaïci, W., Ghorab, M. & Entchev, E. 2013, 'Numerical analysis of heat and energy recovery ventilators performance based on CFD for detailed design', *Applied Thermal Engineering*, vol. 51, no. 1–2, pp. 770-80.

Yi, C. 2016, 'Modeling and experimental studny of plate type indirect evaporative cooler (IEC) for energy recovery in hot and humid regions', The Honk Kong Polytechnic University, Honk Kong.

Zeng, C., Liu, S. & Shukla, A. 2017, 'A review on the air-to-air heat and mass exchanger technologies for building applications', *Renewable and Sustainable Energy Reviews*, vol. 75, pp. 753-74.

Zhan, C., Duan, Z., Zhao, X., Smith, S., Jin, H. & Riffat, S. 2011, 'Comparative study of the performance of the M-cycle counter-flow and cross-flow heat exchangers for indirect evaporative cooling – Paving the path toward sustainable cooling of buildings', *Energy*, vol. 36, no. 12, pp. 6790-805.

Zhan, C., Zhao, X., Smith, S. & Riffat, S. 2011, 'Numerical study of a M-cycle cross-flow heat exchanger for indirect evaporative cooling', *Building and Environment*, vol. 46, no. 3, pp. 657-68.

Zhang, L.-Z. 2010, 'Heat and mass transfer in a quasi-counter flow membrane-based total heat exchanger', *International Journal of Heat and Mass Transfer*, vol. 53, no. 23–24, pp. 5478-86.

Zhao, X., Yang, S., Duan, Z. & Riffat, S.B. 2009, 'Feasibility study of a novel dew point air conditioning system for China building application', *Building and Environment*, vol. 44, no. 9, pp. 1990-9.

Zheng, B., Guo, C., Chen, T., Shi, Q., Lv, J. & You, Y. 2019, 'Development of an experimental validated model of cross-flow indirect evaporative cooler with condensation', *Applied Energy*, vol. 252, p. 113438.

Zhou, B., Huang, X. & Di, Y. 2003, 'Effects of Water Sprays in Indirect Evaporative Coolers on Heat and Mass Transfer', *Building Energy and Environment.*

Zou, Y., Zhao, X. & Chen, Q. 2018, 'Comparison of STAR-CCM+ and ANSYS Fluent for simulating indoor airflows', *Building Simulation*, vol. 11, Springer, pp. 165-74.